2012

Analytical Design and Experimental Validation of a Plate-Confined, Unbonded, Post-Tensioned Precast Concrete Wall Panel

Jeffrey Scott Weidner
Lehigh University

Follow this and additional works at: http://preserve.lehigh.edu/etd

Analytical Design and Experimental Validation of a Plate-Confined,

Unbonded, Post-Tensioned Precast Concrete Wall Panel

By

Jeffrey Weidner

A Thesis

Presented to the Graduate and Research Committee

of Lehigh University

in Candidacy for the Degree of

Master of Science

in

Civil and Environmental Engineering

Lehigh University

May 2012

This thesis is accepted and approved in partial fulfillment of the requirements for the Master of Science.

_____

Date

_____

Thesis Advisor

_____

Chairperson of Department

Acknowledgements

I first want to thank my wife, Jennifer, and my parents for being supportive and understanding throughout my entire educational experience, both at Lehigh University and elsewhere.

I would like to thank the ATLSS staff for working so hard to pull together my experiment while juggling other larger projects. I appreciate all the advice and guidance provided by the faculty of the Civil Engineering Department, particularly that of Dr. John Wilson, who was always available to his students. Additionally, I would like to thank Trevor Williamson and Eric Putnam for providing assistance leading up to and during the experiment.

Finally, I would like to thank my advisor, Dr. Richard Sause, for providing me with the opportunity to carry out this research absent a specific grant to fund it, and for guiding me along the development and execution of a large scale experimental laboratory test, with which I was a novice.

Contents

List of Figures

List of Tables

Abstract

This thesis presents the design, construction and experimental evaluation of an unbonded, precast, post-tensioned concrete shear wall panel system intended to provide large lateral drift level capacity with minimal damage. Prior work indicated the potential for this shear wall panel system to undergo large levels of drift while retaining the ability to self-center. However this occurred with substantial damage at the base of the first story wall panel.

The scope of this research included developing, designing, constructing and testing a more robust first story wall panel design concept. Several options were considered and analyzed. A steel plate-confined detail was chosen, designed, and tested. Performance goals were based on the results achieved during prior work, including a lateral drift capacity of 6% and a base shear capacity of 140 kips.

A quasi-static, cyclic load test of a post-tensioned shear wall with the plate-confined wall panel was conducted. With a maximum of 197 kips, the base shear capacity exceeded the performance goal of 140 kips. The system failed at a drift of 2.7%. It was found that the damage in the contact zone at the base of the bottom panel observed in the prior tests was completely eliminated up to the failure drift level. However, a confinement failure occurred at a different and unexpected location.

1

1 Introduction

1.1 Overview

Past research has shown the potential for unbonded, post-tensioned precast construction to resist seismic loading while providing capacity for large lateral displacements without serious damage (Perez et al. 2004). Current earthquake engineering research has moved beyond providing basic life safety to systems which sustain limited damage. Typically after an earthquake event, many current earthquake-resistant systems would have to be repaired due to substantial structural damage. The purpose of this research is to improve the unbonded post-tensioned shear wall system studied by Perez et al. (2004) to reach larger lateral drift while sustaining little or no structural damage.

1.2 Background

Precast earthquake-resistant structural systems were investigated within a program known as PRESSS (PREcast Seismic Structural Systems) in the 1990s (Priestly 1991). This work showed that unbonded post-tensioned frame structures exhibited nonlinear-elastic lateral force-displacement responses in which yielding of the PT strands was delayed by the independent strain behavior resulting from being unbonded (Priestly 1993).

This idea was extended to unbonded post-tensioned precast shear walls under flexure at Lehigh University. Kurama (1997) showed analytically that an unbonded post-tensioned

precast wall structure could undergo large lateral drifts without fracture of the post-tensioning steel. Additionally, Kurama (1997) showed that unbonded post-tensioned walls have substantial self-centering capability.

Experimental verification of the analytical results from Kurama (1997) was provided by Perez et al. (2004). A parametric experimental study was conducted to determine the effects of various parameters including amount of PT steel, initial PT force, and different concrete confinement details (Perez et al. 2004). The experimental results were correlated with the analytical model results with good correlation under certain conditions. The results of the experimental study showed the potential for the system to perform well under seismic loading, though some damage was observed. Spalling of the cover concrete near the base of the first story panel of the shear wall was seen at drift levels as low as 0.6%. This spalling would need repair after a moderate earthquake. The wall behavior depended on the prestress force. Generally, a smaller PT force would provide larger displacement capacity before failure, but would provide a smaller lateral force capacity, and vice versa.

1.3   Objective

The objectives of this research are to develop details for the first story panel of the unbonded post-tensioned precast shear wall system to extend the drift capacity of the system without sacrificing lateral force capacity, and to decrease or altogether eliminate

damage to the wall system at lower drift levels. The results of this study will be compared

with those of Perez et al. (2004) to demonstrate any improvements that are obtained.

1.4   Organization of Thesis

Chapter 2 presents analytical closed form expressions for the behavior of unbonded post-

tensioned walls as presented by Perez et al. (2004) with modifications to account for

changes in the wall panel geometry developed by the present research. Chapter 3 presents

the options considered for improving the first story panel of the wall system where

damage was observed in the experiments by Perez et al. (2004). The system selected for

the experiment is described. Chapter 4 presents the experimental test setup, data

acquisition, and test plan used to conduct tests on the selected panel design. Chapter 5

presents the results of the tests while Chapter 6 compares these results with those of

Perez et al. (2004). An assessment of the selected design is presented in Chapter 7.

Chapter 8 presents conclusions and recommendations for future work.

1.5   Notation

A_0 = shear area of standard panel

A_1 = shear area of modified 1st story panel

A_i = area under stress-strain curve at step i

A_{Oh} = area under stress-strain curve (Oh Confined Concrete Model)

A_{pi} = area of PT group i

A_{trib} = tributary area of a single bolt

A_{bolt} = cross-sectional area of a single bolt

$\bar{B}$ = distance from corner to horizontal centroid of bolt group

c = depth of compression

c_{llp} = depth of compression for linear limit of post-tensioning stage

c_{cf} = depth of compression for compressive failure stage

c_1 = depth of compression for panel Option 1

c_2 = depth of compression for panel Option 2

c_3 = depth of compression for panel Option 3

c_4 = depth of compression for panel Option 4

C = total compressive resultant force

C_{Di} = compressive resultant at decompression due to area A_i

C_{Ei} = compressive resultant at elastic linear limit due to area A_i

C_{Li} = compressive resultant at linear limit of post-tensioning due to area A_i

5

C_{Ci} = compressive resultant at compressive failure due to area A_i

C_{steel} = compressive resultant on a single steel plate

d = distance to a bolt from the ICR

d_{bolt} = horizontal component of distance from bolt to corner

d_{CDi} = distance from corner to compressive resultant at decompression

d_{CEi} = distance from corner to compressive resultant at elastic linear limit

d_{CLi} = distance from corner to compressive resultant at linear limit of post-tensioning

d_{CCi} = distance from corner to compressive resultant at compressive failure

$\overline{D}$ = distance from corner to total steel compressive resultant

e_c = horizontal eccentricity of steel compressive resultant relative to the bolt group

e_p = eccentricity of PT groups from centroid of the wall

E_c = modulus of elasticity of concrete

E_p = modulus of elasticity of steel confinement plates

f'_{c1} = concrete strength of panel option #1

f'_{c2} = concrete strength of panel option #2

f'_{c3} = concrete strength of panel option #3

f'_{c4} = concrete strength of panel option #4

F_{bolt} = force in bolt after pretensioning

F_{ev} = total force to be transferred by shear between plates and concrete panel

F_R = Resultant force at the bolt to be resisted by friction between the plate and concrete

F_{fr1} = direct shear force resisted by friction

G_0 = shear modulus of standard panel

G_1 = shear modulus of modified 1st story panel

H_{act} = height of the actuator

H_{cr} = critical confined concrete crushing height

H_{unb} = unbonded height of wall

H_w = height of wall

I_0 = moment of inertia of standard panel

I_1 = moment of inertia of modified 1st story panel

J = polar moment of inertia

l_c = confined length

l_i = length to centroid of PT steel group i

l_w = length of the wall panel

M_{fr} = moment due to eccentric compressive resultant, relative to bolt centroid

n = number of bolts

N = total gravity load applied to the wall

N_i = gravity load applied at each story, i

r_{Fi} = force factor for each story, i

r_{Fr} = force factor for roof

r_{Hi} = height factor for each story, i

r_{Hr} = height factor for roof

t_1 = thickness of panel option #1

t_2 = thickness of panel option #2

t_3 = thickness of panel option #3

t_4 = thickness of panel option #4

t_p = thickness of steel confining plates

t_w = thickness of uncracked wall (not including steel plates)

t'_w = thickness of cracked wall

T_i = initial tension in PT rods

T_1 = Tension force in PT group #1

T_2 = Tension force in PT group #2

T_3 = Tension force in PT group #3

V_{dec} = base shear at decompression stage

V_{ell} = base shear at elastic linear limit stage

V_{ell-1} = base shear at elastic linear limit stage from method #1

V_{ell-2} = base shear at elastic linear limit stage from method #2

V_{llp} = base shear at linear limit of post-tensioning stage

V_{cf} = base shear at compressive failure stage

$\bar{x}$ = centroid of area under stress-strain curve

$\bar{x}_i$ = moment arm to area at step i

y = vertical distance to location where bolt spacing variation is being investigated

α = concrete stress block parameter

β = concrete stress block parameter

Δ_{dec} = total roof displacement at decompression stage

$\Delta_{Fr,dec}$ = roof displacement at decompression stage due to flexure

$\Delta_{Sr,dec}$ = roof displacement at decompression stage due to shear

$\Delta_{Pr,dec}$ = roof displacement at decompression stage due to eccentric axial load

Δ_{ell} = total roof displacement at elastic linear limit stage

$\Delta_{Fr,ell}$ = roof displacement at elastic linear limit stage due to flexure

$\Delta_{Sr,ell}$ = roof displacement at elastic linear limit stage due to shear

$\Delta_{Pr,ell}$ = roof displacement at elastic linear limit stage due to eccentric axial load

Δ_{llp} = total roof displacement at linear limit of post-tensioning stage

$\Delta_{llp,go}$ = roof displacement at linear limit of post-tensioning stage due to gap opening

$\Delta_{llp,el}$ = roof displacement at linear limit of post-tensioning stage due to elastic deformation

$\Delta_{Fr,llp}$ = roof displacement at linear limit of post-tensioning stage due to flexure

$\Delta_{Sr,llp}$ = roof displacement at linear limit of post-tensioning stage due to shear

$\Delta_{Pr,llp}$ = roof displacement at linear limit of post-tensioning stage due to axial load

Δ_{cf} = total roof displacement at compressive failure stage

$\Delta_{cf,go}$ = roof displacement at compressive failure stage due to gap opening

$\Delta_{cf,el}$ = total roof displacement at compressive failure stage due to elastic deformation

$\Delta_{Fr,cf}$ = roof displacement at compressive failure stage due to flexure

$\Delta_{Sr,cf}$ = roof displacement at compressive failure stage due to shear

$\Delta_{Pr,cf}$ = roof displacement at compressive failure stage due to eccentric axial load

Δ_{v1} = gap opening at PT group #1

ε_{cef} = maximum compressive strain in the extreme fiber of the panel

ε_{cu} = maximum longitudinal strain

ε_i = strain at step i

$\varepsilon_{max,D}$ = maximum longitudinal strain at decompression

$\varepsilon_{max,E}$ = maximum longitudinal strain at elastic linear limit

$\varepsilon_{max,L}$ = maximum longitudinal strain at linear limit of post-tensioning

$\varepsilon_{max,C}$ = maximum longitudinal strain at compressive failure

ε_{pi} = strain in PT group i

ε_{10c} = maximum longitudinal strain for confined concrete

ε_{10} = maximum longitudinal strain for unconfined concrete

φ_c = confining ratio

φ_{cf} = curvature of critical confined concrete crushing region

σ_i = stress at step i

σ_y = yield stress of steel plates

σ_{avg} = average stress under stress-strain curve

σ_{cp} = confinement stress from a bolt

σ_{ev} = effective shear stress at a bolt location

σ_{pi} = initial value of prestress in PT rods

σ_{py} = yield stress of post-tensioning rods

θ_{llp} = rigid body rotation of wall at linear limit of post-tensioning stage

θ_{cf} = rigid body rotation of wall at compressive failure stage

Θ_{dec} = roof drift at decompression stage

Θ_{ell} = roof drift at elastic linear limit stage

Θ_{llp} = roof drift at linear limit of post-tensioning stage

Θ_{cf} = roof drift at compressive failure stage

2   Analysis of First-Story Panel Design Options

2.1   Introduction

This chapter describes the analysis of first-story panel design options. As discussed in

Chapter 1, the goal of this research is to increase the drift capacity of the unbonded post-

tensioned precast wall system and reduce damage of the first-story wall panel at lower

drift levels without sacrificing lateral force capacity. As shown later, the drift capacity

before wall failure is increased by reducing the strain in the concrete (for a given drift

level), which is achieved by reducing the length of the contact zone, c, of the wall panel

at the base. Reducing c also increases lateral force capacity (which is quantified in terms

of base shear capacity) by increasing the moment arm between the post-tensioning steel

force and the compressive resultant in the contact zone. A detailed explanation of the

system tested by Perez et al. (2004) is provided in Section 2.2. Four different panel

options were considered including a base case from previous work done by Perez et al.

(2004). The four options considered are as follows: Option 1 is the base case; Option 2 is

a thicker panel; Option 3 is a higher strength concrete panel; and Option 4 is a steel plate-

confined panel. These options are explained in detail in Section 2.3.

2.2   First-story Panel Design from Perez et al. (2004)

Figure 2-1 shows the first-story test panel as constructed by Perez et al. (2004). The panel

is comprised of two distinct sections; a traditionally reinforced portion and a heavily

13

reinforced portion. The heavily reinforced portion utilizes either hoop or spiral

reinforcement in a tight layout to achieve confinement of the end regions of the concrete

wall panel. There are two heavily reinforced sections, or confined regions, on both ends

of the panel in the horizontal direction. The traditionally reinforced unconfined region

uses vertical and horizontal rebar in a grid layout, but does not include any additional

reinforcement. This region is in the middle of the panel.

The dimension of the confined regions is defined by the parameter l_c which is the

confinement length in the horizontal direction. Specifically, the length of each confined

region is l_c, and the length of the remaining traditional region is the length of the entire

panel, l_w, less the two confined regions.

Through the unconfined region there are seven ducts used to house the unbonded, post-

tensioning steel bars. The post-tensioning bars are sub-divided into three groups

numbered PT1 through PT3 from west to east. Two types of first-story panel are

presented in Perez et al. (2004); hoop-confined and spiral-confined. The spiral

confinement was used for the first two experiments presented in Perez et al. (2004) but

was abandoned in favor of hoop confinement for the final three tests due to a global

buckling of the panel observed in TW2. Figure 2-2 shows the rebar cage for a hoop-

confined panel with the PT ducts in place.

The general geometric and material parameters for hoop-confined first-story panels from

Perez et al. (2004) are presented in Table 2-1 for reference. Section 3.2 provides more

detail on the test parameters for the hoop-confined panels. Section 4.3 describes the experimental setup in more detail.

2.3   Plate-Confined Panel Concept

Figure 2-3 shows a schematic of the plate-confined first-story panel design concept investigated in this research. Confinement is achieved through casting steel plates cast in-plane with the faces of the wall. The plates are stressed against the concrete with debonded bolts which are installed before the concrete is cast. The bolts are tightened to a predetermined level after the concrete panel has cured. The confined region is defined by l_c, and is similar to the length of the confined regions of the hoop or spiral-confined panels. The interface between the steel and the concrete in the plane of the wall panel is softened using a transition material to prevent premature spalling of the cover concrete in the unconfined region. The ends of the wall are capped with an end plate this is welded to the confinement plates after curing. The end plate was not cast with the panel because it would make it impossible to ensure that there were not voids during pouring. This end plate provides passive confinement in the horizontal direction of the wall, while the confinement plates provide active confinement through the thickness. The plate-confined wall uses the same duct layout and three PT groups as the hoop and spiral confined panels.

The thickness of the concrete wall between the plates, t_w, is equivalent to thickness of the walls tested by Perez et al. (2004), 6 inches. This is to ensure that the confinement plates

15

do not bear against the second story panel, as the stiffness change would cause premature

damage. For the plate-confined panel, the unconfined region is thicker than the walls

tested by Perez et al. (2004) by twice the confinement plate thickness.

2.4   Panel Design Options

Figure 2-4, 2-5, 2-6 and 2-7 show schematics of the four options including relevant

dimensions and material properties. The majority of the wall dimensions are maintained

from Perez et al. (2004) with slight modifications to increase the lateral displacement

(i.e., lateral drift) capacity.   Option 1 is the base case, shown in Figure 2-4. Confinement

of the concrete in the critical region of the first-story panel for Option 1 is achieved

through steel hoops cast into the wall as previously described in Section 2.2. Figure

2-8(a) shows a schematic of the anticipated concrete stress distribution acting on the wall

at maximum drift. Option 2 is a thicker panel, shown in Figure 2-5. Confinement for

Option 2 is also achieved through steel hoops. Figure 2-8(b) shows the anticipated stress

distribution at maximum drift. Note that because $t_2 > t_1$ and $f'_{c2} = f'_{c1}$, c_2 is less than c_1

when the PT steel is kept constant. Option 3 is a higher strength concrete panel, shown in

Figure 2-6. Confinement is again achieved through steel hoops. Figure 2-8(c) shows the

anticipated stress distribution at maximum drift. Note that in this case, because $f'_{c3} > f'_{c1}$

and $t_3 = t_1$, c_3 is less than c_1 when the PT steel is kept constant. Option 4 is a steel plate-

confined panel, shown in Figure 2-7. Figure 2-8(d) shows the anticipated stress

distributions on both the concrete and steel portions that will be contact with the

16

foundation at the maximum drift. Again c_4 is less than c_1 but for this option $t_4 = t_1$ and f'_{c4} $= f'_{c1}$. As shown later, the presence of steel plates causes the decrease in contact zone length.

2.5   Limit States

Limit states for unbonded post-tensioned precast concrete walls were previously identified by Kurama (1997) and described again by Perez et al. (2004). The limits states considered are: (1) decompression, (2) effective linear limit, (3) yielding of PT steel, (4) base shear capacity, (5) loss of prestress, (6) crushing of confined concrete, (7) fracture of PT steel. These limit states are generally adopted here but are modified as presented in Sections 2.5.1 through 2.5.7.

2.5.1   Decompression (DEC)

The decompression state is defined as the point at which the stress at one edge of the base of the first-story wall panel becomes zero due to the overturning moment at the base of the wall. Figure 2-9 shows the assumed equilibrium conditions of the wall at DEC for Options 1, 2, and 3. Figure 2-10 shows the assumed equilibrium condition of the wall at DEC for Option 4. The base shear at this stage is referred to as V_{dec}. The roof drift at this stage is referred to as Θ_{dec}. Expressions for these variables are derived in Section 2.6.1 and Section 2.6.2.

17

2.5.2 Effective Linear Limit (ELL)

The effective linear limit state is defined as the point at which softening of the wall lateral force-displacement behavior becomes apparent. There are two components to softening; nonlinear stress-strain behavior of the concrete and gap opening at the base of the first-story panel. ELL varies based on the makeup of the wall panel. Figure 2-11 shows assumed equilibrium conditions of the wall at ELL for Options 1, 2, and 3. Figure 2-12 shows assumed equilibrium conditions of the wall at ELL for Option 4. The base shear at ELL is denoted V_{ell}. The roof drift at ELL is denoted as Θ_{ell}. Expressions for these variables are derived in Section 2.6.3 and Section 2.6.4.

2.5.3 Yielding of Post-Tensioning Steel (LLP)

The yielding of the PT steel occurs when gap opening along the base of the wall has progressed enough to strain the PT steel group closest to the edge of the wall where gap opening initiated to its yield value. Figure 2-13 shows assumed equilibrium conditions at LLP for Options 1, 2, and 3. Figure 2-14 shows assumed equilibrium conditions at LLP for Option 4. The base shear at LLP is denoted as V_{llp}. The roof drift at LLP is denoted as Θ_{llp}. Expressions for these variables are derived in Section 2.6.5 and Section 2.6.6.

2.5.4 Base Shear Capacity

The wall is assumed to reach its base shear capacity at the LLP stage. The base shear capacity is assumed to be controlled by the base flexural capacity, which is reached when the PT steel yields. Strain hardening effects in the PT steel are ignored, the moment arm between the PT steel force and the concrete compressive stress resultant is assumed to remain constant beyond the LLP state.

2.5.5 Loss of Prestress

Loss of prestress begins at the LLP state. As soon as the PT steel begins to deform plastically, prestress will be lost during subsequent elastic unloading. The amount of prestress lost is proportional to the plastic deformation of the PT steel.

2.5.6 Compressive Failure (CF)

Perez et al. (2004) defined the failure state of the wall as crushing of the confined concrete (CCC). The name for this state has been changed to compressive failure (CF) for the present research. The name has been altered because Option 4 would fail by combined concrete and steel plate failure. The failure of all options would be localized in the compressive contact zone of the wall panel, so compressive failure is an appropriate label. CF is defined to be the state when the concrete strain value in the through-thickness direction of the wall panel reaches a certain value (as described later). Figure 2-15 shows

19

the assumed equilibrium conditions at CF for Options 1, 2, and 3. Figure 2-16 shows the

assumed equilibrium conditions at CF for Option 4. The base shear at CF is denoted V_{cf}.

The roof drift at CF is denoted Θ_{cf}. Expressions for these variables are derived in Section

2.6.7 and Section 2.6.8.

2.5.7 Fracture of Post-Tensioning Steel

Fracture of PT steel occurs when gap opening progresses to a stage where the PT steel

group closest to the edge of the wall where gap opening initiated reaches its ultimate

strain value. Fracture of PT steel occurs after significant loss of prestress, at large levels

of drift.

2.6 Predictive Expressions for Lateral Force Response

Predictive expressions for lateral force response behavior of unbonded post-tensioned

precast wall panel system are developed in the subsequent sections. Perez et al. (2004)

developed expressions considering uniform section properties up the height of the wall;

these expressions are modified to account for potential variation in the properties of the

first story panel. The modifications shown are for a variation in section properties (i.e.,

moment of inertia and area). Figure 2-17 shows schematically how variation of properties

of the first panel can affect the curvature of the wall system under lateral force. Similar

20

modifications could be made for changes to the effective shear area or material properties (i.e., modulus of elasticity and shear modulus).

Perez et al. (2004) also developed expressions considering a single compressive resultant force in the contact zone of the concrete. For the present research, the compressive resultant has several components, which are treated as a summation of forces and distances in moment equilibrium equations. The areas of the base of the wall upon which these compressive forces act are shown explicitly in each section.

The expressions assume that the gravity load, N, is concentric and causes no additional moment. Perez et al. (2004) included a term for moment due to eccentric gravity loading. This term is neglected here.

The expressions developed in Section 2.6.1 through Section 2.6.8 are derived considering the prototype wall setup seen in Figure 2-18, but they are modified to apply to the experimental test wall setup seen in Figure 2-19.

All expressions are developed for lateral forces applied to the right. The sign convention is shown in Figure 2-20.

2.6.1 Base Shear at Decompression, V_{dec}

This section develops an expression to determine the base shear at the decompression state. Figure 2-19 shows the experimental test wall. V_{dec} is estimated by summing moments about point O as follows:

$$V_{dec} = \frac{T_1\left(\frac{l_w}{2} + e_p\right) + (T_2 + N)\frac{l_w}{2} + T_3\left(\frac{l_w}{2} - e_p\right) - \sum_j C_{D_j} d_{CD_j}}{H_{act}} \tag{2.1}$$

with:

$$T_{1i} = T_{2i} = T_{3i} = T_i$$

$$N = \sum_{i=1,r} N_i$$

$$C_{D1} = \frac{1}{2} l_w t_w \left(\varepsilon_{max,D} E_c\right)$$

$$C_{D2} = (l_w - 2l_c)(t_p)\left(\varepsilon_{max,D} E_c\right)$$

$$C_{D3} = \left(\frac{l_c(2l_w - l_c)}{l_w}\right)(t_p)\left(\varepsilon_{max,D} E_{pl}\right)$$

$$C_{D4} = \left(\frac{l_c^{\,2}}{l_w}\right)(t_p)\left(\varepsilon_{max,D} E_{pl}\right)$$

$$d_{CD1} = \frac{l_w}{3}$$

$$d_{CD2} = l_c + \frac{(l_w - 2l_c)(l_w - l_c)}{3l_w}$$

$$d_{CD3} = \frac{l_c}{3} \cdot \frac{(3l_w - 2l_c)}{(2l_w - l_c)}$$

$$d_{CD4} = l_w - \frac{2}{3}l_c$$

$$\varepsilon_{max,D} = \frac{(T_1 + T_2 + T_3 + N)}{l_w \left(\frac{t_w}{2} + t_p \right) E_c + 2 l_c t_p \left(E_{pl} - E_c \right)}$$

In the above expressions, T_{1i}, T_{2i}, and T_{3i} are the initial prestress forces in each post-tensioning group (assumed to be the same). N is a summation of the gravity force acting on the wall. $C_{Di\ (i=1...4)}$ are compressive resultants acting on the bottom of the wall, shown in Figure 2-9 and Figure 2-10. $d_{CDi\ (i=1...4)}$ are the locations of the compressive resultants from point O. The number and location of compressive resultants included in the last term of the numerator of Eqn. 2.1 is dependent on the panel option. H_{act} is the height of the actuator. E_c and E_{pl} are the moduli of elasticity for the concrete and the steel plate, respectively. l_w is the length of the wall panel, while t_w is the thickness of the panel, excluding the steel plates for Option 4. l_c is the length of the confined area on each edge of the wall, which directly corresponds to the length of the plate for Option 4. t_p is the thickness of a single confinement plate. At DEC, the contact zone length, c, is defined as l_w because gap opening has not initiated. The maximum strain at decompression, $\varepsilon_{max,D}$, is determined from vertical equilibrium.

23

2.6.2 Lateral Drift at Decompression, Θ_{dec}

This section develops a set of expressions for lateral drift at the decompression stage. The lateral force considered is shown in Figure 2-9 and Figure 2-10. Section properties are elastic, uncracked, and if needed, transformed. Θ_{dec} is estimated with the following equation:

$$\Theta_{dec} = \frac{\Delta_{dec}}{H_w} \tag{2.2}$$

with:

$$\Delta_{dec} = \Delta_{Fr,dec} + \Delta_{Sr,dec} \tag{2.3}$$

Δ_{dec} is the total lateral roof deflection at the decompression stage. $\Delta_{Fr,dec}$ is the roof deflection due flexural deformation of the wall panel from V_{dec}. $\Delta_{Sr,dec}$ is the roof deflection due to shear deformation of the wall panel from V_{dec}. H_w is the height of the entire wall. These quantities were derived for an unbonded post-tensioned wall panel system with variable properties of the first section using virtual work. The resulting expressions, derived from Figure 2-18 are shown below:

$$\Delta_{Fr,dec} = \sum_{i=1,r} \left(\begin{array}{l} \dfrac{1}{2EI_0} \cdot r_{Fi} \cdot V_{dec} \cdot r_{Hi}^2 \cdot H_w^3 \cdot \left(r_{Hr} - \dfrac{r_{Hi}}{3} \right) - \\[2ex] \left(\dfrac{EI_1 - EI_0}{EI_1 EI_0} \right) \cdot r_{Fi} \cdot V_{dec} \cdot r_{H1} \cdot H_w^3 \cdot \left(r_{Hi} - \dfrac{1}{2} r_{H1} - \dfrac{1}{2} r_{Hi} \cdot r_{H1} + \dfrac{1}{3} r_{H1}^2 \right) \end{array} \right) \tag{2.4}$$

$$\Delta_{Sr,dec} = \sum_{i=1,r} \left(\dfrac{1}{GA_0} \cdot r_{Fi} \cdot V_{dec} \cdot r_{Hi} \cdot H_w - \left(\dfrac{GA_1 - GA_0}{GA_1 GA_0} \right) \cdot r_{Fi} \cdot V_{dec} \cdot r_{H1} \cdot H_w \right) \tag{2.5}$$

The first term of these equations is the same as developed by Perez et al. (2004). The second term accounts for the section properties of the first story panel being different that the properties of the other panels. EI_1 is the stiffness of the first-story wall panel and EI_0 is the stiffness of the base case panels as described in Section 2.2. When $EI_1 = EI_0$, the second term of Eqn. 2.4 becomes zero, and the expression is equivalent with those developed in Perez et al. (2004). Similarly, GA_1 is the shear stiffness of the first-story wall panel, and GA_0 is the shear stiffness of the base case wall panels. When these values are equivalent, the second term in Eqn. 2.5 becomes zero.

The equations are modified to represent the experimental test setup shown in Figure 2-19 as follows; H_w is taken as H_{act}, where the load is applied. This means that r_{Fr}, the force ratio corresponding to the location of the force, is equal to 1 while all other r_{Fi} factors are equal to zero. r_{H1} is taken as 0.2283 from the ratio of the height of the first wall panel to the height of the wall.

2.6.3   Base Shear at Effective Linear Limit, V_{ell}

In this section an expression is developed for the base shear at the effective linear limit state. The basis for this analysis is presented in El-Sheikh (1997). ELL occurs when there is a "substantial reduction in lateral stiffness" or softening (Perez et al. 2004). As described previously, this point is not clearly defined and has two contributing factors; gap opening and nonlinear material behavior. The expression for V_{ell} is as follows:

$$V_{ell} = \min \begin{cases} V_{ell-1} \\ V_{ell-2} \end{cases} \qquad (2.6)$$

V_{ell-1} is based on equilibrium conditions of the wall and assumes the concrete behaves as if it were unconfined. Using Figure 2-19, V_{ell-1} is estimated by summing moments about point O as follows:

26

$$V_{ell-1} = \frac{T_1\left(\dfrac{l_w}{2} + e_p\right) + (T_2 + N)\dfrac{l_w}{2} + T_3\left(\dfrac{l_w}{2} - e_p\right) - \sum_j C_{Ej}\, d_{CEj}}{H_{act}} \tag{2.7}$$

with:

$$T_{1i} = T_{2i} = T_{3i} = T_i$$

$$N = \sum_{i=1,r} N_i$$

$$C_{E1} = \alpha\,\beta\, f'_c\, t_w\, c$$

$$C_{E2} = \frac{1}{2}\left(\frac{\varepsilon_y}{\varepsilon_{max,E}}\right)\sigma_y\, t_p\, c$$

$$C_{E3} = \left(1 - \frac{\varepsilon_y}{\varepsilon_{max,E}}\right)\sigma_y\, t_p\, c$$

$$d_{CE1} = \frac{\beta\, c}{2}$$

$$d_{CE2} = \left(1 - \left(\frac{2}{3}\frac{\varepsilon_y}{\varepsilon_{max,E}}\right)\right)c$$

$$d_{CE3} = \left(1 - \frac{\varepsilon_y}{\varepsilon_{max,E}}\right)c$$

$$c = \frac{T_1 + T_2 + T_3 + N}{\alpha \beta f'_c t_w + \left(1 - \dfrac{\varepsilon_y}{\varepsilon_{max,E}}\right)\sigma_y t_p}$$

In the above expressions, T_{1i}, T_{2i}, and T_{3i} are the initial prestress forces in each post-tensioning group. N is a summation of the gravity force at each story. Figure 2-11 shows the equilibrium condition of the experimental test wall at the effective linear limit for Options 1, 2, and 3. Figure 2-12 shows the equilibrium condition of the experimental test wall at the effective linear limit for Option 4. $C_{Ei\ (i=1\ldots4)}$ are compressive resultants acting on the bottom of the wall, derived from Figure 2-11 or Figure 2-12 depending on the panel option. $d_{CEi\ (i=1\ldots4)}$ are the locations of the compressive resultants from point O. H_{act} is the height of the applied force, l_w is the length of the wall and t_w is the thickness of the concrete portion of the unspalled wall. For Option 4, t_p is the thickness of one of the confinement plates. σ_y is the yield stress of the steel confinement plates and ε_y is the yield strain. At ELL, the concrete is treated as unconfined. An equivalent stress block is used to define the concrete compressive distribution. The unconfined concrete is assumed to be at its ultimate capacity ($\varepsilon_{max,E} = .003$; $\alpha = 0.85$; $\beta = 1.0$) Typical unconfined concrete stress-strain behavior is shown schematically in Figure 2-21.

V_{ell-2} is based on the gap opening behavior of the wall. An empirical relationship to determine V_{ell-2} was described in Perez et al. (2004) and is used here. V_{ell-2} is determined as follows:

28

$$V_{ell-2} = 2.5 \cdot V_{dec} \qquad (2.8)$$

2.6.4   Lateral Drift at Effective Linear Limit, Θ_{ell}

This section develops a set of expressions for lateral drift at the effective linear limit state. Section properties are elastic, uncracked, and if needed, transformed. Θ_{ell} is estimated with the following equation:

$$\Theta_{ell} = \frac{\Delta_{ell}}{H_w} \qquad (2.9)$$

with:

$$\Delta_{dec} = \Delta_{Fr,dec} + \Delta_{Sr,dec} \qquad (2.10)$$

Δ_{ell} is the total elastic roof deflection at the ELL stage. $\Delta_{Fr,ell}$ is the roof deflection due flexural deformation of the wall panel from V_{ell}. $\Delta_{Sr,ell}$ is the roof deflection due to shear deformation of the wall panel from V_{ell}. These quantities were derived for an unbonded

29

post-tensioned wall panel system with variable properties of the first panel using virtual

work. The resulting expressions, derived based on Figure 2-18, are shown below:

$$\Delta_{Fr,ell} = \sum_{i=1,r} \left[\begin{array}{l} \dfrac{1}{2EI_0} \cdot r_{Fi} \cdot V_{ell} \cdot r_{Hi}{}^2 \cdot H_w{}^3 \cdot \left(r_{Hr} - \dfrac{r_{Hi}}{3} \right) - \\ \left(\dfrac{EI_1 - EI_0}{EI_1 EI_0} \right) \cdot r_{Fi} \cdot V_{ell} \cdot r_{H1} \cdot H_w{}^3 \cdot \left(r_{Hi} - \dfrac{1}{2}r_{H1} - \dfrac{1}{2}r_{Hi} \cdot r_{H1} + \dfrac{1}{3}r_{H1}{}^2 \right) \end{array} \right] \qquad (2.11)$$

$$\Delta_{Sr,ell} = \sum_{i=1,r} \left(\dfrac{1}{GA_0} \cdot r_{Fi} \cdot V_{ell} \cdot r_{Hi} \cdot H_w - \left(\dfrac{GA_1 - GA_0}{GA_1 GA_0} \right) \cdot r_{Fi} \cdot V_{ell} \cdot r_{H1} \cdot H_w \right) \qquad (2.12)$$

The equations are modified to represent the experimental test setup shown in Figure 2-19

as follows; H_w is taken as H_{act}, where the load is applied. This means that r_{Fr}, the force

ratio corresponding to the location of the force, is equal to 1 while all other r_{Fi} factors are

equal to zero. r_{H1} is taken as 0.2283 from the ratio of the height of the first wall panel to

the height of the wall.

30

2.6.5 Base Shear at Yielding of Post-Tensioning Steel, V_{llp}

This section develops an expression for the base shear at the point where the post-tensioning steel begins to yield. At this stage, the distribution of the confined concrete stress at the panel base is not known. A stress block is assumed based on parameters as it would for the ultimate condition. ($\alpha = 0.9$; $\beta = 1.0$). Figure 2-13 shows the assumed equilibrium conditions of the experimental test wall at the LLP state for Options 1, 2, and 3. Figure 2-14 shows the assumed equilibrium conditions of the experimental test wall at the LLP state for Option 4. At LLP, neither the contact zone length nor the maximum strain is known, so one value must be assumed in order to calculate the other. In this case, $\varepsilon_{max,L}$ is assumed to be equivalent to the concrete strain in the longitudinal direction of the wall (global vertical direction) when the confined concrete reaches its peak compressive strength as presented by Oh (2002) and defined by Richart (1928). The following gives an expression for the strain when the confined concrete reaches its peak strength:

$$\varepsilon_{max,L} = \varepsilon_{10C} = \varepsilon_{10}\left(1 + 20.5\phi_c\right) \tag{2.13}$$

where ε_{10} is the strain when unconfined concrete reaches its peak compressive strength. ε_{10} can be determined from a concrete stress-strain model or from experimental data. An iterative approach similar to that used in Perez et al. (2004) to determine the contact zone length, c, is shown below:

Step 1 - Estimate the contact zone length by assuming yielding in all PT steel and that the

contact zone length, c, is less that the confined length, l_c, and using vertical equilibrium of

the forces shown in Figure 2-13 or Figure 2-14. The derivation of c is presented with

formulas based on Option 4. For Options 1, 2, and 3, the value of t_p is zero and the

equations reduce to simpler versions for a concrete panel without steel plates.

$$c_{llp} = \frac{T_1 + T_2 + T_3 + N}{\alpha \beta f`_c t`_w + \left(\dfrac{\varepsilon_y}{\varepsilon_{max,L}}\right)\sigma_y t_p + 2\left(1 - \dfrac{\varepsilon_y}{\varepsilon_{max,L}}\right)\sigma_y t_p} \tag{2.14}$$

with:

$$T_1 = T_2 = T_3 = A_p f_{py}$$

Cover concrete is assumed to have spalled off in the contact zone for Option 1, 2, and 3

so t'_w, which is the wall thickness neglecting the cover concrete, is used. In the case of

Option 4, t_w is used as spalling will not occur. A_p is the area of one PT steel group and f_{py}

is the yield stress of the PT steel. The assumption that all the PT steel is yielded is the

start of the iteration process.

Step 2 - Define the location of each PT steel group from the NA.

$$l_1 = \frac{l_w}{2} - c + e_p \qquad (2.15\text{a})$$

$$l_2 = \frac{l_w}{2} - c \qquad (2.15\text{b})$$

$$l_3 = \frac{l_w}{2} - c - e_p \qquad (2.15\text{c})$$

Step 3 - Determine the gap opening, Δ_{v1}, at the post-tensioning group when yielding first occurs (PT1 assuming Eastward loading).

$$\Delta_{v1} = \frac{\left(f_{py} - f_{p1} \right)}{E_p} \cdot H_{unb} \qquad (2.16)$$

where H_{unb} is the unbonded height of the PT steel, f_{pi} is the initial prestress in the PT steel, and $f_{p1} = f_{py}$ for eastward loading.

Step 4 - Determine the strain in each PT steel group.

33

$$\varepsilon_{p1} = \frac{f_{pi}}{E_p} + \frac{\Delta_{v1}}{H_{unb}} \cdot \left(\frac{l_1}{l_1}\right) \qquad\qquad (2.17a)$$

$$\varepsilon_{p2} = \frac{f_{pi}}{E_p} + \frac{\Delta_{v1}}{H_{unb}} \cdot \left(\frac{l_2}{l_1}\right) \qquad\qquad (2.17b)$$

$$\varepsilon_{p3} = \frac{f_{pi}}{E_p} + \frac{\Delta_{v1}}{H_{unb}} \cdot \left(\frac{l_3}{l_1}\right) \qquad\qquad (2.17c)$$

Step 5 - Determine the force in each PT steel group.

$$T_1 = A_{p1} \cdot \varepsilon_{p1} \cdot E_p \qquad\qquad (2.18a)$$

$$T_2 = A_{p2} \cdot \varepsilon_{p2} \cdot E_p \qquad\qquad (2.18b)$$

$$T_3 = A_{p3} \cdot \varepsilon_{p3} \cdot E_p \qquad\qquad (2.18c)$$

Step 6 - Recalculate the contact zone length, c with Eqn. 2.15 using the new PT steel forces. Iterate steps 2 through 6 until c converges to a final value, c_{llp}.

V_{llp} is estimated by summing moments about point O in Figure 2-19:

$$V_{llp} = \frac{T_1\left(\frac{l_w}{2} + e_p\right) + (T_2 + N)\left(\frac{l_w}{2}\right) + T_3\left(\frac{l_w}{2} - e_p\right) - \sum_j C_{Lj}\, d_{CL_j}}{H_{act}} \tag{2.19}$$

with:

$$C_{L1} = \alpha\, \beta\, f'_c\, t'_w\, c_{llp}$$

$$C_{L2} = \frac{1}{2}\left(\frac{\varepsilon_y}{\varepsilon_{max,L}}\right)\sigma_y\, t_p\, c_{llp}$$

$$C_{L3} = \left(1 - \frac{\varepsilon_y}{\varepsilon_{max.L}}\right)\sigma_y\, t_p\, c_{llp}$$

$$d_{CL1} = \frac{\beta\, c_{llp}}{2}$$

$$d_{CL2} = \left(1 - \left(\frac{2}{3}\frac{\varepsilon_y}{\varepsilon_{max,L}}\right)\right)c_{llp}$$

$$d_{CL3} = \frac{1}{2}\left(1 - \frac{\varepsilon_y}{\varepsilon_{max,L}}\right)c_{llp}$$

35

Figure 2-13 shows the equilibrium condition of the experimental test wall at the yielding of PT Steel for Options 1, 2, and 3. Figure 2-14 shows the equilibrium condition of the experimental test wall at the effective linear limit for Option 4. $C_{Li\ (i=1...4)}$ are compressive resultants acting on the bottom of the wall, derived from Figure 2-13 or Figure 2-14 depending on the panel option. $d_{CLi\ (i=1...4)}$ are the locations of the compressive resultants from point O. H_{act} is the height of the actuator, l_w is the length of the panel, t'_w is the thickness of the panel after spalling for Options 1, 2, and 3 and t_w is the thickness of the confined concrete portion of the plate-confined wall. For Option 4, t_p is the thickness of one of the confinement plates. σ_y is the yield stress of the steel confinement plates and ε_y is the yield strain.

2.6.6   Lateral Drift at Yielding of Post-Tensioning Steel, Θ_{llp}

This section develops a set of expressions for lateral drift at first yielding of the post-tensioning steel. Section properties are elastic, uncracked, and if needed, transformed. This stage differs from the previous two in that the drift at LLP includes both gap opening behavior and elastic deformation. Θ_{llp} is estimated with the following equation:

$$\Theta_{llp} = \frac{\Delta_{llp}}{H_w} \tag{2.20}$$

36

with:

$$\Delta_{llp} = \Delta_{llp,el} + \Delta_{llp,go}$$

$$\Delta_{llp,el} = \Delta_{Rr,llp} + \Delta_{Sr,llp} + \Delta_{Pr,llp}$$

$$\Delta_{llp,go} = \theta_{llp} \cdot H_w$$

$$\theta_{llp} = \frac{\Delta_{v1}}{l_1}$$

Δ_{llp} is the total elastic roof deflection at the LLP stage. $\Delta_{Fr,llp}$ is the roof deflection due

flexural deformation of the wall panel from V_{llp}. $\Delta_{Sr,llp}$ is the roof deflection due to shear

deformation of the wall panel from V_{llp}. $\Delta_{Pr,llp}$ is the roof deflection due to flexural

deformation resulting from any difference in the post-tensioning steel forces T_1 and T_3.

$\Delta_{llp,go}$ is the roof deflection due to rigid body rotation from gap opening at the base of the

wall. θ_{llp} is the rotation, in radians, at the base of the wall due to gap opening. This

calculation assumes that the gap opening is only a function of the rigid body rotation of

the wall and that this rotation can be calculated using small angle theory. Δ_{v1} is the gap

opening at post-tensioning group PT1 (Eqn. 2.16), and l_1 is the distance from the ICR to

PT1, (Eqn.2.15a) along the base of the wall panel. The elastic roof deformation

quantities were derived for an unbonded post-tensioned wall panel system with variable

properties of the first panel using virtual work, as seen in Figure 2-18. The resulting

expressions are shown as follows:

37

$$\Delta_{Fr,llp} = \sum_{i=1,r} \left(\begin{array}{l} \dfrac{1}{2EI_0} \cdot r_{Fi} \cdot V_{llp} \cdot r_{Hi}^2 \cdot H_w^3 \cdot \left(r_{Hr} - \dfrac{r_{Hi}}{3} \right) - \\[2mm] \left(\dfrac{EI_1 - EI_0}{EI_1 EI_0} \right) \cdot r_{Fi} \cdot V_{llp} \cdot r_{H1} \cdot H_w^3 \cdot \left(r_{Hi} - \dfrac{1}{2} r_{H1} - \dfrac{1}{2} r_{Hi} \cdot r_{H1} + \dfrac{1}{3} r_{H1}^2 \right) \end{array} \right) \quad (2.21)$$

$$\Delta_{Sr,llp} = \sum_{i=1,r} \left(\dfrac{1}{GA_0} \cdot r_{Fi} \cdot V_{llp} \cdot r_{Hi} \cdot H_w - \left(\dfrac{GA_1 - GA_0}{GA_1 GA_0} \right) \cdot r_{Fi} \cdot V_{llp} \cdot r_{H1} \cdot H_w \right) \quad (2.22)$$

$$\Delta_{Pr,llp} = \dfrac{e_p \cdot (T_3 - T_1)}{2EI_0} \cdot H_w^2 - e_p \cdot (T_3 - T_1) \cdot \left(\dfrac{EI_1 - EI_0}{EI_1 EI_0} \right) \cdot H_w^2 \cdot \left(r_{H1} - \dfrac{1}{2} r_{H1}^2 \right) \quad (2.23)$$

The equations are modified to represent the experimental test setup shown in Figure 2-19 as follows; H_w is taken as H_{act}, where the load is applied. This means that r_{Fr}, the force ratio corresponding to the location of the force, is equal to 1 while all other r_{Fi} factors are equal to zero. r_{H1} is taken as 0.2283 from the ratio of the height of the first wall panel to the height of the wall.

2.6.7 Base Shear at Compressive Failure, V_{cf}

The base shear between LLP and CF is assumed to be constant. Strain hardening of the PT bars and the small increase in post-tensioning forces after yield of the first PT steel group are neglected.

2.6.8 Lateral Drift at the Compressive Failure, Θ_{cf}

This section develops equations for the roof drift at the compressive failure of the wall. The lateral forces are shown in Figure 2-15 and Figure 2-16. Section properties are elastic, uncracked, and if needed, transformed. Θ_{cf} is estimated with the following equation:

$$\Theta_{cf} = \frac{\Delta_{cf}}{H_w} \tag{2.24}$$

with:

$$\Delta_{cf} = \Delta_{cf,el} + \Delta_{cf,go}$$

$$\Delta_{cf,el} = \Delta_{Rr,cf} + \Delta_{Sr,cf}$$

$$\Delta_{cf,go} = \theta_{cf} \cdot H_w$$

Δ_{cf} is the total elastic roof deflection at the CF stage. $\Delta_{Fr,cf}$ is the roof deflection due flexural deformation of the wall panel from V_{cf}. $\Delta_{Sr,cf}$ is the roof deflection due to shear deformation of the wall panel from V_{cf}. $\Delta_{cf,go}$ is the roof deflection due to rigid body rotation from gap opening at the base of the wall. θ_{cf} is the rotation, in radians, at the base of the wall due to gap opening. The elastic deformation quantities were derived for an unbonded post-tensioned wall panel system with variable properties of the first panel using virtual work, based on Figure 2-18.

For the calculation of elastic deformation of the wall, the deformations within the critical confined concrete crushing region at the bottom of the wall (H_{cr}) are ignored. The resulting equations are as follows:

$$\Delta_{Fr,cf} = \sum_{i=1,r} \left(\begin{array}{l} \dfrac{1}{2EI_0} \cdot r_{Fi} \cdot V_{cf} \cdot \left(r_{Hi} \cdot H_w - H_{cr} \right)^2 \cdot \left(H_w - H_{cr} \right) \left(r_{Hr} - \dfrac{r_{Hi}}{3} \right) - \\ \left(\dfrac{EI_1 - EI_0}{EI_1 EI_0} \right) \cdot r_{Fi} \cdot V_{cf} \cdot r_{H1} \cdot \left(H_w - H_{cr} \right)^3 \cdot \left(r_{Hi} - \dfrac{1}{2} r_{H1} - \dfrac{1}{2} r_{Hi} \cdot r_{H1} + \dfrac{1}{3} r_{H1}^2 \right) \end{array} \right)$$

(2.25)

$$\Delta_{Sr,cf} = \sum_{i=1,r} \left(\dfrac{1}{GA_0} \cdot r_{Fi} \cdot V_{cf} \cdot r_{Hi} \cdot \left(H_w - H_{cr} \right) - \left(\dfrac{GA_1 - GA_0}{GA_1 GA_0} \right) \cdot r_{Fi} \cdot V_{cf} \cdot r_{H1} \cdot \left(H_w - H_{cr} \right) \right)$$

(2.26)

The bottom portion of the wall up to a height of H_{cr} is assumed to be the critical confined concrete crushing region. H_{cr} is defined as:

$$H_{cr} = \begin{cases} 2t'_w & if\ 2t'_w > c \\ c\ if\ 2t'_w < c \end{cases}$$

(2.27)

Note that for Option 4, t'_w is replaced with t_w. The roof deflection due to gap opening $\Delta_{cf,go}$ is calculated based on an assumption of constant curvature of the critical height, H_{cr}. This curvature, φ_{cf}, is determined through the following relationship developed by Perez et al. (2004):

$$\phi_{cf} = \frac{\varepsilon_{cu}}{c_{cf}}$$

(2.28)

with ε_{cu} equal to the concrete strain in the longitudinal direction of the wall (global vertical direction) at failure of the confined concrete. Confined concrete failure is often controlled by failure of the confining material (e.g., hoops or spiral reinforcement) under strain in the transverse direction due to dilation of the concrete. ε_{cu} is determined from a confined concrete stress-strain model or experimental values. c_{cf} equals the contact zone length, calculated using vertical equilibrium, resulting in the following relationship:

41

$$c_{cf} = \frac{T_1 + T_2 + T_3 + N}{\alpha \beta f'_c t'_w + \left(\dfrac{\varepsilon_y}{\varepsilon_{cu}}\right)\sigma_y t_p + 2\left(1 - \dfrac{\varepsilon_y}{\varepsilon_{cu}}\right)\sigma_y t_p} \tag{2.29}$$

With c_{cf} determined, ϕ_{cf} is calculated and then θ_{cf}, which is a rigid body rotation of the wall along H_{cr}, is determined using the following equation:

$$\theta_{cf} = \phi_{cf} H_{cr} \tag{2.30}$$

This rotation applied to the entire height, H_w, to determine a roof deflection, $\Delta_{cf,go}$. This is used in Eqn. 2.25 to determine the overall lateral drift at the ultimate condition.

Though not specifically required for the calculation of base shear or lateral drift at the CF limit state, the compressive resultants at this stage are used throughout the design and are explicitly included here:

$$C_{C1} = \alpha \beta f'_c t'_w c_{cf}$$

$$C_{C2} = \frac{1}{2}\left(\frac{\varepsilon_y}{\varepsilon_{cu}}\right)\sigma_y t_p c_{cf}$$

$$C_{C3} = \left(1 - \frac{\varepsilon_y}{\varepsilon_{cu}}\right)\sigma_y t_p c_{cf}$$

with respective moment arms about point O, as seen in Figure 2-16 of:

42

$$d_{CC1} = \frac{\beta c_{cf}}{2}$$

$$d_{CC2} = \left(1 - \left(\frac{2}{3}\frac{\varepsilon_y}{\varepsilon_{cu}}\right)\right)c_{cf}$$

$$d_{CC3} = \frac{1}{2}\left(1 - \frac{\varepsilon_y}{\varepsilon_{cu}}\right)c_{cu}$$

2.7   Comparison of Panel Design Options

2.7.1   Input Parameters for Panel Design Comparison

In order to select a panel design option, predictions were made using the previously described equations. The input parameters used for the predictions are presented in Table 2-2, Table 2-3 and Table 2-4. The PT steel material behavior is shown in Figure 2-22. The unconfined and confined concrete behavior is shown in Figure 2-23. The assumed elastic-plastic material behavior of the steel confinement plates is shown in Figure 2-24.

2.7.2   Panel Design Comparison Results

Figure 2-25 compares the expected lateral force deformation behavior of the four options for the base panel of the unbonded post-tensioned precast wall system. All three "new" options (i.e., those different than tested by Perez et al. (2004)) exhibit improved base shear capacity. Since the contact zone length becomes smaller during the LLP and CF

stages with any of the three new options, the moment arm between the compressive resultant and the PT steel forces and gravity loads increases, thereby increasing the overturning moment. Assuming the height of the wall is the same, the base shear is equivalently increased.

The three options exhibit similar base shear capacities as seen in Figure 2-25. However, it also clear that they have varying lateral drift capacities. Option 3, using higher strength concrete, shows a drift capacity of approximately 4.5%. This does not reach the goal capacity of 6%. Both the plate confinement and thicker panel options achieve drifts in excess of 6%. The thicker panel option (Option 2) would reach a drift capacity of 8.4% which is larger than the 6.9% drift that the plate confinement option (Option 4) would reach. However, to avoid spalling of the cover concrete at lower drift levels, the plate confinement option was chosen.

Table 2-1 – General Wall Parameters (Perez et al. 2004)

General Wall Parameters (Perez)	Length, l_w	100 in.
	Panel Height	65 in.
	Thickness, t_w	6 in.
	Confined length, l_c	26.875 in.
	$f'c$	8 ksi
	E_c	5098 ksi
	$f'cc$	13 ksi

Table 2-2 - Input Parameters for Comparison - Geometry

Design Option	H_{unb} (in.)	H_{act} (in.)	l_w (in.)	t_w (in.)	t'_w (in.)	t_p (in.)
Option 1	390	284.75	100	6	4.75	-
Option 2	390	284.75	100	12	11	-
Option 3	390	284.75	100	6	4.75	-
Option 4	390	284.75	100	6	6	0.5

Table 2-3 - Input Parameters for Comparison - Panel Material and Confinement Properties

Design Option	f'_c (ksi)	f'_{cc} (ksi)	α	β	σ_{yp} (ksi)
Option 1	8	13.1	0.9	1	-
Option 2	8	13.1	0.9	1	-
Option 3	14	21.9	0.9	1	-
Option 4	6	12.1	0.73	0.88	50

Table 2-4 - Input Parameters for Comparison - Prestress Parameters

Design Option	E_p (ksi)	f_{pi} (ksi)	e_{pi} (in./in.)	e_p (in.)	N (kips)
Option 1	29000	88.5	0.003052	17.25	173.4
Option 2	29000	88.5	0.003052	17.25	173.4
Option 3	29000	88.5	0.003052	17.25	173.4
Option 4	29000	88.5	0.003052	17.25	173.4

West   East

Confined Region   Unconfined Region   Confined Region

t_w PT steel group #1   PT steel group #2   PT steel group #3 l_c

l_w
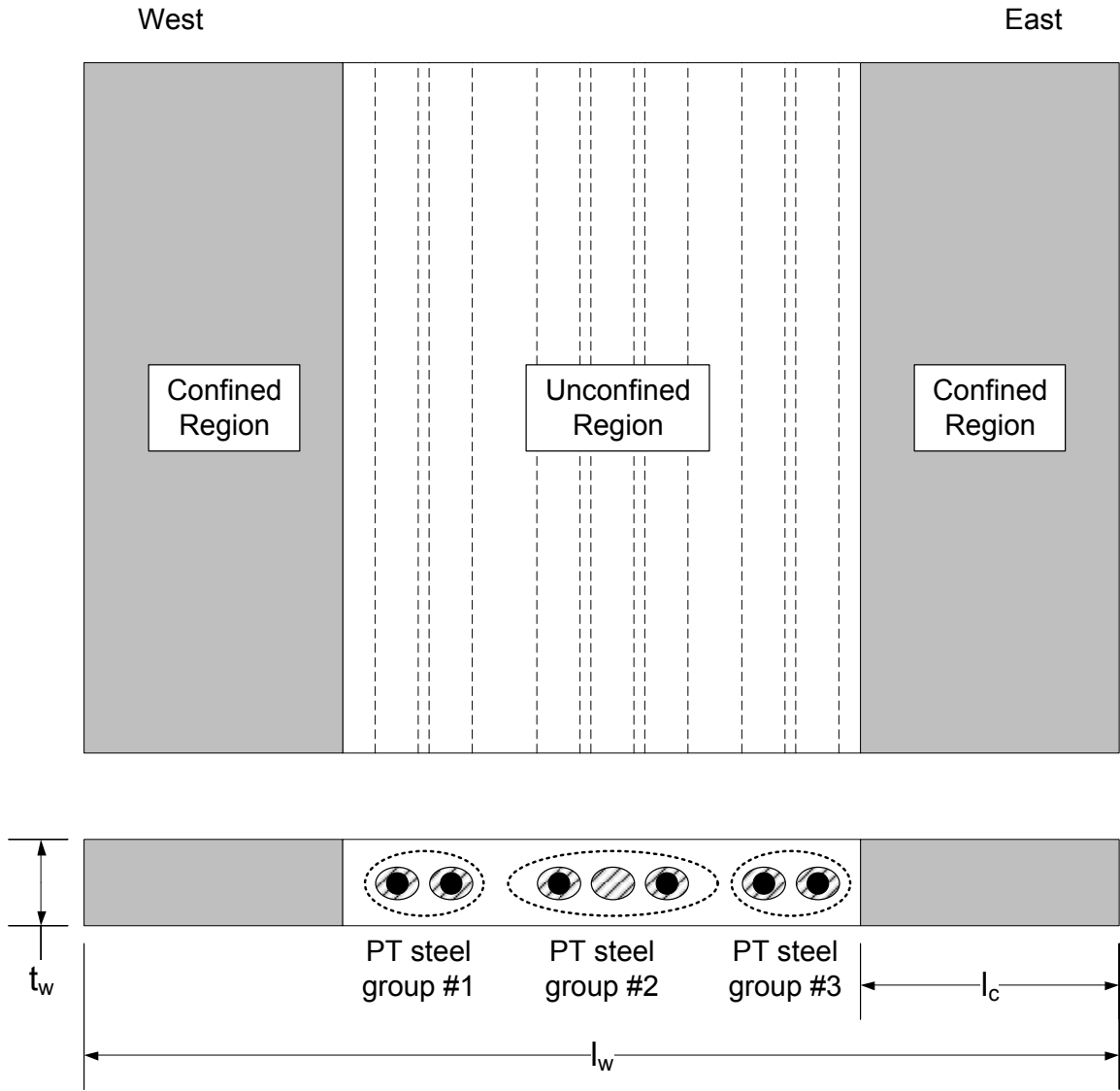
Figure 2-1 – Elevation and Section Schematics of First-story Panel (Perez et al. 2004)

Figure 2-2 - Rebar Cage from Hoop-Confined Panel (Perez et al. 2004)

West   East

Confined Region   Unconfined Region   Confined Region

t_p

t_w

PT steel group #1   PT steel group #2   PT steel group #3

l_c

l_w
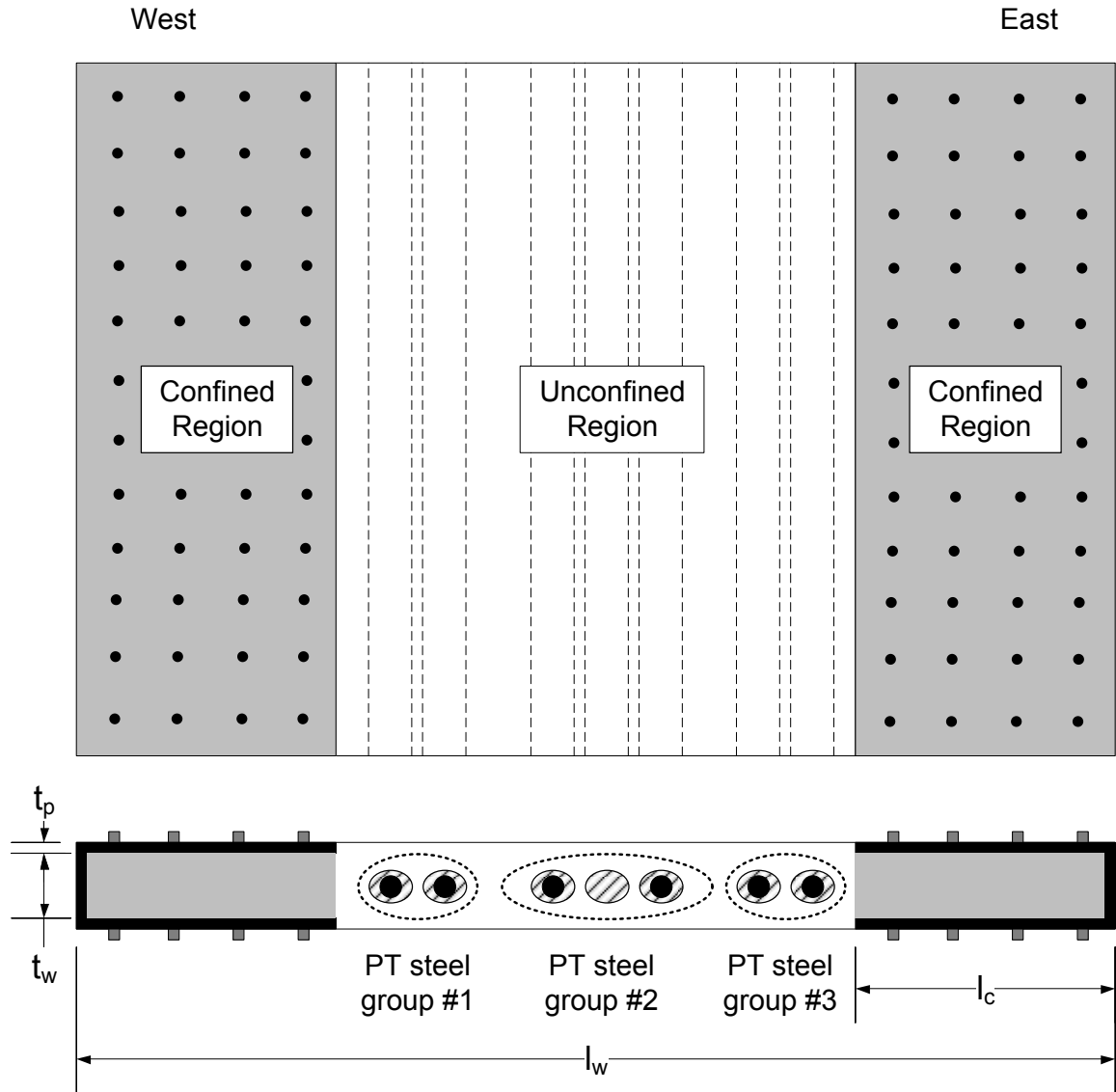
Figure 2-3 – Elevation and Section Schematics of Plate-confined Panel Design
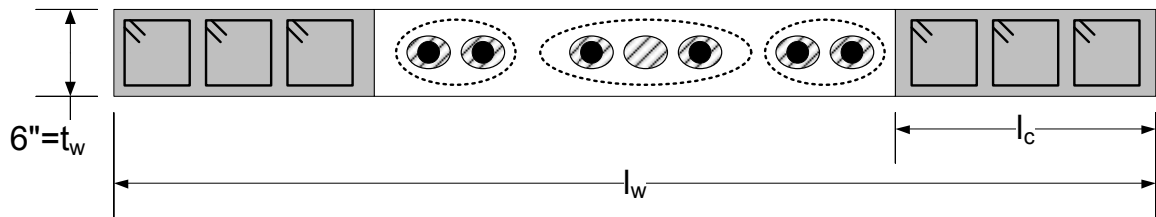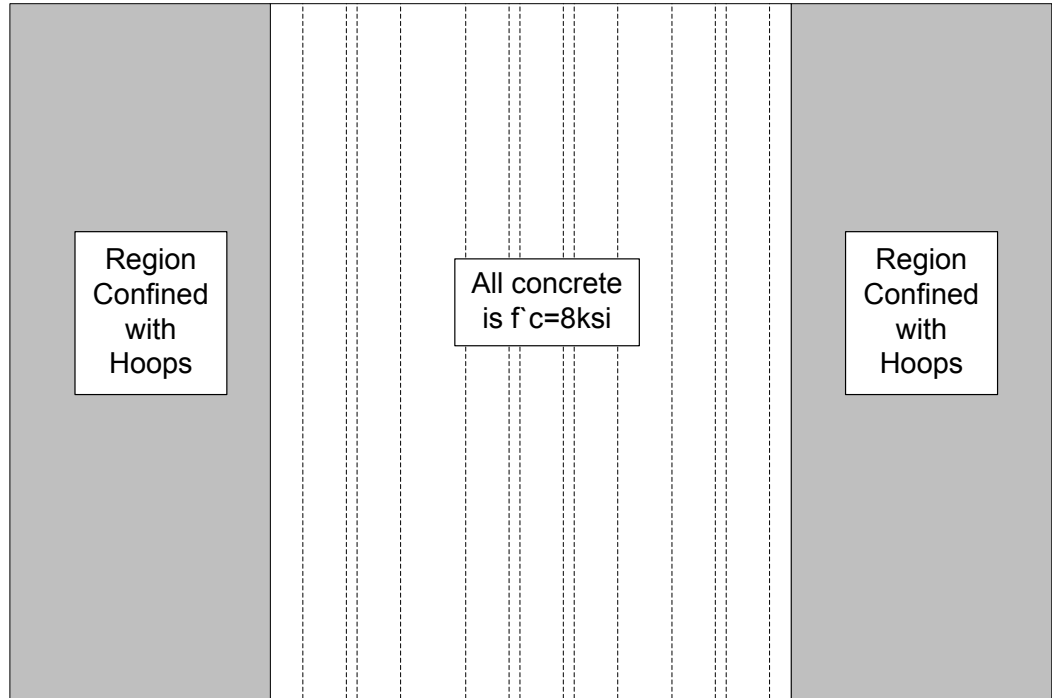
Figure 2-4 - Panel Design Option #1 – Base Case

Region
Confined
with
Hoops

All concrete
is f`c=8ksi

Region
Confined
with
Hoops

12"=t_w

l_c

l_w
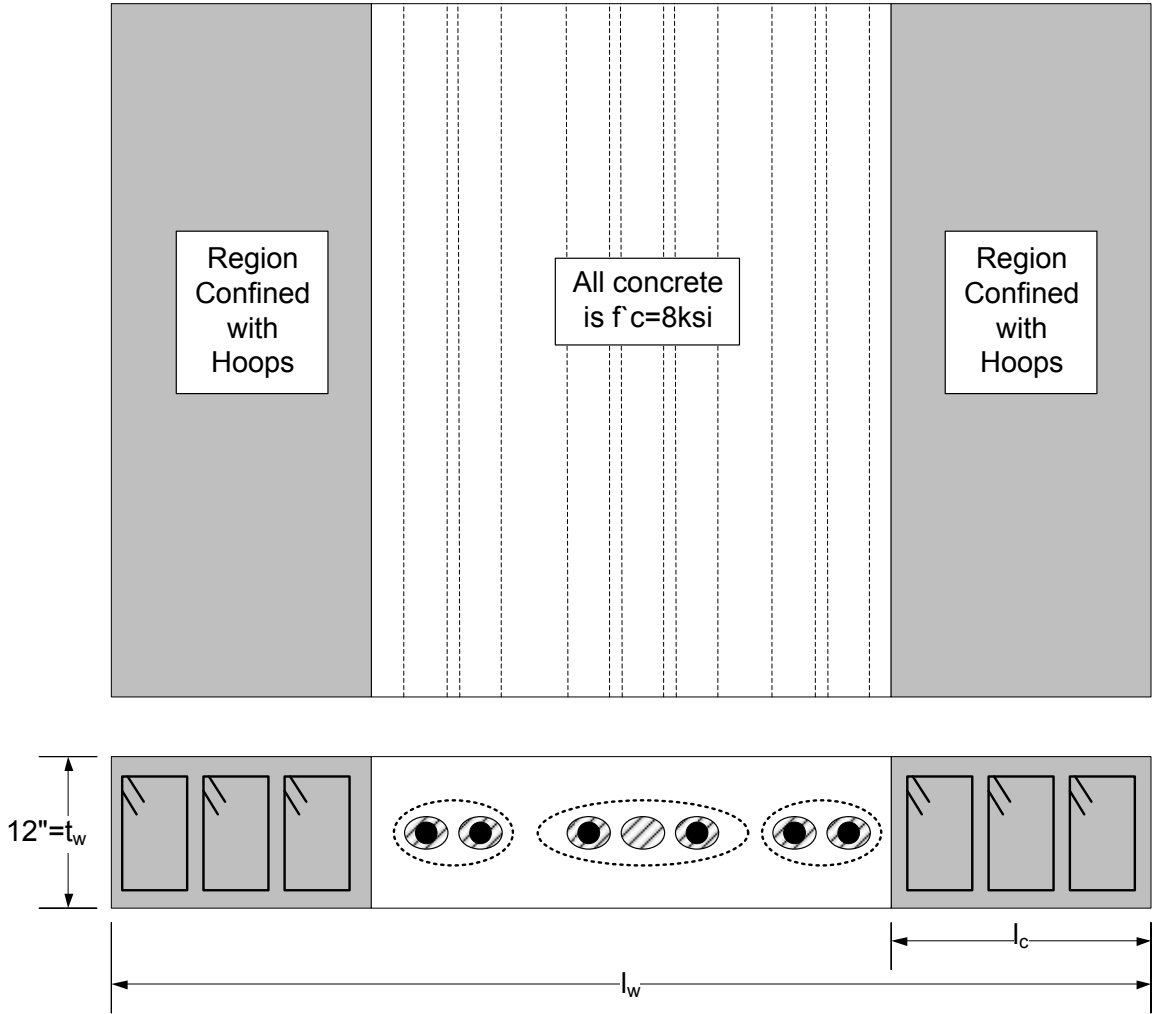
Figure 2-5 - Panel Design Option #2 - Thicker Panel
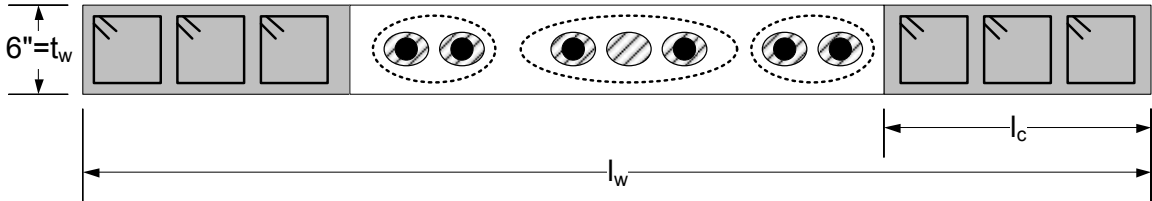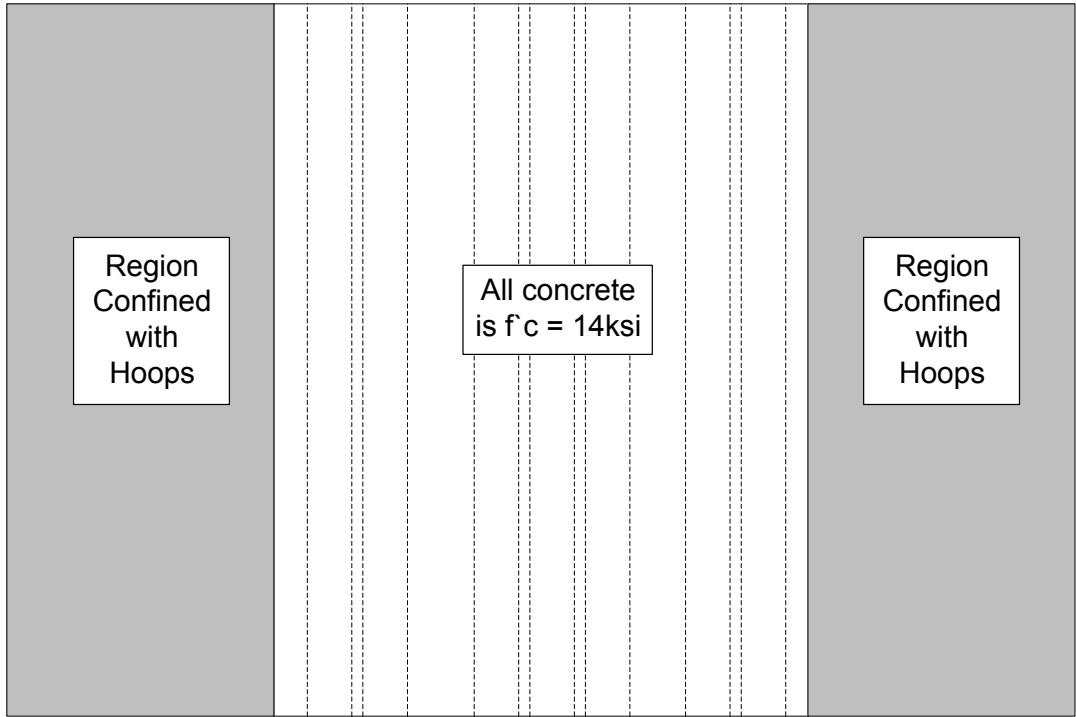
Figure 2-6 - Base Panel Option #3 - High Strength Concrete
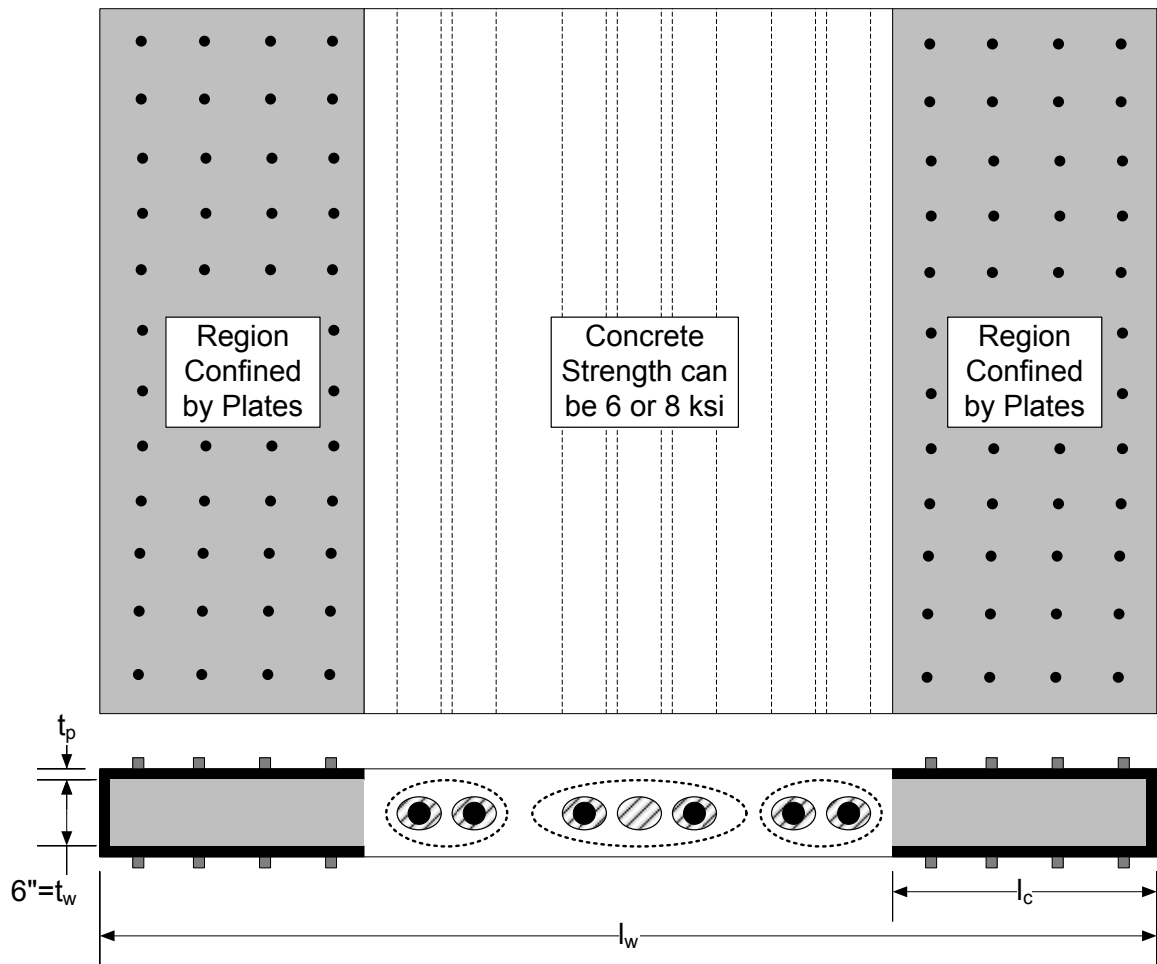
Figure 2-7 - Base Panel Option #4 - Plate-confined
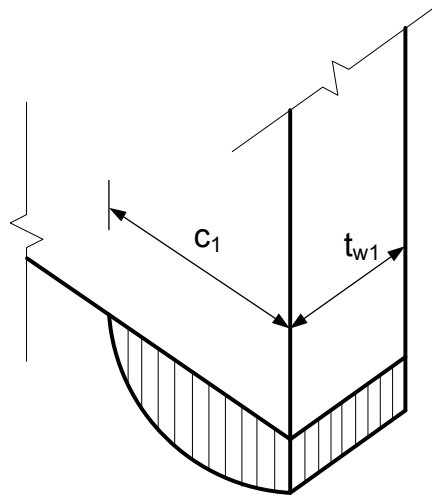
(a) Base Case
Panel

$f'_{c2} = f'_{c1}$
$t_{w2} > t_{w1}$
$c_2 < c_1$

(b) Thicker Panel

Figure 2-8 – Stress Distributions at the Base of the Panel Options

$f'_{c3} > f'_{c1}$
$t_{w3} = t_{w1}$
$c_3 < c_1$
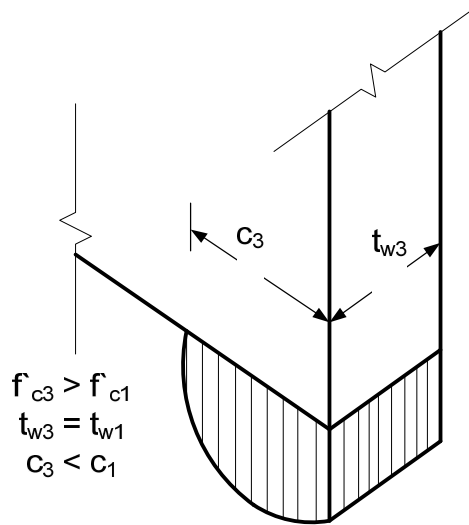
(c) Higher Strength
Concrete Panel

$f'_{c4} = f'_{c1}$
$t_{w4} = t_{w1}$
$c_4 < c_1$
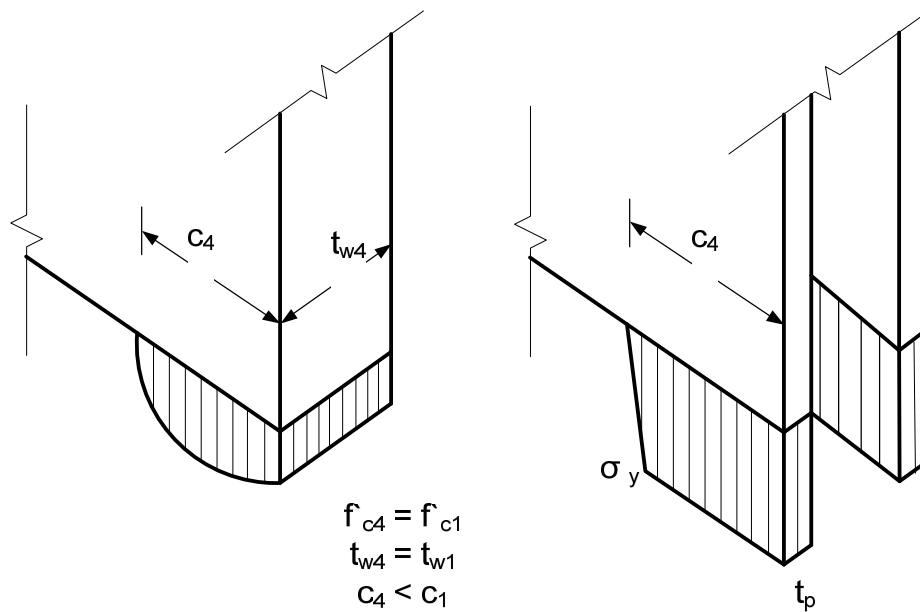
) ᵔ ᶦte-confined Panel

Figure 2-8 – Stress Distributions at the Base of the Panel Options (Continued)
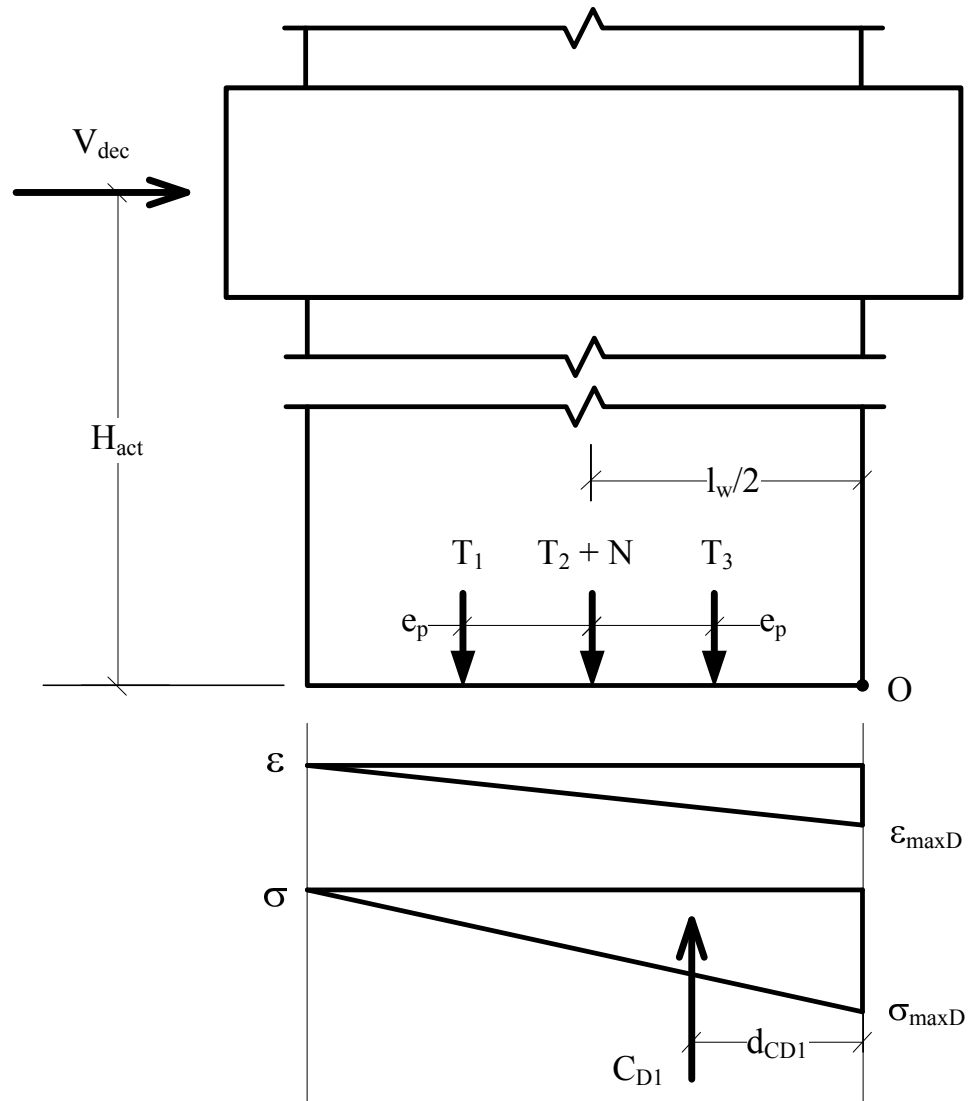
Figure 2-9 – Equilibrium at DEC for Options 1, 2, and 3

56
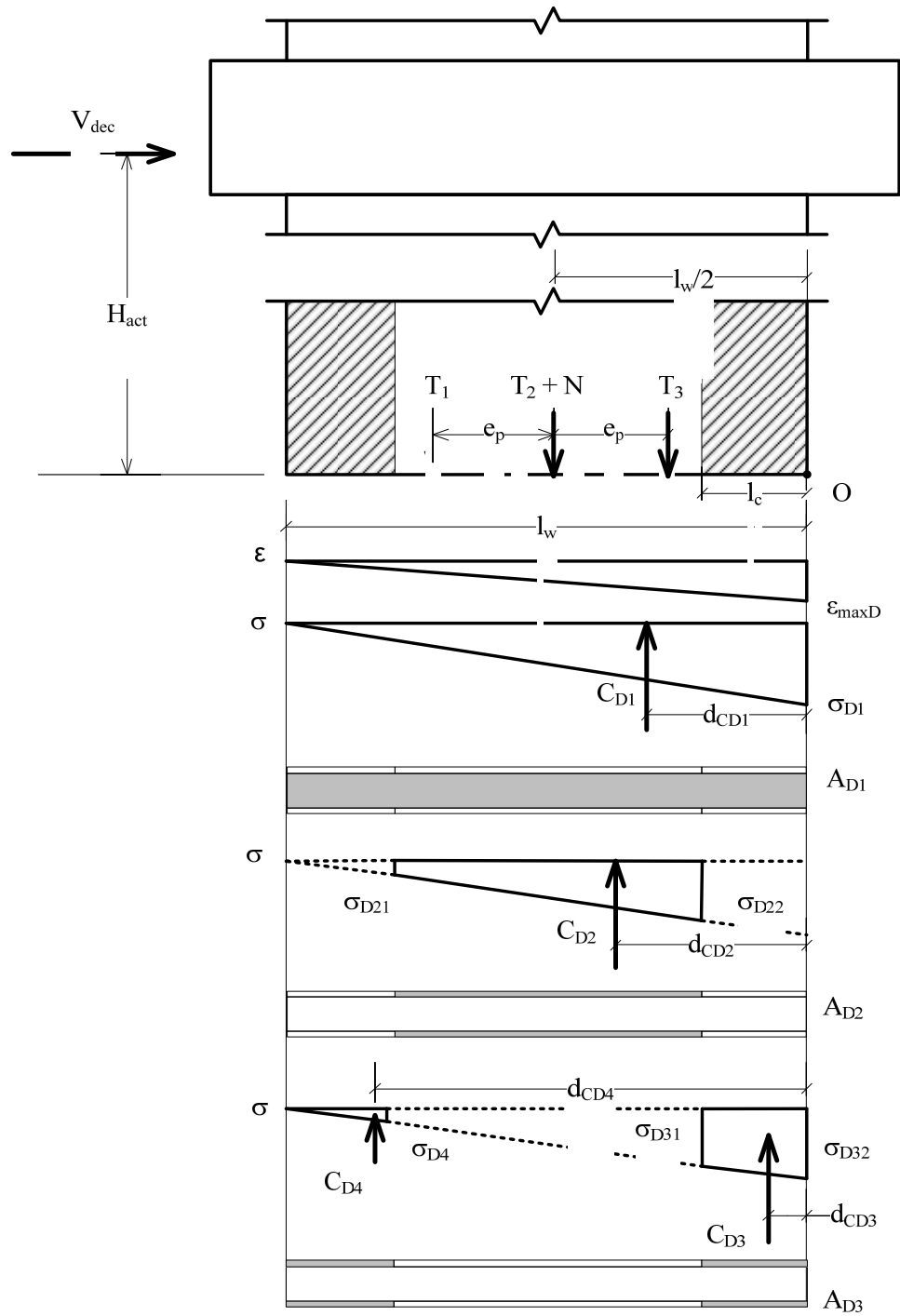
Figure 2-10 – Equilibrium at DEC for Option 4
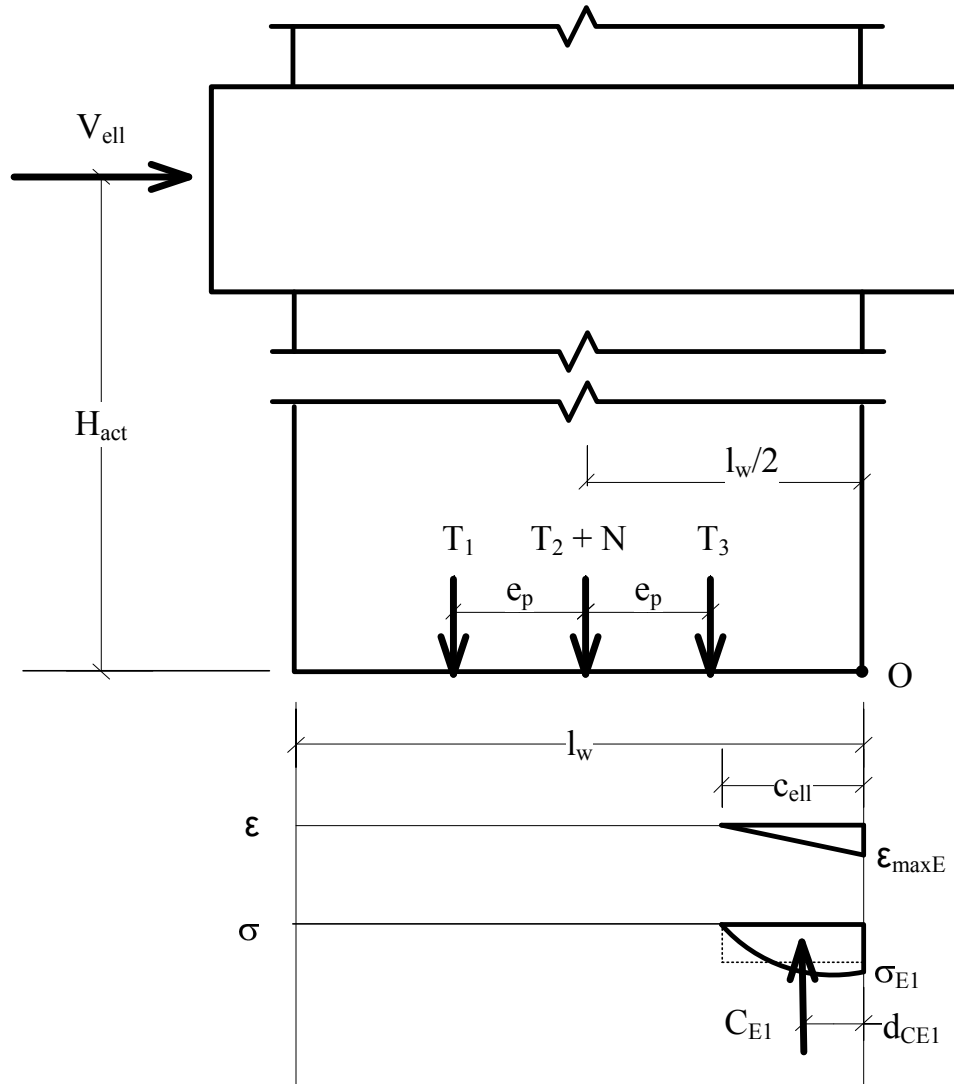
Figure 2-11 – Equilibrium at ELL for Options 1, 2, and 3

58
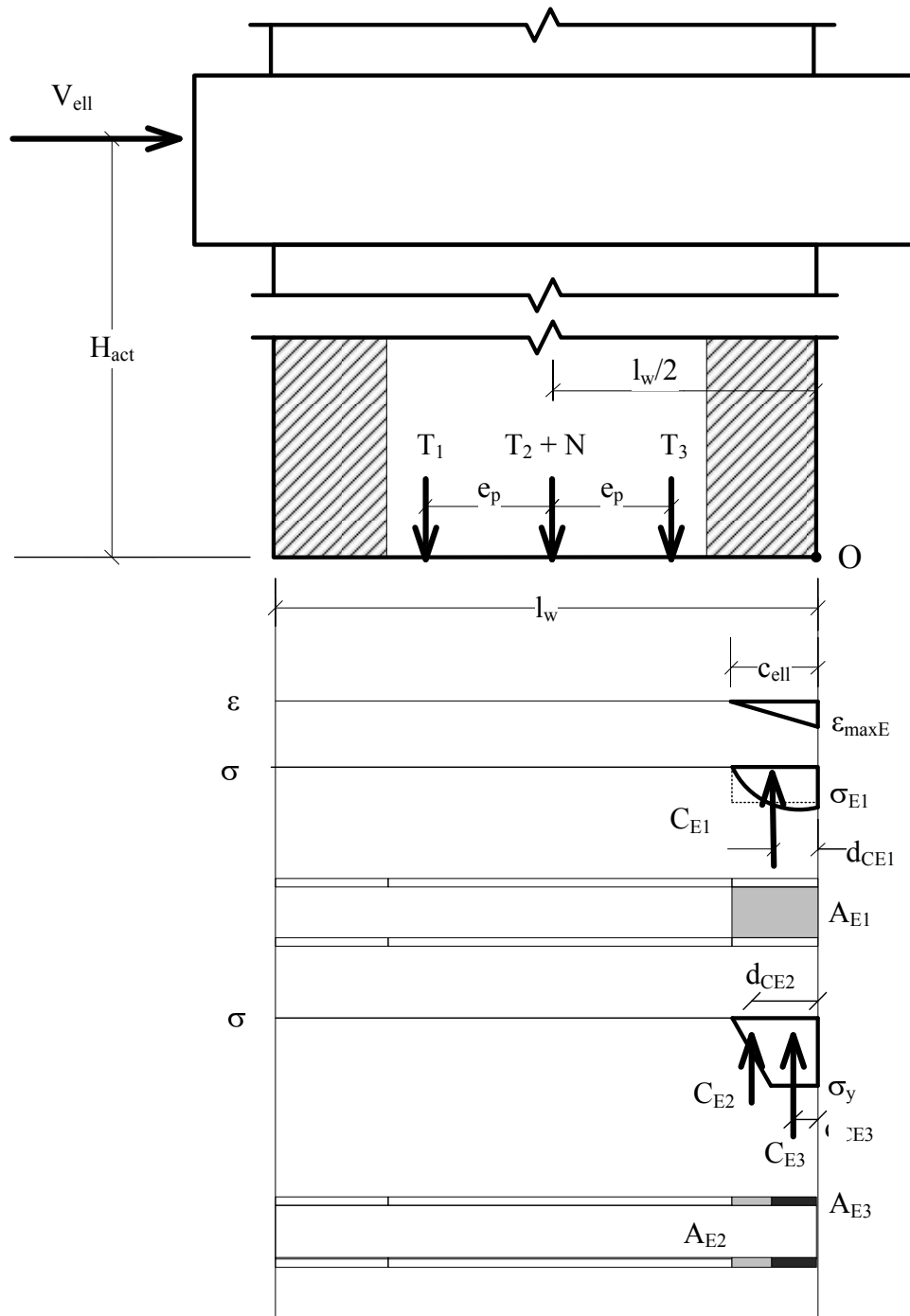
Figure 2-12 – Equilibrium at ELL for Option 4
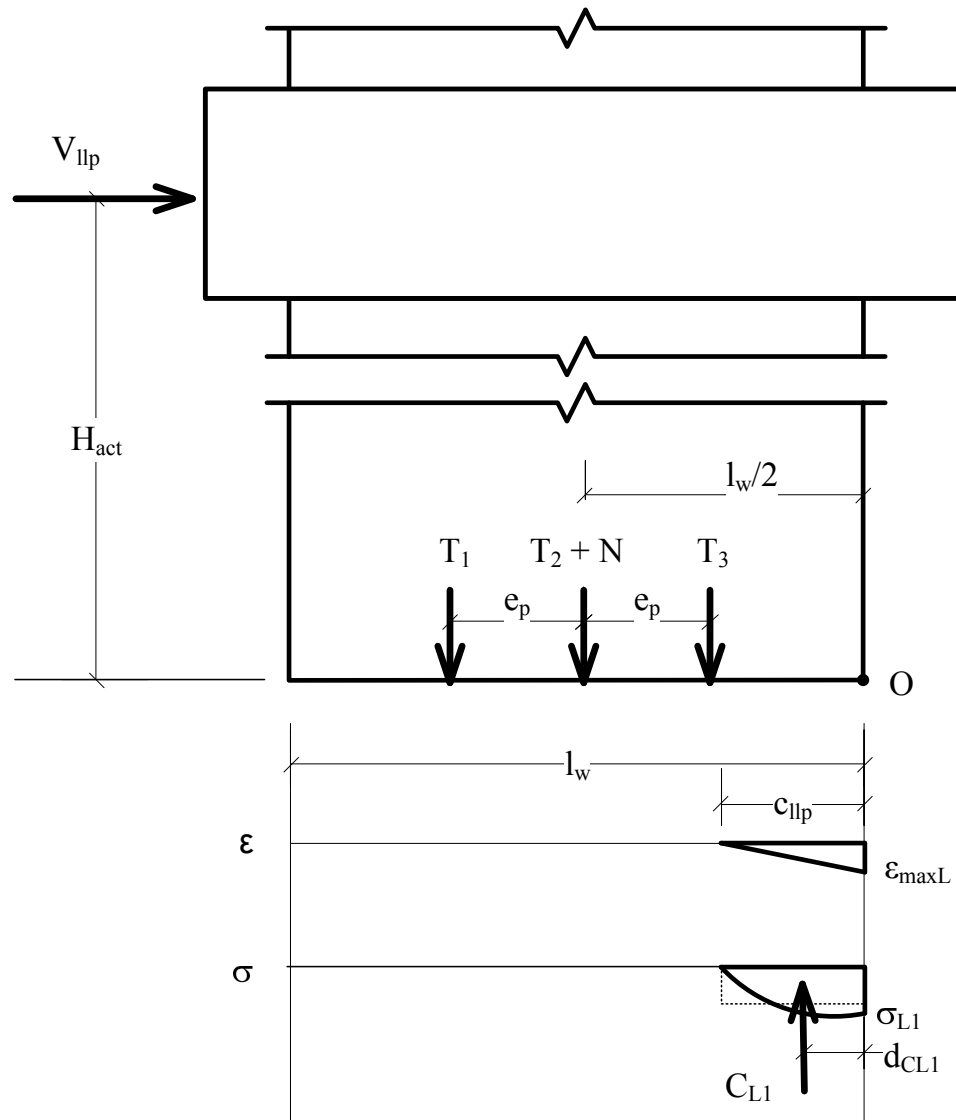
Figure 2-13 – Equilibrium at LLP for Options 1, 2, and 3
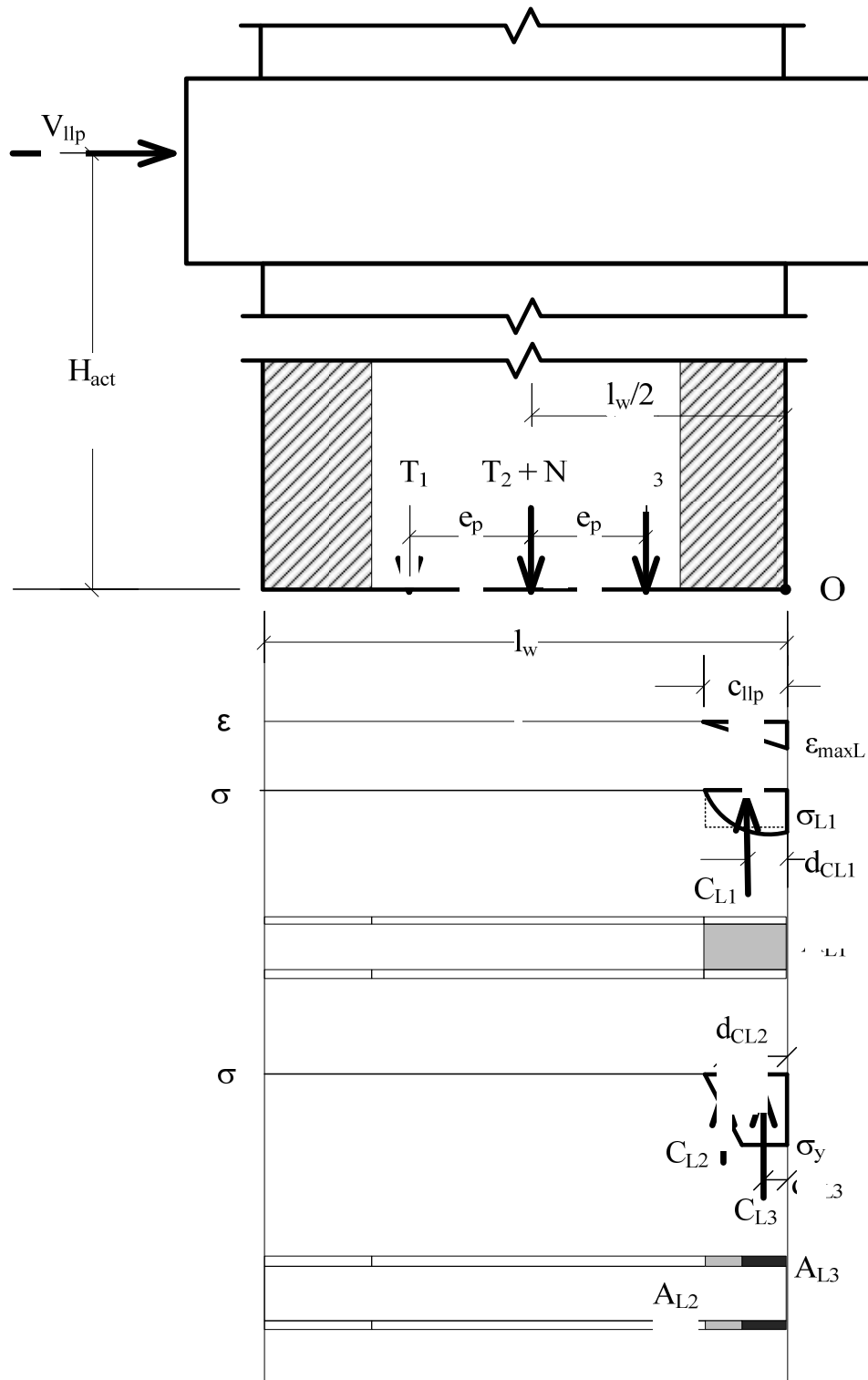
Figure 2-14 –Equilibrium at LLP for Option 4
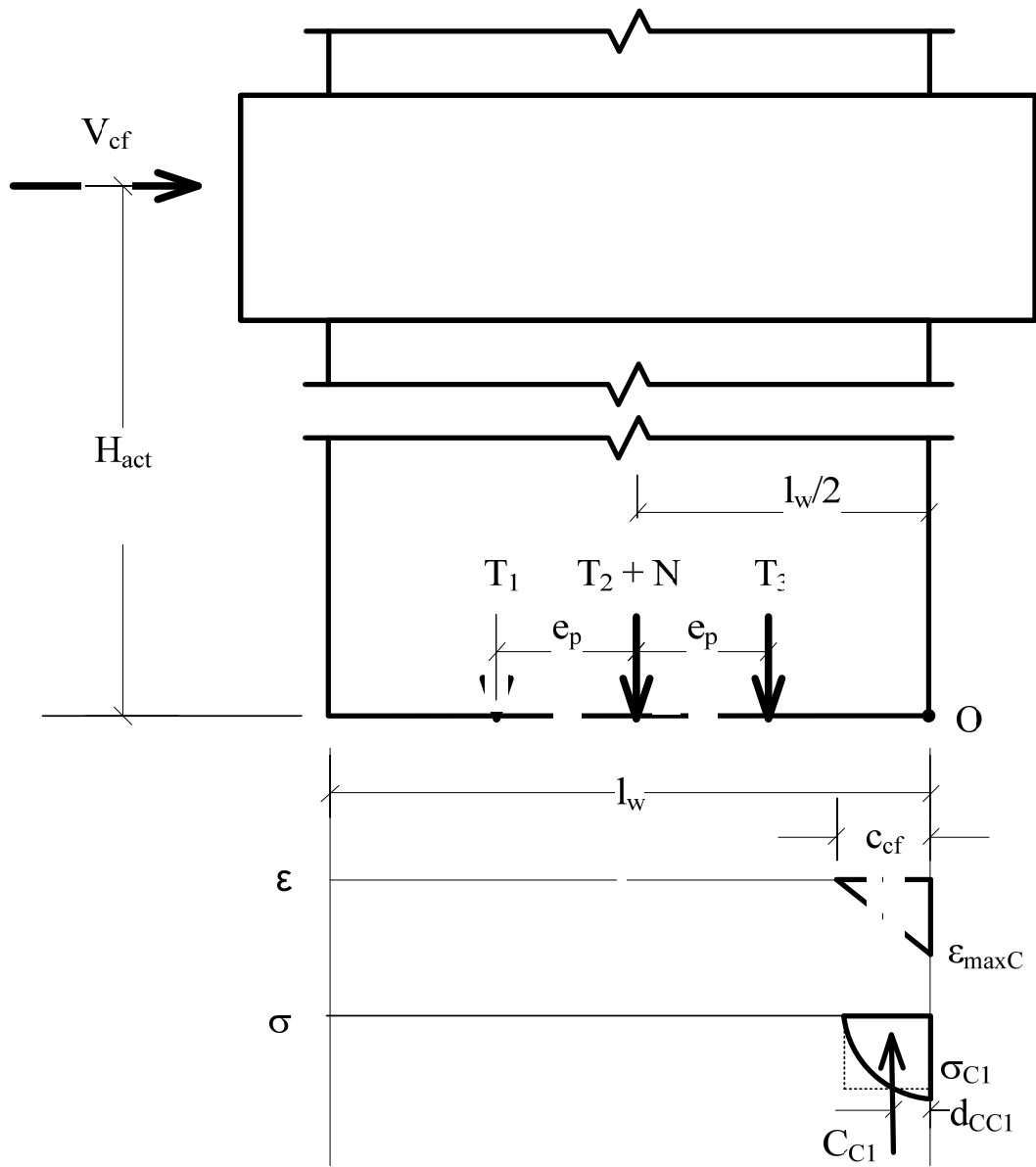
Figure 2-15 – Equilibrium at CF for Options 1, 2, and 3

Figure 2-16 – Equilibrium at CF for Option 4

Shear wall with Force at some level, i | Curvature when $I_1 = I_0$ | Curvature when $I_1 \neq I_0$
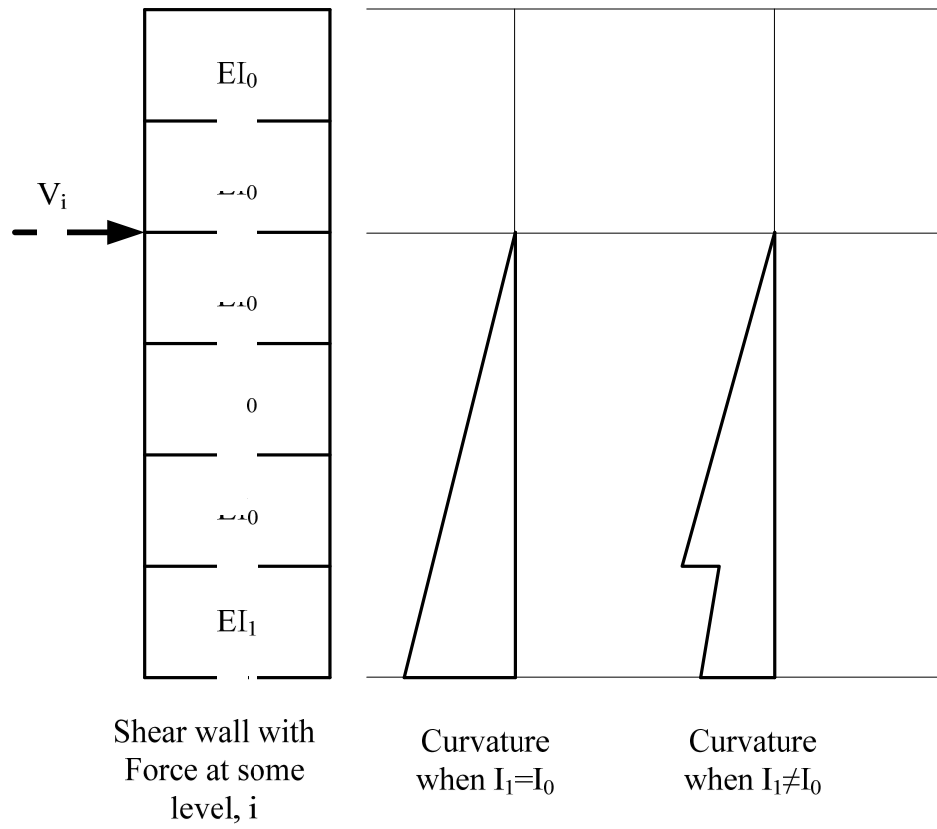
Figure 2-17 – Schematic of Curvature Change due to Different Panel Cross-Section Properties
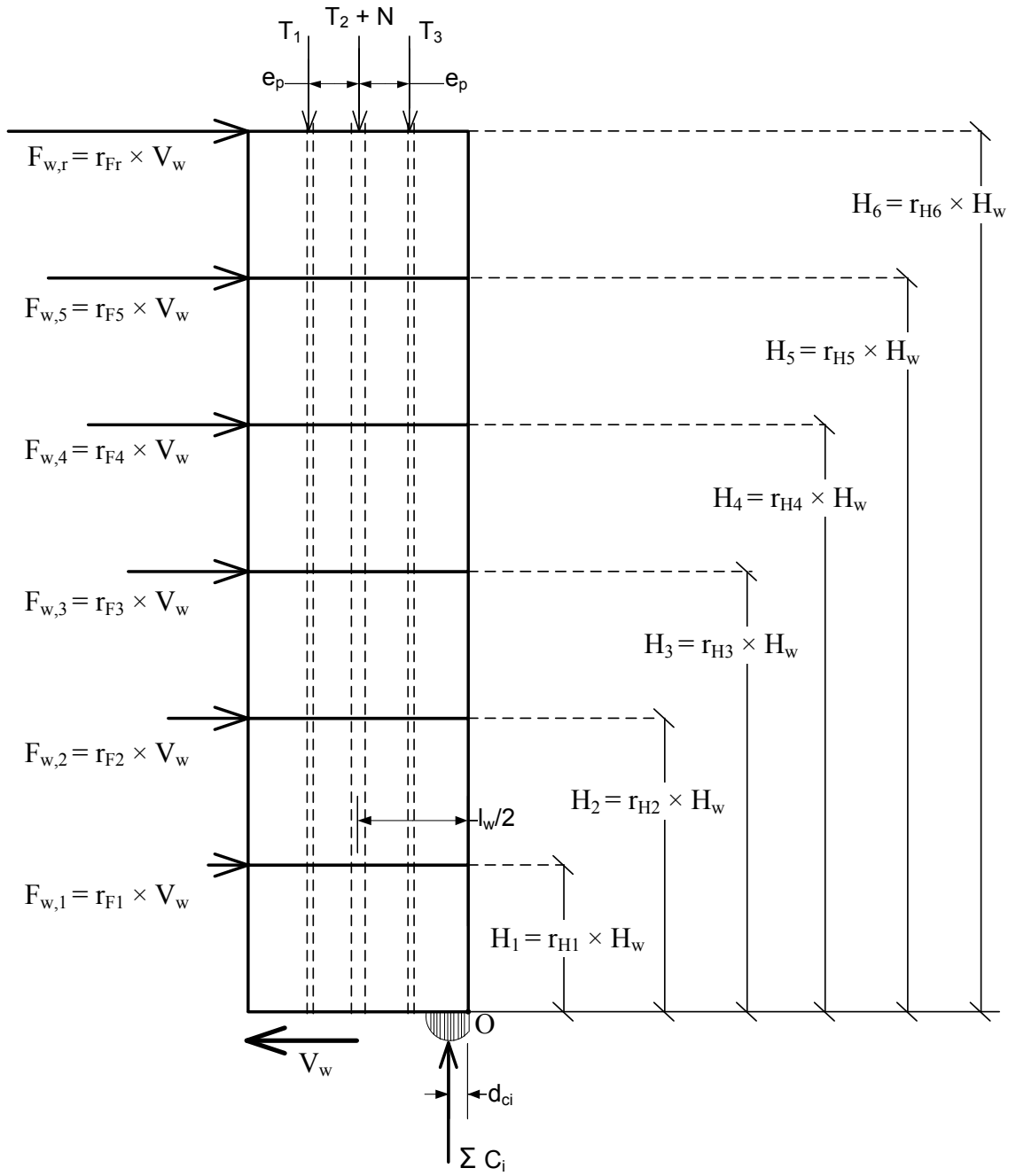
Figure 2-18 - Scaled Prototype Wall Geometry

65
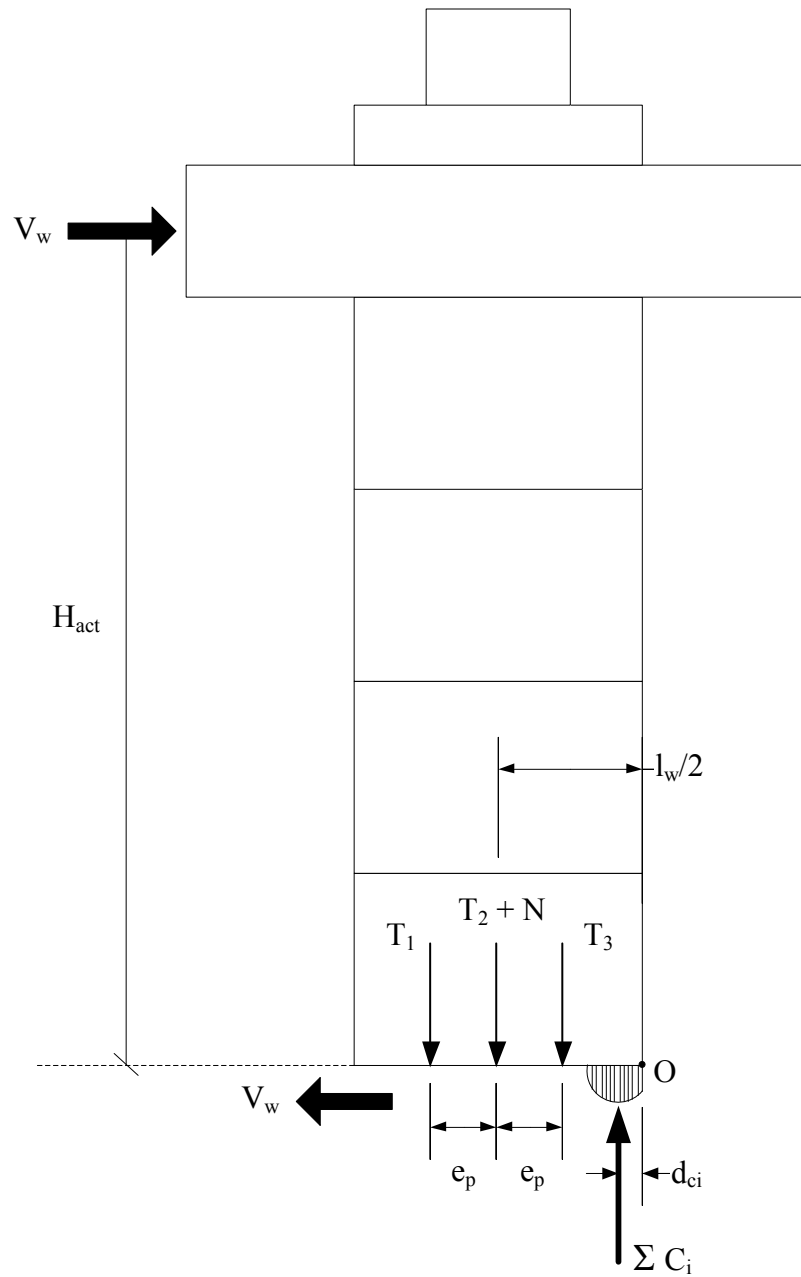
Note: The number, location and magnitude of the compressive resultants depends on the panel option

Figure 2-19 - Experimental Test Setup used for Derivation of Predictive Expressions
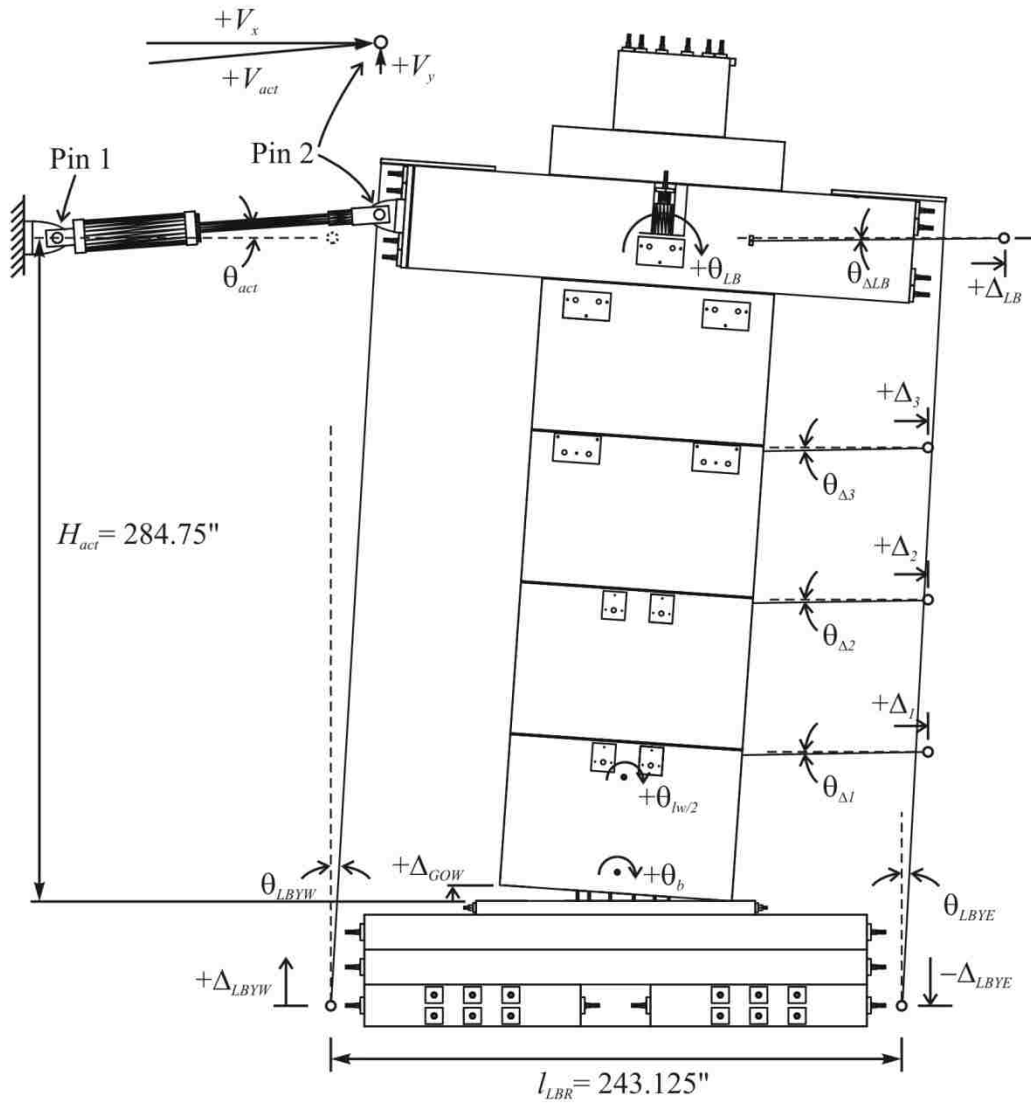
Figure 2-20 – Global Sign Convention (Perez et al. 2004)

67
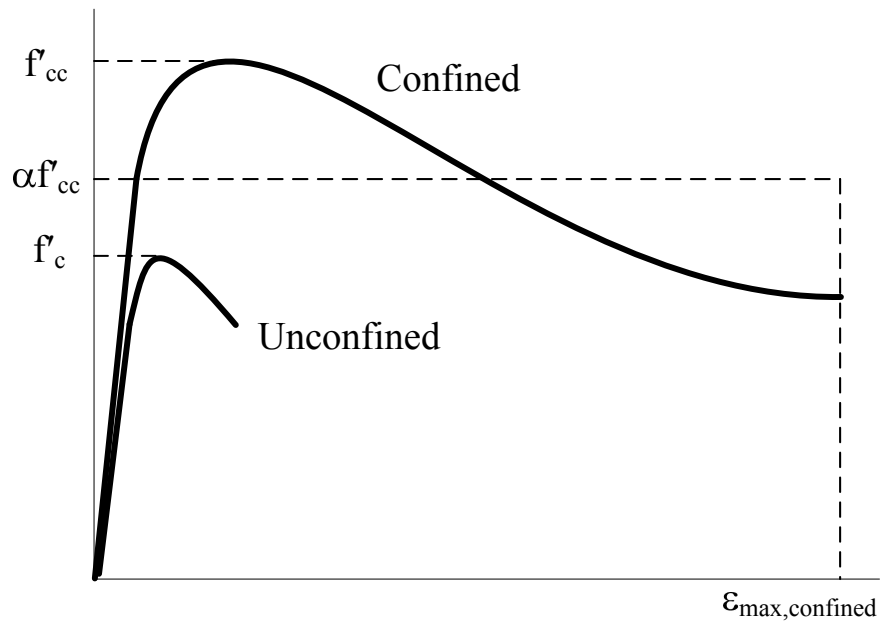
Figure 2-21 – Schematic of Stress-Strain Behavior for Unconfined and Conﬁned Concrete
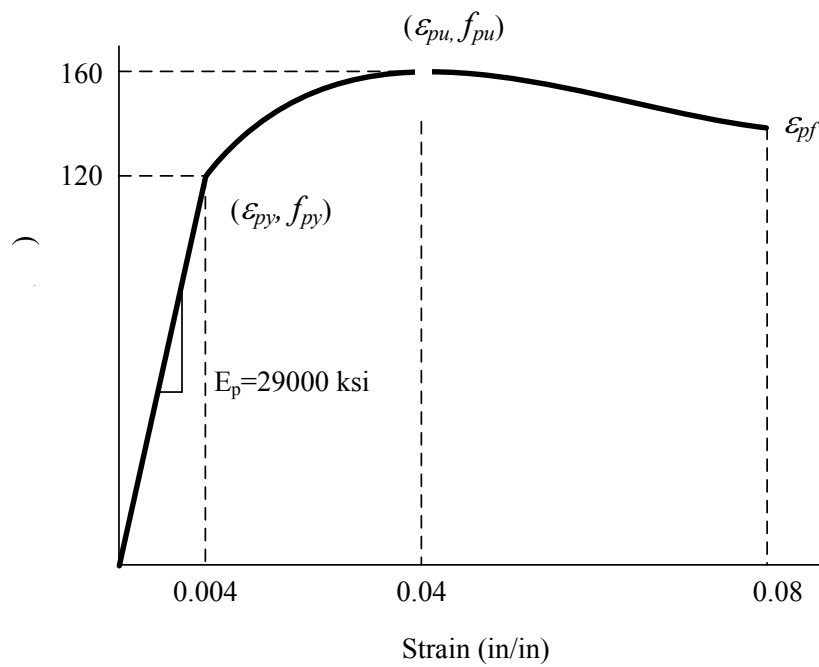
Figure 2-22 - PT Stress-Strain Relationship (Perez et al. 2004)

68
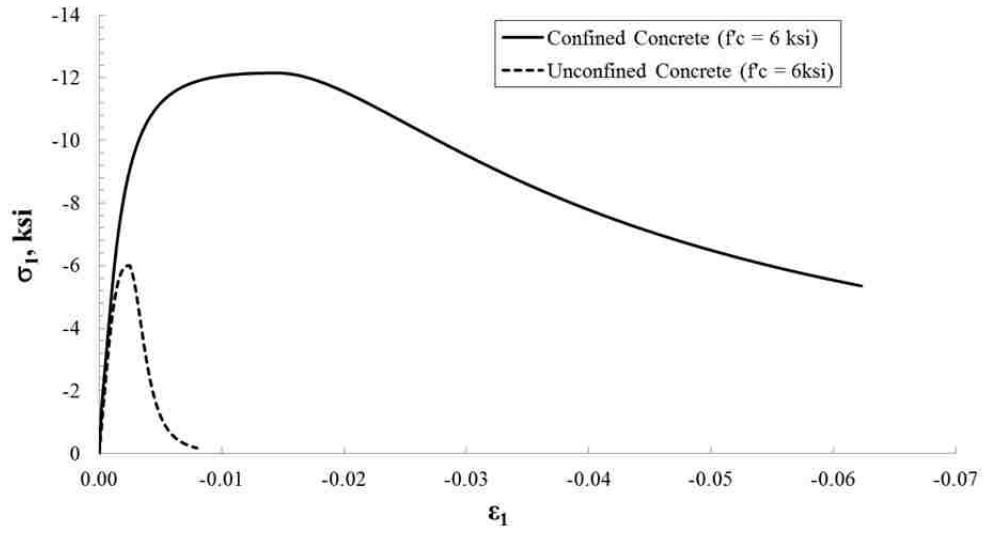
Figure 2-23 - Confined and Unconfined Behavior of 6 ksi Concrete

50

$(\varepsilon_{py}, f_{py})$

$E_p = 29000$ ksi

0.001724

Strain (in/in)
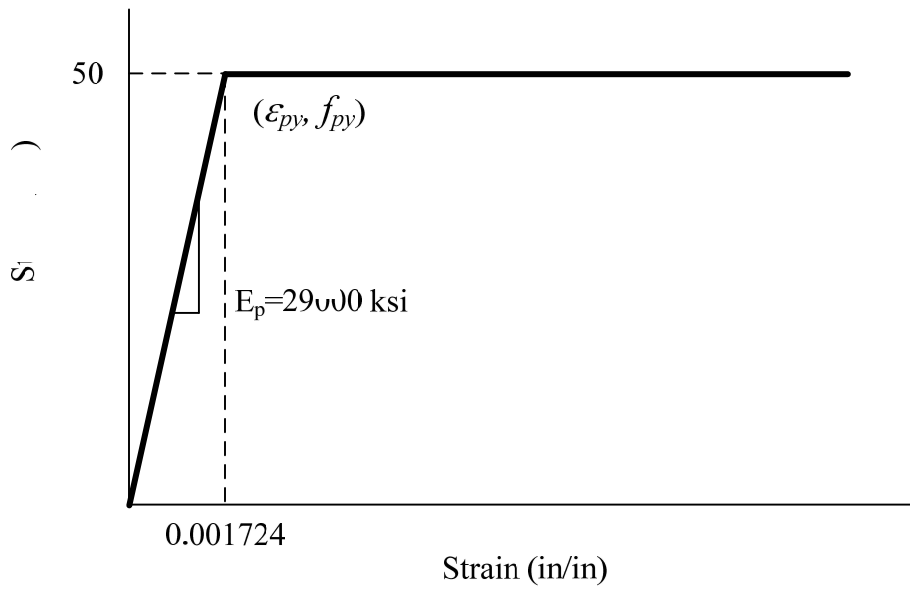
Figure 2-24 - Assumed Elastic-Plastic Material   ior of Steel Confinement Plates
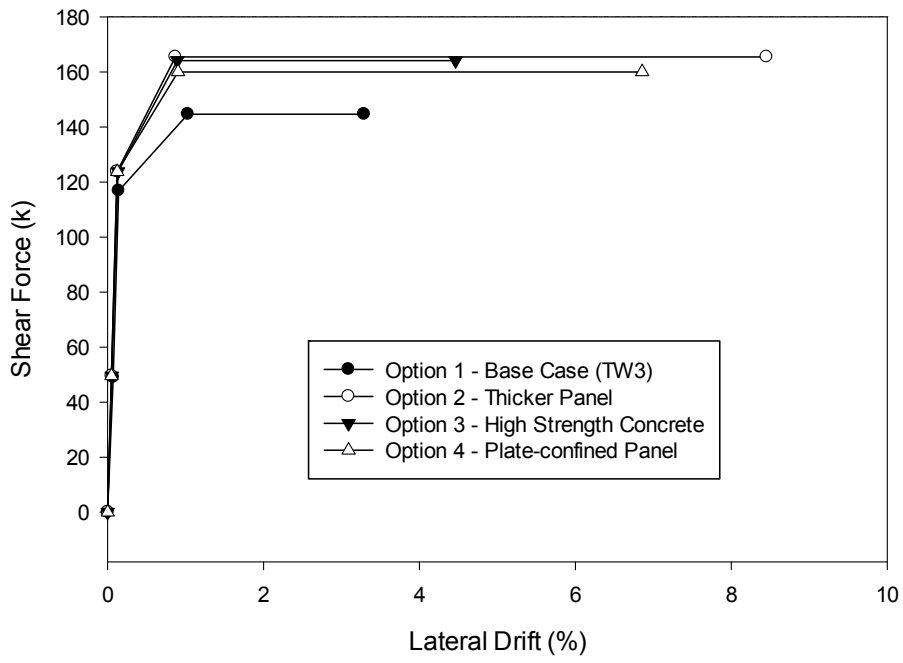
Figure 2-25 – Comparison of Analytical Results for Different Panel Design Options

3 Plate-Confined Wall Panel Analysis and Design

3.1 Introduction

This section describes the analysis and design process for a plate-confined wall panel. Section 3.2 provides a summary of the performance of TW3 and TW5 from Perez et al. (2004). Section 3.3 presents the goals for performance of the wall panel in relation to previous work. Section 3.4 describes the basis of design which is comprised mainly of parameters which have been kept constant from Perez et al. (2004). Section 3.5 describes assumptions made in order to define the ultimate limit state for a plate-confined wall panel. Section 3.6 describes the design process of a plate-confined wall panel. Section 3.7 presents the final selected design.

3.2 Summary of Relevant Prior Tests

A total of five tests were conducted by Perez et al. (2004). The first two, TW1 and TW2, used spiral reinforcement for confinement. TW2 failed via buckling of the confined region, which was undesirable. Therefore, the remaining tests used hoop confinement, which mitigated the buckling failure mode. Of these three tests, TW3 was the base case, TW4 used a reduced initial post-tensioning force, and TW5 used fewer PT bars. Table 3-1 shows the test parameters for these three wall panels. Table 3-2 shows the performance levels of these three wall panels in terms of lateral drift and base shear

71

capacity. From these results, performance targets are established for the plate-confined wall panel.

3.3   Performance Targets

This section explains the selection of targets for the performance of the selected plate-confined wall panel design option. Perez et al. (2004) tested five walls. TW3 had a base shear capacity of approximately 140 kips and TW5 had a drift capacity that exceeded 6% as shown in Table 3-2. The base shear of 140k and drift capacity of 6% were not achieved in the same test wall. The main performance target for the present work is a wall that achieves 6% or greater drift, while maintaining or exceeding a base shear capacity of 140 k. Qualitatively, a second performance target is to delay cover concrete spalling to a level of drift beyond the level observed by Perez et al. (2004), approximately 1% drift. Ideally, spalling would be eliminated altogether.

3.4   Basis of Design

This section lists the parameters of the wall design that remain unchanged with the use of Option 4. Recall that the overall wall thickness is 7 inches, which is thicker than the walls tested by Perez et al. (2004). The post-tensionsing steel parameters of A_p and f_{pi} are taken from TW3.

3.5 Ultimate Limit State Assumptions

This section highlights several assumptions made in order to define the ultimate limit state for the plate-confined wall panel. Perez et al. (2004) found the failure state of the wall panels to be crushing of confined concrete. This occurred when the confinement steel fractured. For a plate-confined wall with bolts providing the confinement force, the equivalent limit state would be bolt fracture. A325 bolts are used to provide the confinement force. Pretensioned, the ultimate limit state, compression failure, is controlled by the change in strain of the bolts between the pretension strain and the ultimate bolt strength. Figure 3-1 shows a stress-strain curve for an A325 bolt. The strain at pretension and the strain at ultimate strength are marked on the plot. The difference is the allowable change in strain used to define the ultimate limit state.

3.6 Design of Plate-Confined Wall Panel

This section describes in detail the process of designing a plate-confined wall panel. A model for confined concrete by Oh (2005) is used to model both the confined and unconfined concrete of the wall panel. This model plays an important role in the design process. The most important parameter in the Oh model for confined concrete is the confinement ratio, ϕ_c. The confinement ratio, in conjunction with concrete strength, will define the predicted stress-strain behavior of the confined concrete. Figure 3-2 shows an overview of the design process starting from base design presented in Section 3.3.

3.6.1 Unconfined Concrete Strength

There were two options for concrete strength considered for the wall panel design; 6 ksi or 8 ksi. Perez et al. (2004) used 8 ksi concrete for TW3 and TW5, but because the lack of ductility of the confined higher strength concrete was a concern, 6 ksi was considered. Figure 3-3 shows the stress-strain behavior of the 6 ksi and 8 ksi concrete with the confining ratio, ϕ_c equal to 0.25. The behavior of the 8 ksi concrete after reaching the peak concrete stress is less desirable than that of the 6 ksi concrete. At a given value of strain, the higher strength concrete loses a comparatively larger percentage of its peak stress. The selection of concrete strength is presented in Section 3.7.

3.6.2 Bolt Design Parameters

For the initial design of the plate-confined wall panel, a uniform spacing of A325 bolts was selected based on the confinement requirements at the base of the wall. The bolts are assumed to be tensioned to the AISC-specified values for a fully pretensioned bolt (AISC 2005). The two bolt design parameters are the bolt spacing and the bolt diameter.

3.6.3 Plate Design Parameters

The three plate design parameters chosen are the thickness, t_p, the length, l_c and the yield stress, σ_y. The plate length, l_c, is the horizontal dimension along the length of the wall.

The plate height is taken as the height of the first story wall panel. The thickness of the plate is determined by two factors; the out of plane bending of the plate due to dilation of the concrete, and the percentage of the total compressive force at the base of the wall carried by the plate. In the design process, the plate thickness was selected and plate bending and compressive stresses were checked after the design was complete. The length, l_c, corresponds to the confined length from Perez et al. (2004). l_c was usually around 25% of the wall length, though it was minimized where possible to decrease the weight of the plates.

3.6.4 Confining Ratio

Considering the values of $f'c$ described in Section 3.6.1 and the bolt design parameters described in Section 3.6.2, a confining ratio can be calculated. Figure 3-4 shows a bolt and the tributary area of concrete confined by the bolt, A_{trib}, based on the bolt spacing. The confining ratio is calculated as follows:

$$\phi_c = \frac{\sigma_{cp}}{f'_c} \tag{3.1}$$

where σ_{cp} is the confining pressure as follows:

$$\sigma_{cp} = \frac{F_{bolt}}{A_{trib}} \tag{3.2}$$

and F_{bolt} is the pretension force in the bolt. The pretension force is specified by the bolt type (A325) and diameter (AISC 2005). Table 3-3 shows values of confining ratio for various bolt diameters, spacings, and concrete strengths.

3.6.5   Confined Concrete Parameters

This section describes the stress-strain behavior of the confined concrete based on Oh's model (Oh 2002). Perez et al. (2004) assumed the confined concrete stress block parameters were constant (α = 0.9; β = 1.0). These parameter values were used in the present study, initially, for evaluating different wall panel options. However, to design the plate-confined wall, more accurate stress block parameter values based on the shape of the stress-strain curve are desired.

To determine these parameters, the stress-strain curve must be integrated over the range of strain expected to occur. The stress-strain curve is integrated numerically using the trapezoidal rule. Figure 3-5 shows a schematic of a stress-strain curve and the corresponding trapezoids used to integrate the area. The area beneath the curve is:

$$A_{Oh} = \sum_{i=1}^{n-1} \frac{\sigma_{i+1} + \sigma_i}{2} \left(\varepsilon_{i+1} - \varepsilon_i \right) = \sum_{i=1}^{n} A_i \tag{3.3}$$

with n equal to the number of stress and strain values. A_i is the area of one trapezoid. The first moment about the point of zero strain (neutral axis of the cross-section) for each trapezoid, shown in Figure 3-6, is as follows:

$$\bar{x}_i = \varepsilon_i + \frac{(\varepsilon_{i+1} - \varepsilon_i)(2\sigma_{i+1} + \sigma_i)}{3(\sigma_{i+1} + \sigma_i)} \tag{3.4}$$

The distance in the x-direction from the origin of the entire area is calculated as follows:

$$\bar{x} = \frac{\displaystyle\sum_{i=1}^{n} A_i \cdot \bar{x}_i}{A_{Oh}} \tag{3.5}$$

Now that the area and centroid of the stress-strain curve are known, the confined concrete stress block parameters can be calculated as follows:

$$\alpha = \frac{f_{avg}}{f'_{cc}} = \frac{A_{Oh}}{f'_{cc}\,\varepsilon_{cu}} \tag{3.6}$$

$$\beta = \frac{2\,\bar{x}}{\varepsilon_{cu}} \tag{3.7}$$

where ε_{cu} and f'_{cc} are the ultimate strain and confined concrete strength, as shown in Figure 3-3.

Note that in order to use this model, confinement has to be provided in all directions. Confinement through the thickness of the panel is provided by the bolts and the plates. Figure 3-7 defines the other directions which require confinement. Vertical confinement (y-direction as indicated in Figure 3-7) is provided by the post-tensioning and gravity forces in the wall. Longitudinal confinement (x-direction as indicated in Figure 3-7) is provided by the steel end plate.

Figure 3-8 shows the final rebar cage in the plate-confined region. The cage is constructed of vertical and horizontal straight bars spaced at approximately 5 inches o.c. The bars are tied with hoops, spaced at approximately 5 inch intervals. The ends of the longitudinal rebars are capped with U-shaped bars, intended to provide nominal confinement. The rebar cage layout is dimensioned in Figure 3-9.

The end plates were designed based on out of plane bending due to the expansion of the concrete. The height of the plate was determined by looking at the strain along the height and determining the point where little confinement is required. The plate, as installed, is shown in Figure 3-10. Description of the design of the end plate is included in Section 3.6.8.

3.6.6 Θ_{cf} and V_{cf}

The calculation of the roof drift at compressive failure (CF) is explained in Section 2.6.8. Here the confined concrete parameters described in Section 3.6.5 are used. The roof drift at CF, Θ_{cf}, is compared to the performance target of 6% and if the target is met, then the

base shear capacity is calculated. If the target is not met, then the design process is started over with variations to parameters chosen in Sections 3.6.1 through 3.6.3.

The calculation of V_{cf} is explained in Section 2.6.7. Note that V_{cf} is equivalent to V_{llp} as described in Section 2.6.5. The value obtained for base shear capacity is compared to the performance target of 140 kips and if the target is met, then the design is a viable option.

3.6.7   Plate Slip Limit State

A major assumption of the design calculations for a plate-confined wall panel is that bolts through the wall are loaded only in tension, and the bolts are not in shear and bearing against the steel plates. To satisfy this assumption, the friction between the plates and the concrete wall must be adequate to transfer the load applied to the plates. Figure 3-11 shows a free body diagram of the end of the wall in compression. The view is from the end of the wall. The friction force depicted carries shear between the plates and the concrete. This shear must be in equilibrium with the compression resultants at the base of the plates. The design of the bolts is based on the AISC eccentric bolt group analysis (AISC 2005). Figure 3-12 shows a schematic of the forces applied to each bolt. Every bolt is assumed to carry an equal percentage of the direct shear force, and a portion of the induced moment (from eccentricity, *e,* as shown in Figure 3-12) based on the distance from the bolt to instantaneous center of rotation (ICR). The ICR is at the location of the compressive resultant. The total steel compressive resultant on a single plate is determined as follows:

$$C_{steel} = \sum_{j=2}^{3} \frac{C_{X_j}}{2}$$

(3.8)

These expressions are generalized for any load stage. The subscript, X, refers to DEC, ELL, LLP or CF. The forces will be most critical in the CF stage so this stage is used for design at the plate-slip limit state. The expressions for these forces are shown in Section 2.6.8. The eccentricity of the steel compressive resultant relative to the centroid of the bolt group is calculated using Figure 3-13. The eccentricity between the bolt group and the compressive force is:

$$e_C = \overline{B} - \overline{D}$$

(3.9)

The location of the compressive resultant relative to the corner wall is determined as follows:

$$\overline{D} = \frac{\sum_{j=2}^{3} C_{X_j} \cdot d_{X_j}}{\sum_{j=2}^{3} C_{X_j}}$$

(3.10)

where C_{Xj} and d_{Xj} are the magnitude and location of the steel compressive resultants from point O as seen in Figure 2-10, Figure 2-12, Figure 2-14 and Figure 2-16, depending on the limit state. Similarly, the centroid of the bolt group is located using the distances indicated schematically in Figure 3-14 as follows:

$$\overline{B} = \frac{\sum_{j=1}^{\#bolts} A_{bolt} \cdot d_{bolt_j}}{\sum_{j=1}^{\#bolts} A_{bolt}} \tag{3.11}$$

where d_{bolt} is the horizontal component of the distance from the corner of the wall to the bolt. The induced moment is calculated as follows:

$$M_{fr} = C_{steel} \cdot e_c \tag{3.12}$$

Figure 3-15 shows a detail of the most critical bolt, located furthest from the ICR. The two forces shown at the bolt are the components of force to be resisted by friction at each bolt. The direct shear force is calculated as follows:

$$F_{fr_1} = \frac{C_{steel}}{n} \tag{3.13}$$

where n is the number of bolts. The force from the induced moment is calculated as follows:

$$F_{ev} = \frac{M_{fr} \cdot d \cdot A_{bolt}}{J} \qquad (3.14)$$

where d equals the distance from the ICR to the bolt location and J equals the polar moment of inertia of the bolt group.

The bolt forces assigned to each bolt are combined to determine the resultant force, as shown below:

$$F_R = F_{fr_1} + F_{ev} \qquad (3.15)$$

The direction of this force is not critical as the friction between the plate and the concrete wall panel is the same in all directions. This resultant force is compared to the available force from friction to ensure that the plate will not slip.

3.6.8 Constructability and Economy Concerns for Design

Aspects of design related to constructability and economy are considered. A uniform spacing of bolts could be used to provide uniform confinement of the wall panel. However, the concrete axial compressive strains are greater at the bottom portion of the wall. Therefore, to save cost and make the wall easier to build, the bolt spacing was varied, decreasing along the height.

The locations where the spacing is changed are determined from the moment-curvature behavior of the wall panel. Figure 3-16 shows the wall with a section cut at an arbitrary height, y, from the bottom of the wall. Figure 3-17 shows a schematic plot of the moment versus the extreme fiber strain (ε_{cef}.) Figure 3-17 also shows the moment at the section at y calculated from the base shear force and the base moment. The corresponding strain value is the extreme fiber strain at the section at y. As this strain becomes smaller, the bolt spacing can be increased as higher levels of confinement are no longer needed.

Similarly, as the extreme fiber strain decreases, the requirement for confinement in the longitudinal direction (in-plane, transverse, or x-direction shown in Figure 3-7) decreases. After the second transition of bolt spacing, the end plate is no longer required and the rebar cage is adequate to confine the concrete in the longitudinal direction.

3.7   Final Design

This section presents the final design which resulted from the above design process.

Figure 3-18 shows the overall dimensions of the wall and its components. Based on a

qualitative assessment of the predicted confined concrete behavior from the Oh model for

the expected range of confining ratios from the plate-confinement system, it was decided

that 6 ksi concrete would provide more ductile behavior at higher levels of drift and was

selected for the final design. The final bolt spacing is included in Figure 3-18. The end

plate was stopped at 40 inches from the bottom of panel where it was anticipated that the

longitudinal confinement requirements were minimal. The thickness of the end plate was

the same as the main confinement plates to facilitate fillet welding to the panel.   Table

3-4 gives the values of the wall design parameters.

Table 3-1 - Test Parameters for Hoop Confined Tests (Perez et al. 2004)

Test I.D.	Ap (in.^{2})	f_{pi}/f_{pu}	PT Bar Arrangement
TW3	7.5	0.553	xx xox xx
TW4	7.5	0.277	xx xox xx
TW5	3.75	0.553	xo oxo ox

Table 3-2 - Performance Levels of TW3 and TW5 (Perez et al. 2004)

Test Wall	Loading Direction	SPL		LLP		CCC	
		V_{spl} (kips)	Θ_{spl} (%)	V_{llp} (kips)	Θ_{llp} (%)	V_{ccc} (kips)	Θ_{ccc} (%)
TW3	Eastward	139.5	0.83	150.7	1.63	125.1	2.74
	Westward	-74.2	-0.13	-135.8	-1.54	-121.8	-2.54
TW5	Eastward	86.9	0.65	97.8	1.44	**	**
	Westward	-85.9	-0.65	-97.7	-1.50	**	**
Target	NA	NA	±1%	±140	NA	±140	±6.0

Table 3-3 - Bolt Spacing Options

Diameter (in.)	Nominal Area (in.²)	Pretension Force (kips)	Spacing (in.) x (in.)	Tributary Area (in.²)	σ_{cp} (ksi)	φ_c for f′c= 8 ksi	φ_c for f′c = 6 ksi
5/8	0.226	20.7	9 x 9	81	0.256	0.032	0.043
5/8	0.226	20.7	9 x 4.5	40.5	0.511	0.064	0.085
5/8	0.226	20.7	8 x 4.5	36	0.575	0.072	0.096
5/8	0.226	20.7	7 x 4.5	31.5	0.657	0.082	0.110
5/8	0.226	20.7	6 x 4.5	27	0.767	0.096	0.128
5/8	0.226	20.7	5 x 5	25	0.828	0.104	0.138
5/8	0.226	20.7	6 x 4	24	0.863	0.108	0.144
5/8	0.226	20.7	4.5 x 4.5	20.25	1.022	0.128	0.170
5/8	0.226	20.7	4 x 4	16	1.294	0.162	0.216
3/4	0.334	29.8	9 x 9	81	0.368	0.046	0.061
3/4	0.334	29.8	9 x 4.5	40.5	0.736	0.092	0.123
3/4	0.334	29.8	8 x 4.5	36	0.828	0.103	0.138
3/4	0.334	29.8	7 x 4.5	31.5	0.946	0.118	0.158
3/4	0.334	29.8	6 x 4.5	27	1.104	0.138	0.184
3/4	0.334	29.8	5 x 5	25	1.192	0.149	0.199
3/4	0.334	29.8	6 x 4	24	1.242	0.155	0.207
3/4	**0.334**	**29.8**	**4.5 x 4.5**	**20.25**	**1.472**	**0.184**	**0.245**
3/4	0.334	29.8	4 x 4	16	1.863	0.233	0.310
7/8	0.462	40.6	9 x 9	81	0.501	0.063	0.084
7/8	0.462	40.6	9 x 4.5	40.5	1.002	0.125	0.167
7/8	0.462	40.6	8 x 4.5	36	1.128	0.141	0.188
7/8	0.462	40.6	7 x 4.5	31.5	1.289	0.161	0.215
7/8	0.462	40.6	6 x 4.5	27	1.504	0.188	0.251
7/8	0.462	40.6	5 x 5	25	1.624	0.203	0.271
7/8	0.462	40.6	6 x 4	24	1.692	0.211	0.282
7/8	0.462	40.6	4.5 x 4.5	20.25	2.005	0.251	0.334
7/8	0.462	40.6	4 x 4	16	2.538	0.317	0.423

Table 3-4 - Panel Final Design Values

$f\,'c$	6	ksi
φ_c	0.25	
E_c	4415.2	ksi
H_w	284.75	in.
H_{cr}	12	in.
t_w	6*	in.
t'_w	6*	in.
l_w	100**	in.
e_p	17.25	in.
E_p	29000	ksi
H_{unb}	390	in.
f_{pi}	88.5	ksi
ε_{pi}	0.00305	in./in.
A_p	2.5	in.^{2}
E_{pl}	29000	ksi
σ_y	50	ksi
ε_{ply}	0.001724	in./in.
t_p	0.5	in.

*These values are equivalent for the plate-confined design

** Changed during construction to 102 in.
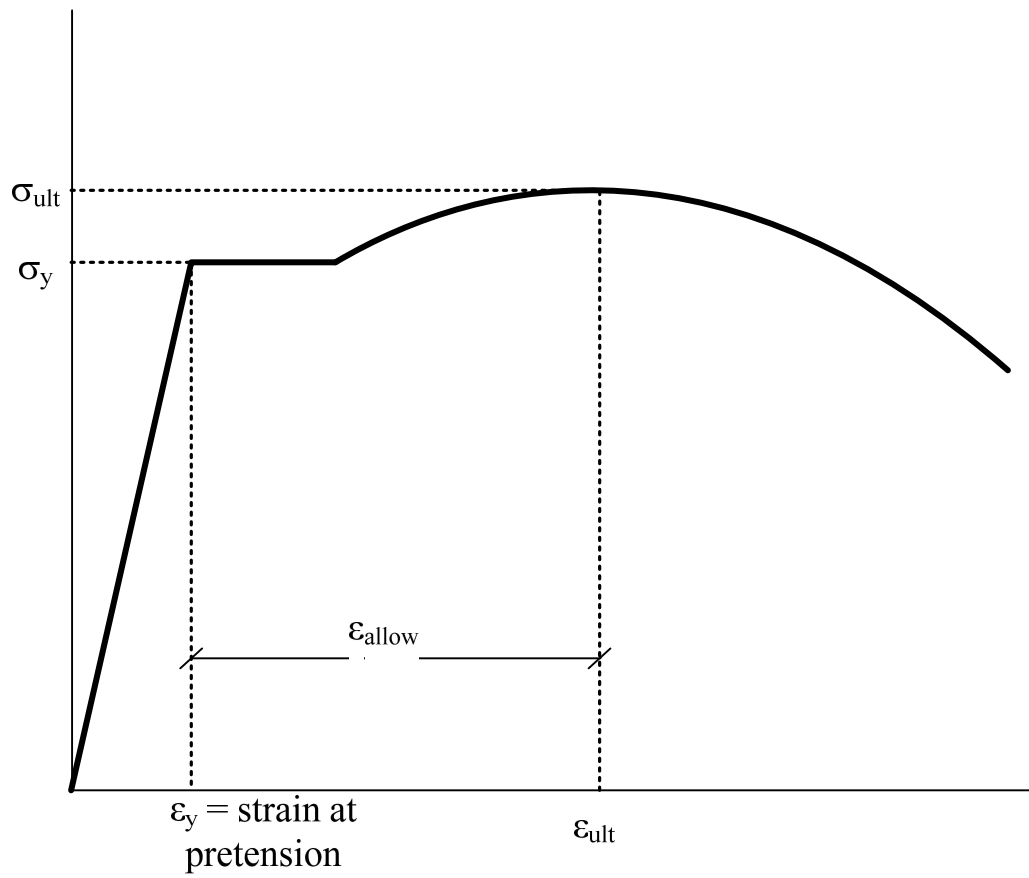
Figure 3-1 – Stress-Strain Behavior of Confinement Bolt
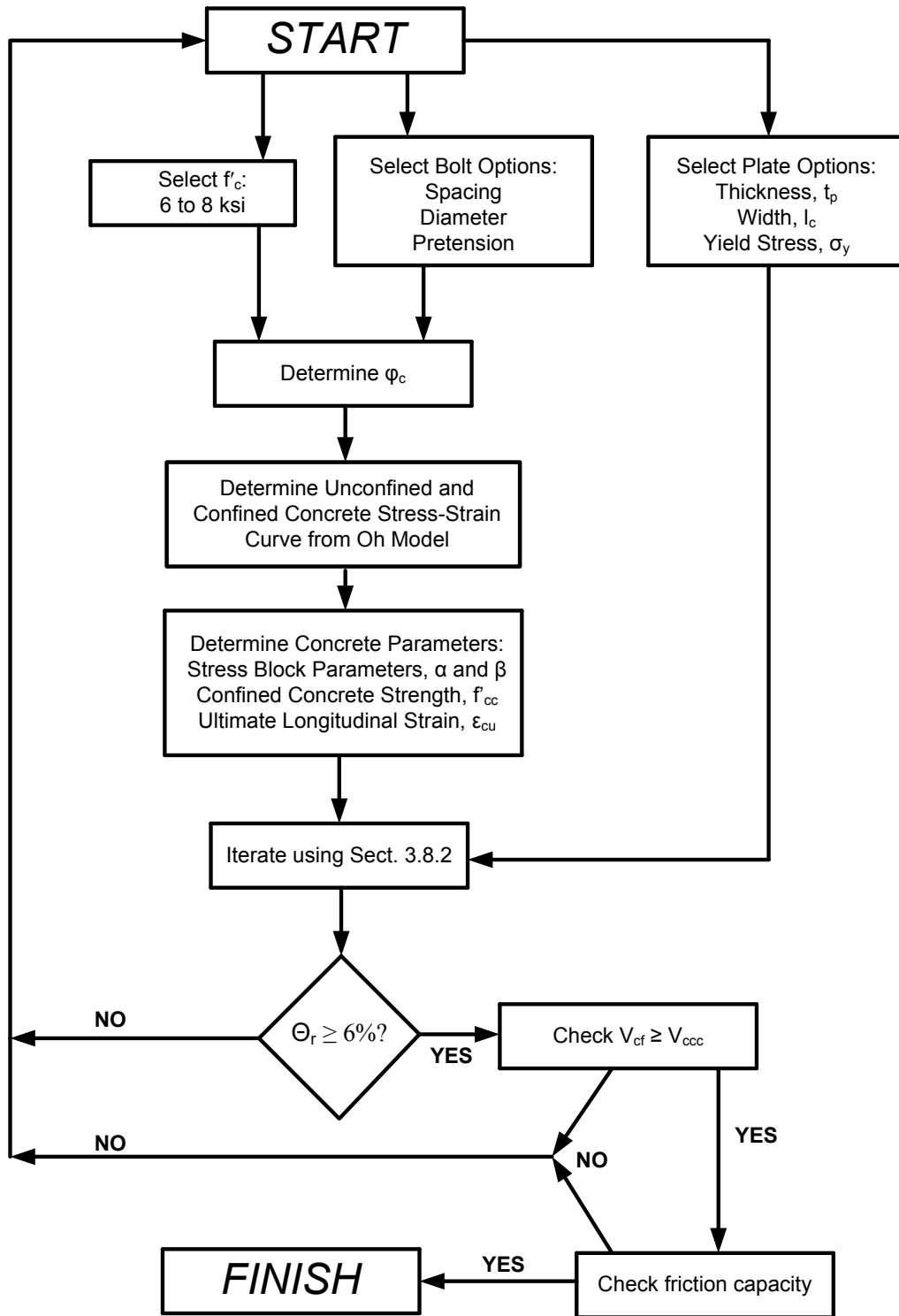
Figure 3-2 – Panel Design Process
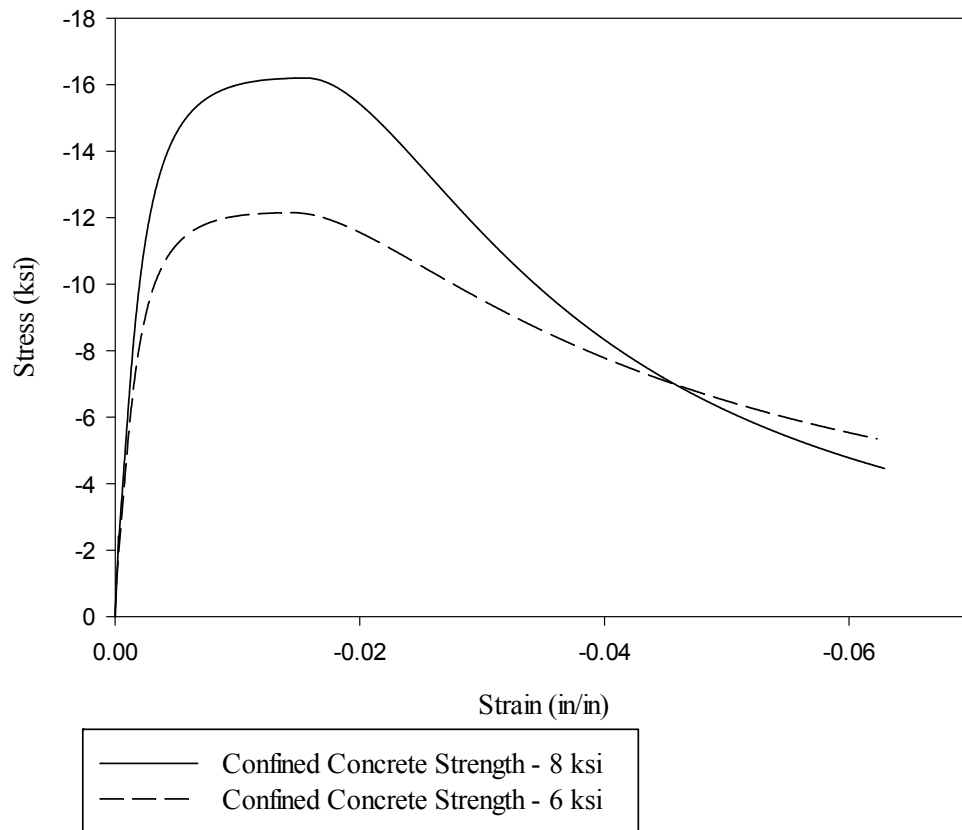
Figure 3-3 – Stress-strain Curves for Confined Concrete based on Oh's Model
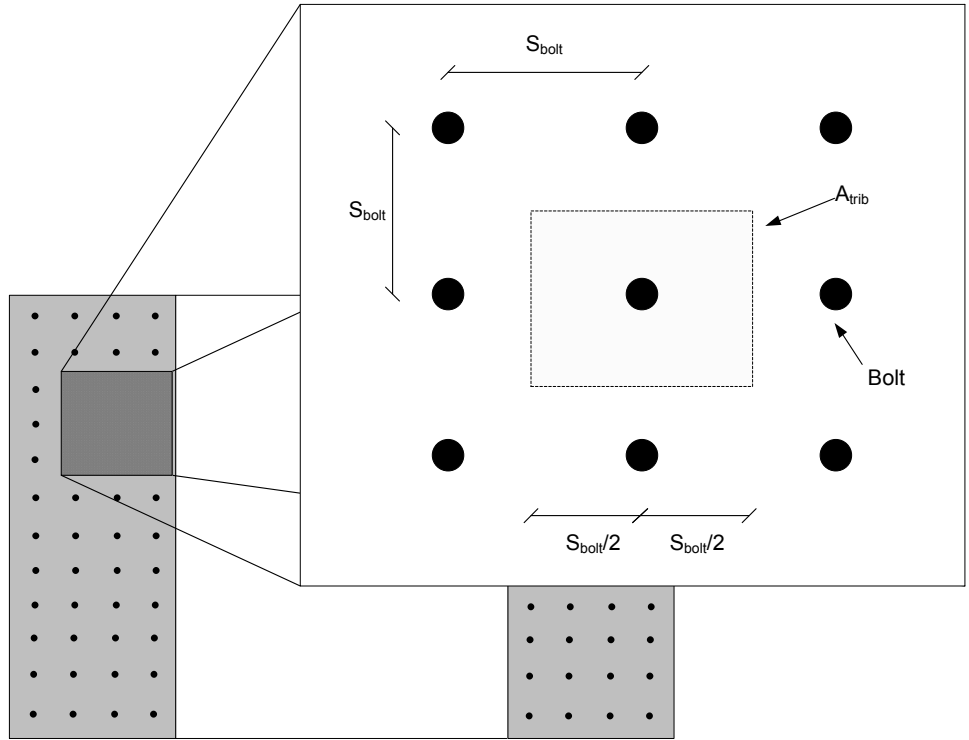
Figure 3-4 – Tributary Area of a Bolt
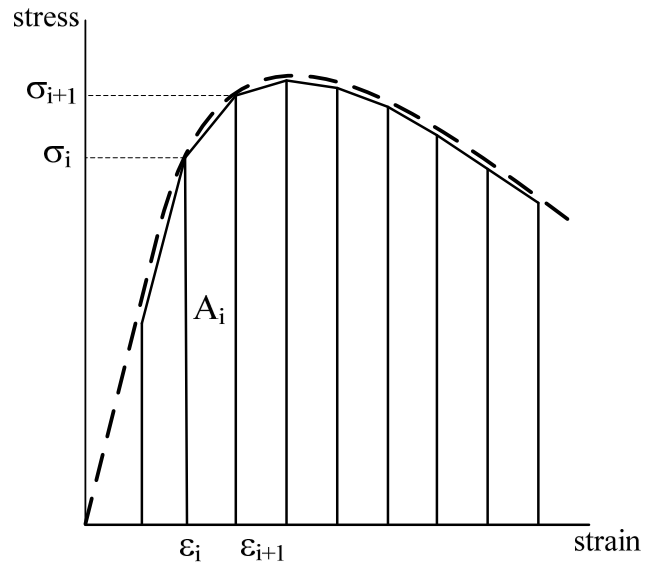
Figure 3-5 – Schematic of Area Calculation using Trapezoidal Rule
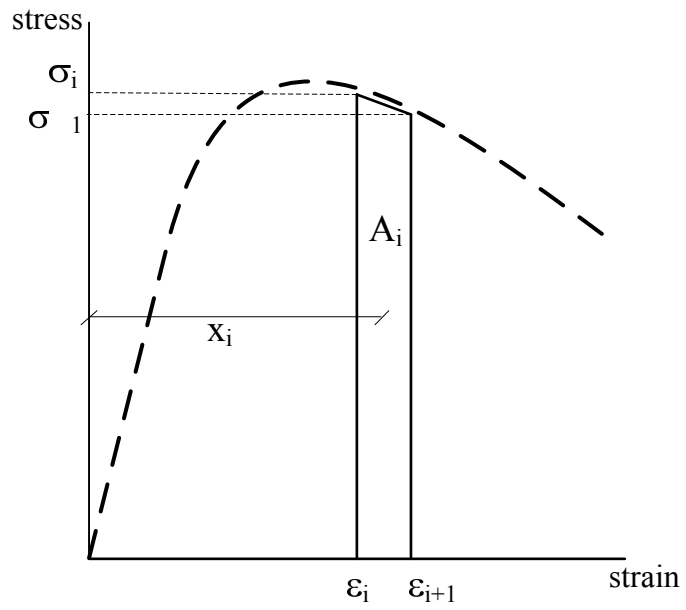
Figure 3-6 – Schematic of Centroid Calculation with Trapezoid Rule

Confinement from gravity
and post-tensioning

y

x

Confinement from rebar
and supplemental end plate
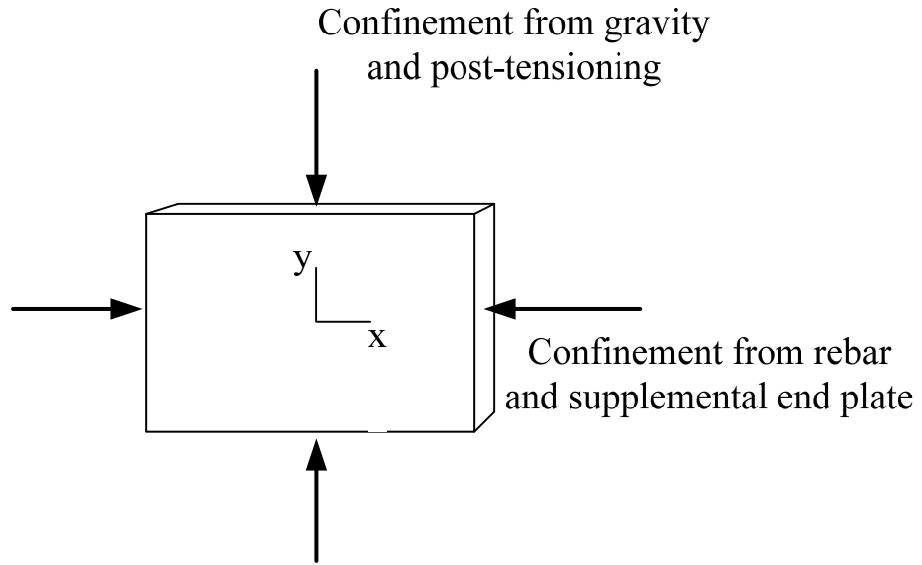
Figure 3-7 - Sources of In-plane Confinement

Figure 3-8 - Detail of the Rebar Cage in the Plate-confined Region

Figure 3-9 - Rebar Cage Layout

Figure 3-10 - End Confinement Plate

$$T1 + T2 + T3 + N$$

Shear
Force

$n * F_{bolt}$

$n * F_{bolt}$

$$\sum_{i=2}^{3}\frac{C_{Xi}}{2}$$

C_{X1}

$$\sum_{i=2}^{3}\frac{C_{Xi}}{2}$$
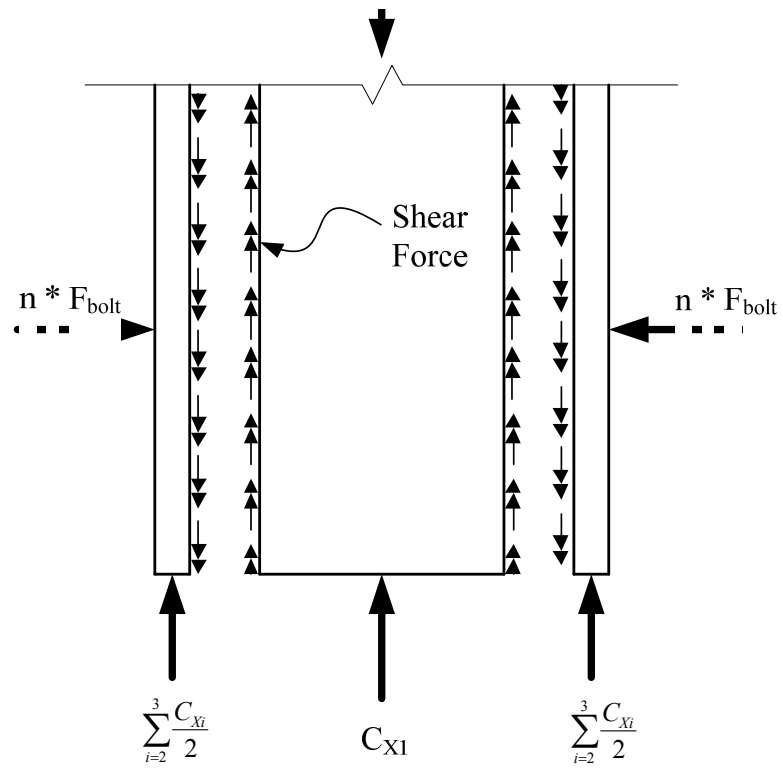
Figure 3-11 – End View at Compression End of /all Showing Shear between Concrete and Steel Wall Components Carried by Friction

$$\sum_{i=2}^{3} \frac{C_{Xi}}{2}$$

ICR

e
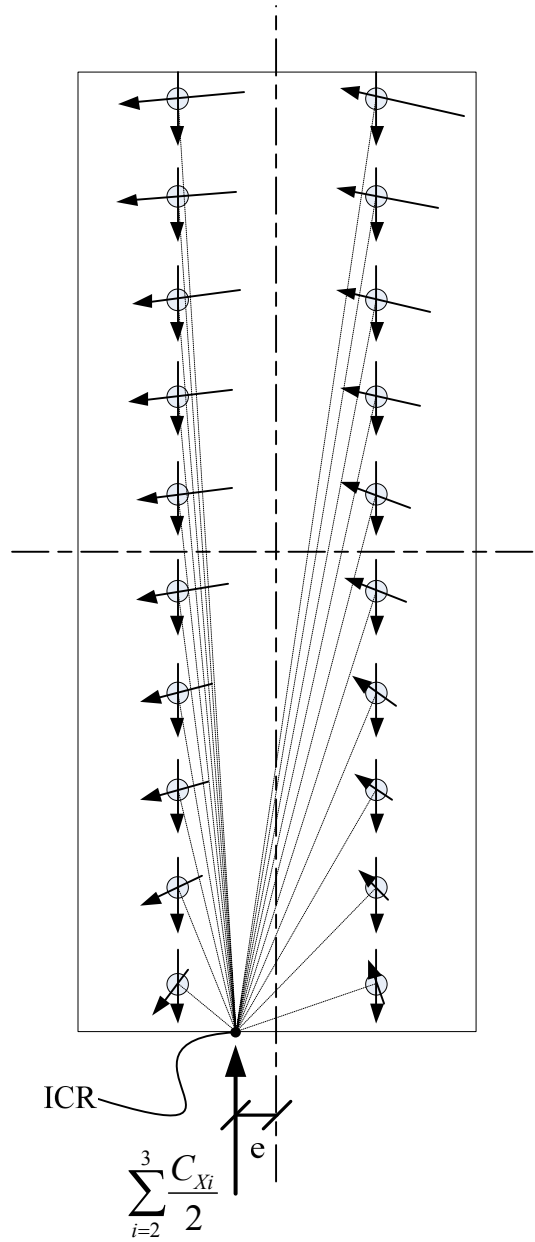
Figure 3-12 – Schematic of Friction Forces Assigned to Bolts

98
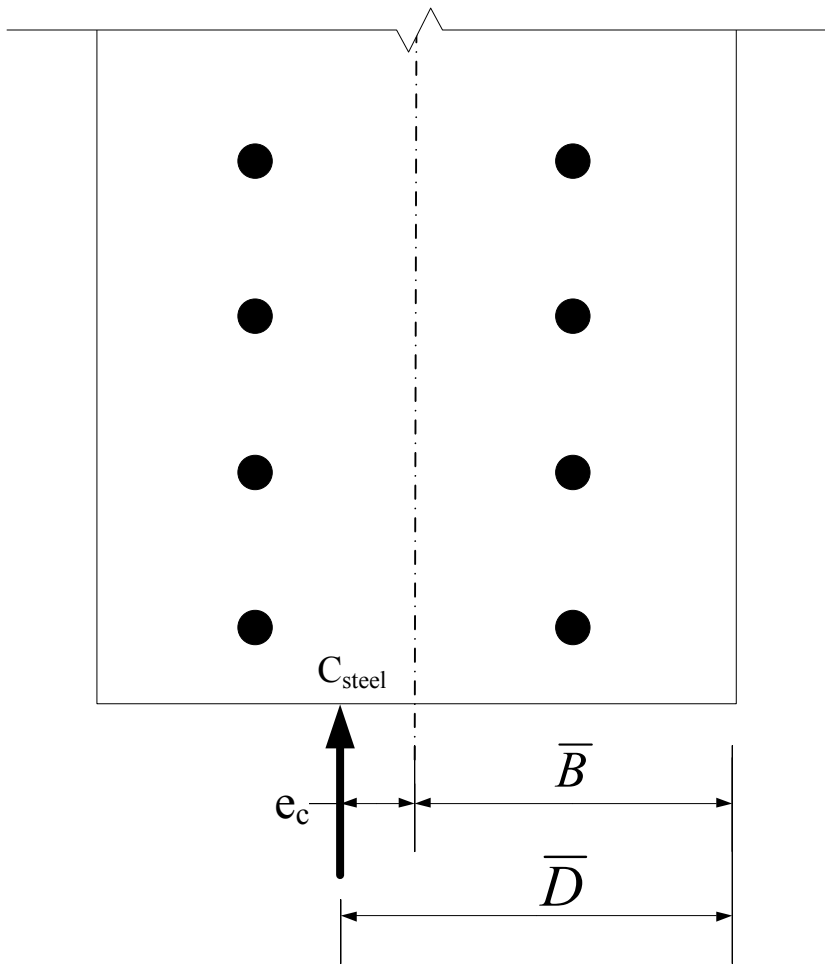
Figure 3-13 - Schematic of Eccentricity between Bolt Group and the Steel Compressive Resultant
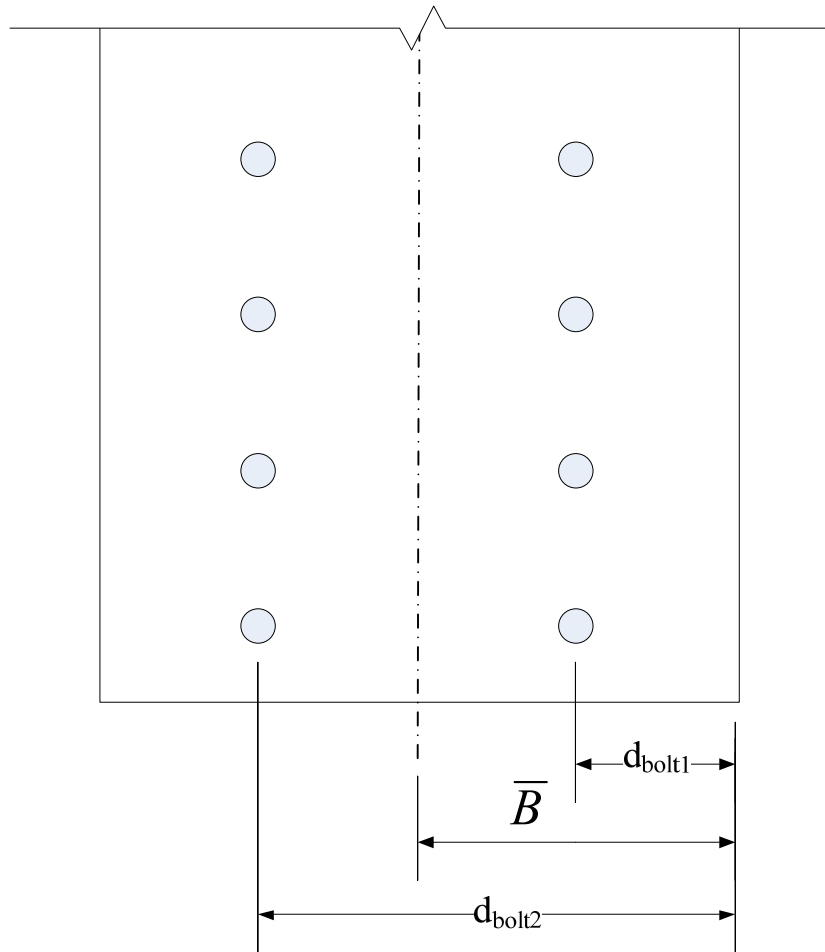
Figure 3-14 - Centroid of the Bolt Group
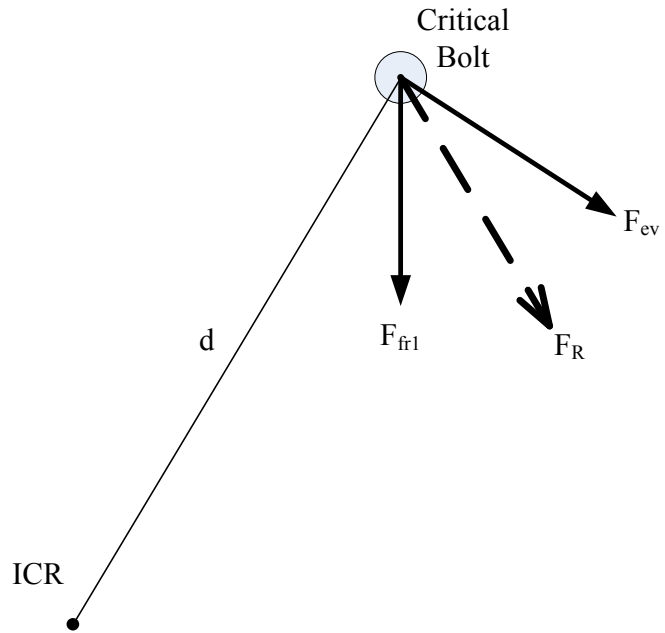
Figure 3-15 – Detail of Friction Forces Assigned to Bolts

$$H_y = H_{act} - y$$

$M(y)$
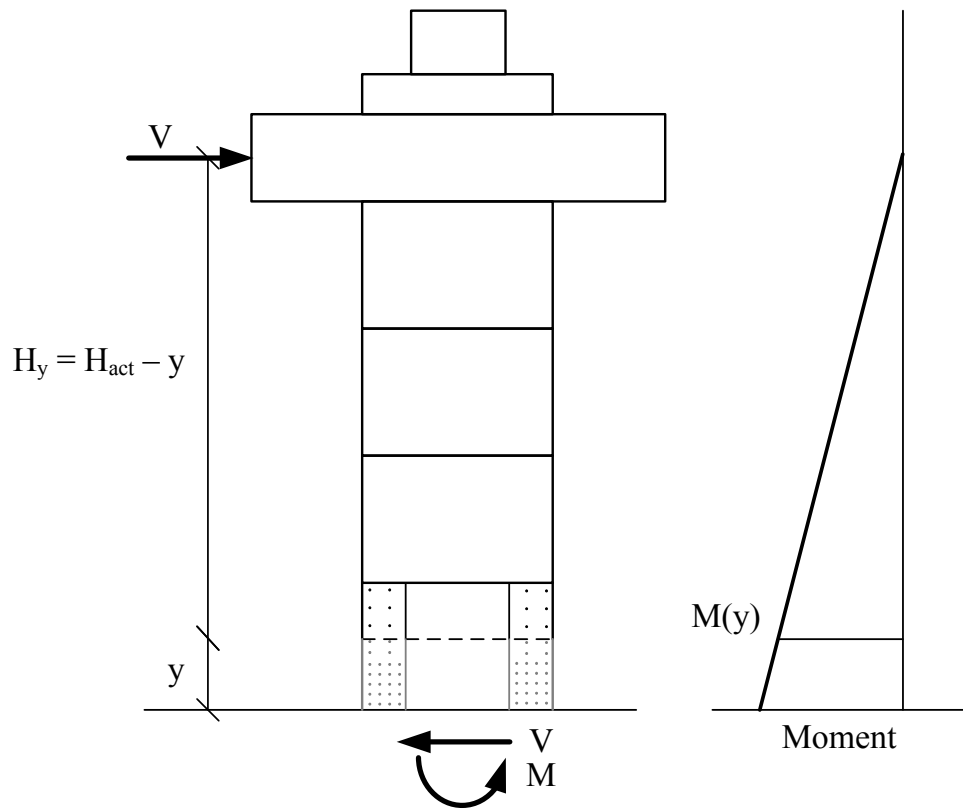
Moment

Figure 3-16 – Experimental Geometry used for Moment-Extreme Fiber Strain Analysis
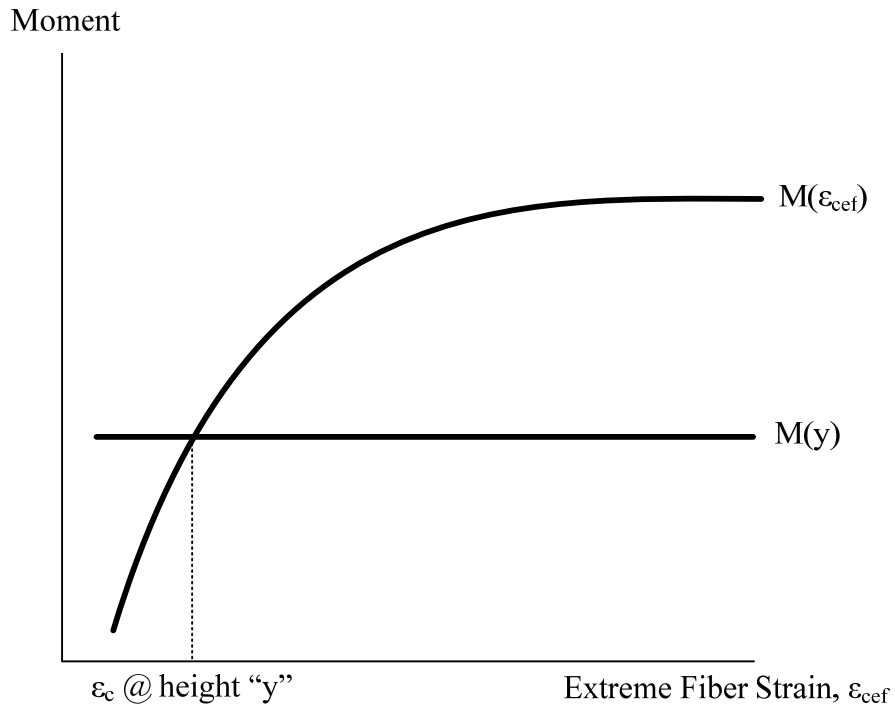
Figure 3-1   Schematic of Moment-Extreme Fiber Strain used to Adjust Bolt Spacing
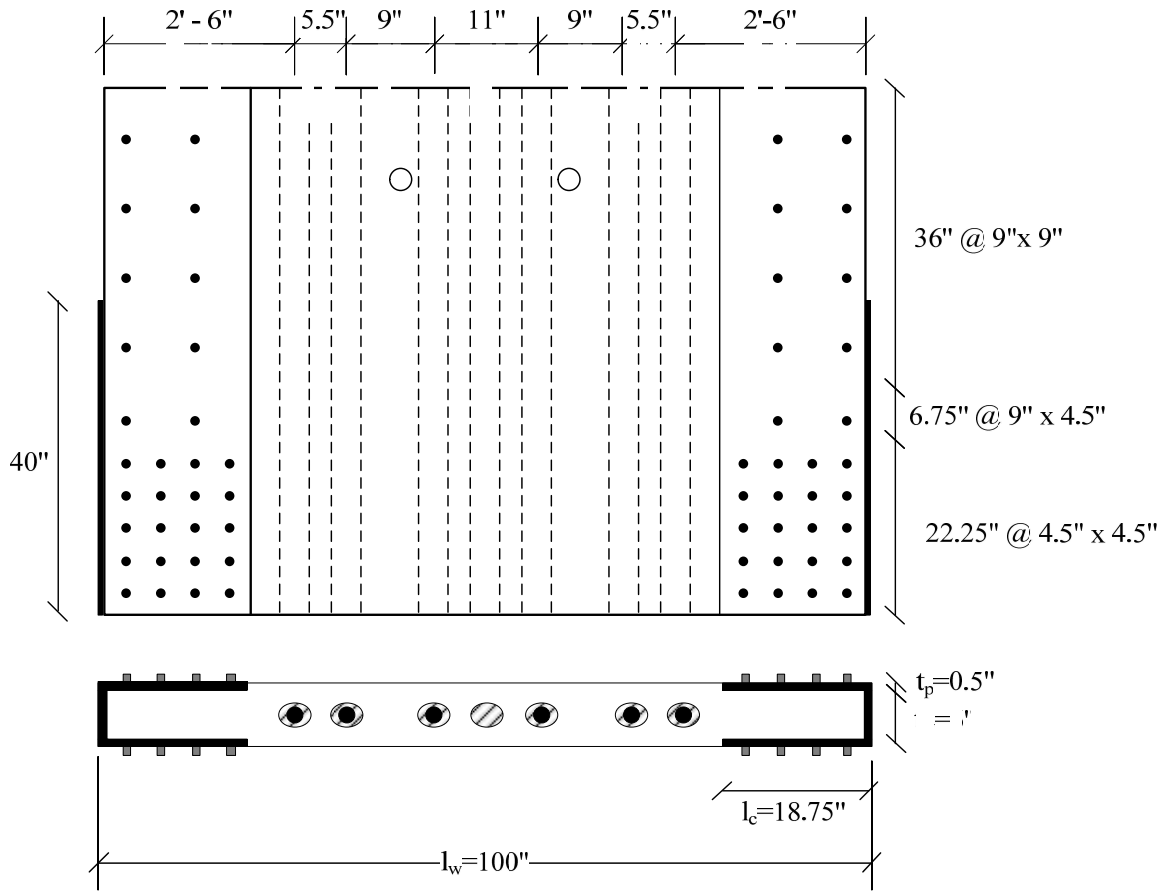
Figure 3-18 – Final First Story Plate-Confined Panel Design

4 Description of the Experiment

4.1 Introduction

This chapter describes the construction, installation, instrumentation, and experimental design for the validation of the plate-confined wall panel option. Section 4.2 describes the process of building the plate-confined wall panel and explains changes in the design which occurred during construction. Section 4.3 presents the scaled experimental test setup used by Perez et al. (2004) and reused for this test. The plate-confined panel installation process is described in Section 4.4. Section 4.5 describes the instrumentation plan and data acquisition system. Section 4.6 presents the test plan, loading scheme, and predictions of the wall panel behavior.

4.2 Plate-Confined Panel Fabrication

The construction of the panel includes the design and construction of the formwork, layout of the rebar cage, placement of the steel plates and debonded bolts in the formwork, and pouring and curing of the concrete. The presence of the plates and bolts creates some difficulties with the design of the formwork. The plates are cast into the panel. The panel was cast flat. Figure 4-1 shows the constructed formwork. Brackets on both sides, top and bottom, of the formwork as seen in Figure 4-2, provide an attachment to support and position the upper confinement plates (i.e., those plates on the outer face of the panel during the casting). The elevation and position of the plates can be adjusted

105

and locked into place to prevent the plates from shifting during the concrete pour. The lower confinement plates (on the bottom face during the casting) were secured to the bottom of the form. Figure 4-3 shows the plates in place within the formwork.

Around the perimeter of the plates, holes were drilled to allow the release of air and to verify the presence of concrete all along the inside edges of the plates. These holes were required to ensure that there were no voids in the concrete created during the pour. There is a strip of foam along the inside edge of each plate, attached with tape as seen in Figure 4-4. This serves as a transition to remediate the effects of the change in stiffness between concrete and steel and prevent cracking.

The original design of the formwork included a strip of foam at the end of the formwork between the plates as well. The purpose of this foam was to provide a gap that would be grouted after the end plate was welded on the panel. However, it was decided that the welding procedure could be altered to alleviate any concern about scorching the concrete behind the plates and the foam was removed. This created an excess length of 1 inch on either side of the panel. This resulted in a final panel length of 102 inches, which is longer than TW3 and TW5 tested by Perez et al (2004). This is also longer than the upper panels from TW5 which were reused in the experiment. These panels were all 100 inches long.

There were two options considered for installing the bolts in the wall panel. They could be cast in the wall from the start or a small duct could be cast in their place and removed. The bolts must be debonded through the thickness of the wall. It was decided that the

bolts would be positioned in the formwork before pouring as this required less work after curing. Figure 4-5 shows the bolt after it has been debonded. Debonding was accomplished by coating the middle portion of the bolt in grease and then wrapping it with plastic wrap. The bolts were placed vertically in holes drilled into the bottom of the formwork, as well as the confinement plates. They were held at the correct elevation by wooden shims underneath the formwork.

Figure 4-6 shows the as-built cage. There are seven post-tensioning ducts cast into the panel in accordance with the original design by Perez et al. (2004). The ducts were located in the same location, and were shown in Figure 3-18.

The concrete was ordered from Koller Concrete in Allentown, PA. The mix, upon arrival, was not as plastic and workable as desired considering the crowded formwork. The initial slump value was 2 inches. Therefore water was added at the time of the pour. The final slump value was 5 inches. Figure 4-7 shows an additional frame built to extend the height of the forms at the middle of the panel. This frame allowed for a substantial head of concrete to be built up. Twelve concrete cylinders were also poured for use in material tests.

The panel was poured first by vibrating the concrete up under the suspended steel confinement plates, then filling in the middle section. The air holes in the formwork were not adequate to ensure that concrete had fully filled all the space between the plates. The plate was separated slightly from the wall of the formwork to create an air-release gap so that the concrete level in the volume between the lower and upper confinement plates

could be verified. Figure 4-8 shows the pour and Figure 4-9 shows concrete in the gap

between the forms and the steel plate, indicating that no air was trapped. The concrete

was vibrated thoroughly during the pour and was finished, covered in burlap and a plastic

tarp, and left to cure. The burlap was kept hydrated for 28 days. As shown, the concrete

strength reached only 94% of the specified f'_c after 28 days. Table 4-1 presents the

concrete strengths from compression tests of the cylinders. The panel was removed from

the formwork at approximately 35 days.

When the formwork was pulled off the edge of the steel plates, excess concrete extended

past the edge of the plates, as seen in Figure 4-10 as a result of the modification to the

forms during the pour. In order to weld on the end plates, this excess concrete was ground

off, leaving a flush surface. The plates were welded on in a piecewise manner, meaning

that small sections of weld were laid down in varying locations to avoid overheating the

concrete.

The as-built dimensions of the panel can be seen in Figure 4-11.

4.3   Scaled Experimental Test Setup

The test setup used by Perez et al. (2004), which is being reused for the present

experiment, is shown in Figure 4-12. The setup of the wall itself includes the foundation,

four wall panels, a large loading block, an extension panel, and a filler panel all post-

tensioned together vertically with steel PT bars. Complete drawings including dimensions

can be found in Perez et al. (2004). The bars are anchored within the foundation and are

anchored on the top of the wall specimen. The prestressing is performed from the top. The foundation is post-tensioned to the laboratory strong floor using standard threaded tie-downs cast in the floor.

This entire fixture is housed within a steel frame designed to prevent out of plane motion. Figure 4-13 and Figure 4-14 are drawings of the out of plane bracing frame. The test specimen is connected to the frame through Teflon friction pads which are welded to the frame and grouted to the wall panels. These pads are located at every story and the loading block. They are large enough in area to remain in contact even at high levels of drift. A complete description of the out of plane bracing frame is included in Perez et al. (2004).

4.4   Plate-Confined First Story Panel Installation

The original test setup from Perez et al. (2004) was left in place because everything above the base panel was deemed to be undamaged and reusable. During the tests by Perez et al. (2004), the entire wall panel was disassembled between test panels. In order to save time and labor, a method of panel installation which did not require removal of the test fixture components was implemented. An attachment was developed used the available gravity-load bars to post tension the second, third and fourth story panels to the loading block. Figure 4-15 shows the lifting attachment which bolts to the second story panel. The panels were post-tensioned together so that the upper panel would not develop tension stress, to protect the grouted joints from cracking. Once the upper portion of the

test setup was post-tensioned together, the entire upper segment (second, third, fourth panels and foundation block) was lifted vertically with Enerpac jacks located under the ends of the loading block.

The first story panel was slid in under the lifted portion using winches and was positioned vertically using shims. Great care was taken not to damage the panel during this process. Formwork was built around the joints and the top and bottom of the first story panel so that the joints could be filled with grout. The grout was a 10 ksi grout mix with an addition of polymer fibers. Foam was inserted in each duct before the pour to prevent the ducts from filling with grout. The grout was cured for 3 days. However, during the grout pour some of the ducts were blocked with grout. The blockages were removed by drilling prior to insertion of the PT bars. The bars were attached at the foundation level and post-tensioned from the top of the wall. The bars were tensioned first to 50% then 100% of the total PT force. The post-tensioning occurred of the bars occurred in the following order: PT4; PT3; PT5; PT2; PT6; PT1. The corresponding bars are labeled in Figure 4-11.

4.5   Instrumentation and Data Acquisition

The instrumentation plan used in the experiments included transducers to measure the lateral displacements and rotations at each floor level up the height of the wall, the gap opening along the base of the wall, and the vertical displacement of the ends of the loading block. The global instrumentation plan is shown in Figure 4-16. Gap opening was measured with LVDTs. Lateral displacement was measured with linear potentiometers

because of the large range which was required. Also included in the plan are load cells on each of the PT bars and on the lateral load actuator.

The instrumentation for this test is much sparser than used by Perez et al. (2004). A large portion of the instrumentation used previously was not necessary based on prior test results. The gap opening displacement transducers are shown in Figure 4-17.

The data acquisition system used was a Campbell Scientific CR9000 unit capable of reading raw voltage input from string potentiometers, LVDTs, load cells, and rotation meters. The actuator was controlled with a Vickers control system, using displacement control. Table 4-2 is a list of all the transducers.

Photos were taken periodically throughout the test and video was taken for the entire test from fixed positions.

4.6   Test Plan and Loading Scheme

Figure 4-18 shows the loading plan used for the experiments. The wall was loaded to each lateral drift level for three cycles before moving to the next drift level. The loading speed was approximately 1% of roof drift per minute. The four load cycles to 0.1% drift were used to assess stiffness degradation throughout the test.

The gravity force was maintained throughout the test manually using a pressure relief valve. The operator of this valve was guided by the measured gravity load

Figure 4-19 shows the expected monotonic behavior of the test setup based on the

calculations outlined in Chapter 3. LLP was expected to occur at 160 kips of lateral load,

at 0.9% drift. A maximum drift level of nearly 7% was expected before CF occurred at

the bottom of the bolted region.

Table 4-1- Concrete Cylinder Compression Tests

Test (#)	Age (days)	Dia. (in.)	Load Rate (kip/min)	Load (kips)	Strength (ksi)	Average (ksi)	% of Specified f'_c
1	16	6.0	60	134	4739	4792	80%
2	16	6.0	60	137	4845		
3	21	6.0	60	155	5482	5382	90%
4	21	6.0	60	153.5	5429		
5	21	6.0	60	148	5234		
6	28	6.0	60	159.8	5650	5618	94%
7	28	6.0	60	157	5553		
8	28	6.0	60	159.8	5650		

Table 4-2 - Instrumentation Description

Plan Designation	DAS Designation	Transducer	Measured Response
Grav LC-S	Gravity_1S	Load Cell	Gravity Force
Grav LC-N	Gravity_2N	Load Cell	Gravity Force
PT_1	PT_1	Load Cell	Post-tension Force
PT_2	PT_2	Load Cell	Post-tension Force
PT_3	PT_3	Load Cell	Post-tension Force
PT_4	PT_4	Load Cell	Post-tension Force
PT_5	PT_5	Load Cell	Post-tension Force
PT_6	PT_6	Load Cell	Post-tension Force
Lat LC	Actuator	Load Cell	Applied Force
Floor 1 SP	Floor_1	String Pot	First Story Disp.
Floor 2 SP	Floor_2	String Pot	Second Story Disp.
Floor 3 SP	Floor_3	String Pot	Third Story Disp.
LB SP-N	SPLBN	String Pot	Loading Block Lateral Disp.
LB SP-S	SPLBS	String Pot	Loading Block Lateral Disp.
LBYE	LB_East	String Pot	Loading Block Vertical Disp.
LBYW	LB_West	String Pot	Loading Block Vertical Disp.
Slip_1	Slip_1	Small Disp.	Confinement Plate Slip
Slip_2	Slip_2	Small Disp.	Confinement Plate Slip
Yield_1	Yield_1	Small Disp.	Local Plate Yielding
Yield_2	Yield_2	Small Disp.	Local Plate Yielding
GO_E	GO_E	LVDT	Gap Opening
GO_1	GO_1	LVDT	Gap Opening
GO_2	GO_2	LVDT	Gap Opening
GO_3	GO_3	LVDT	Gap Opening
GO_4	GO_4	LVDT	Gap Opening
GO_5	GO_5	LVDT	Gap Opening
GO_6	GO_6	LVDT	Gap Opening
GO_7	GO_7	LVDT	Gap Opening
GO_W	GO_W	LVDT	Gap Opening
RMB	ROT_1	Rotation meter	Rotation
RM l/2	ROT_2	Rotation meter	Rotation
RM LB	ROT_3	Rotation meter	Rotation

Figure 4-1 - Formwork with Rebar Cage and Post-Tensioning Steel Ducts in Place

Figure 4-2 - Angle Support Brackets to Position the Upper Confinement Plates

115

Figure 4-3 - Confinement Plate in Place in the Formwork before Pouring

Figure 4-4 - Foam Taped to Confinement Plate for Stiffness Transition

Figure 4-5 – Confinement Bolt Debonded with Grease and Plastic Wrap

Figure 4-6 - Rebar Cage Detail

Figure 4-7 - Additional Frame to Allow for Buildup of Head during Concrete Pour

118

Figure 4-8 - Pouring the Panel

Figure 4-9 - Concrete working through air release gap

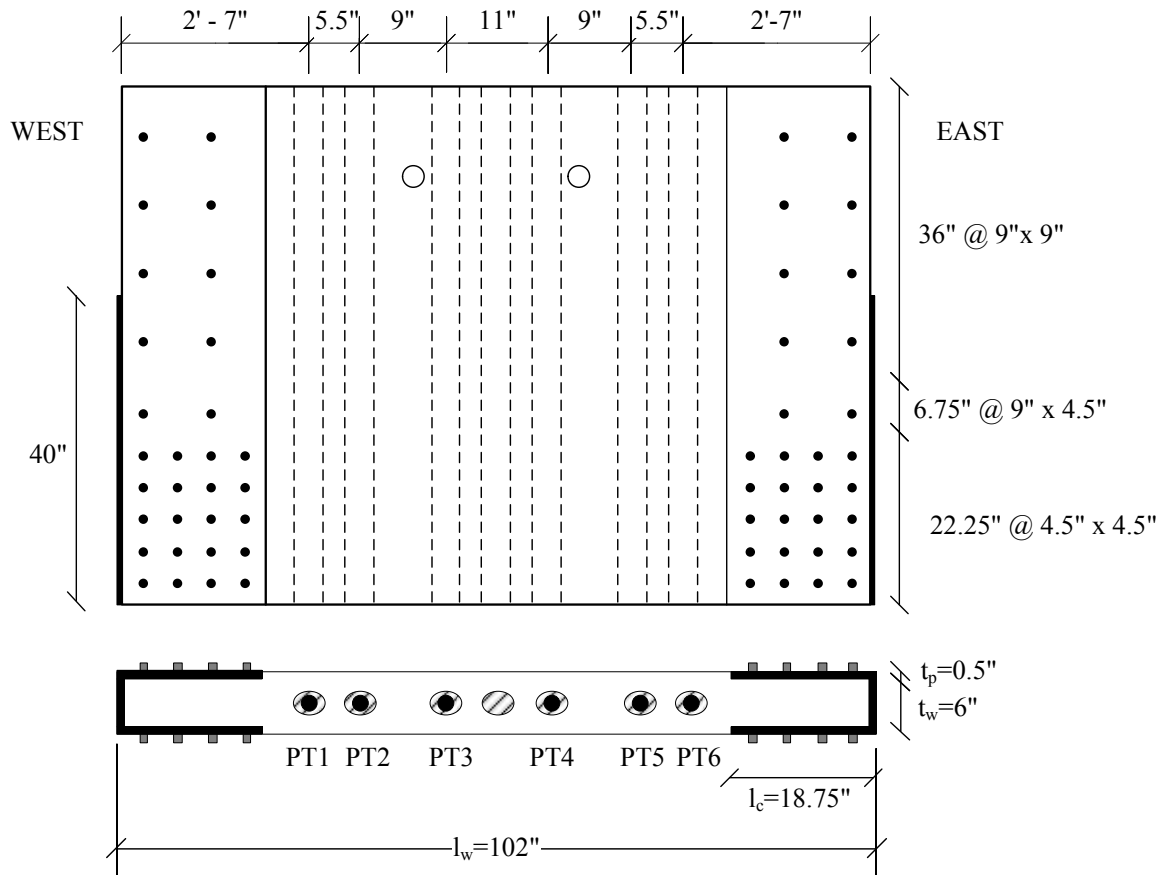**Figure 4-10 - Excess Concrete to be Removed after Curing was Complete**

Figure 4-11 - As-built Plate-confined Panel
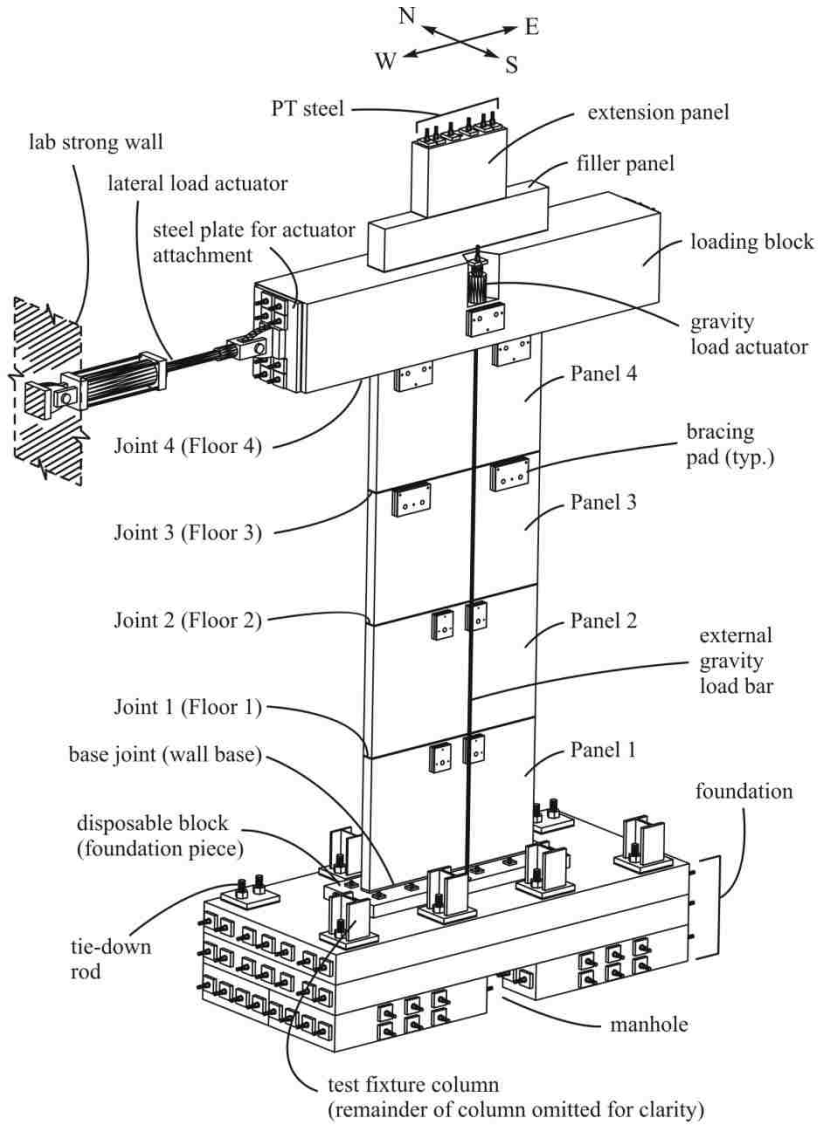
Figure 4-12 - Overall Wall Test Setup (Perez et al. 2004)
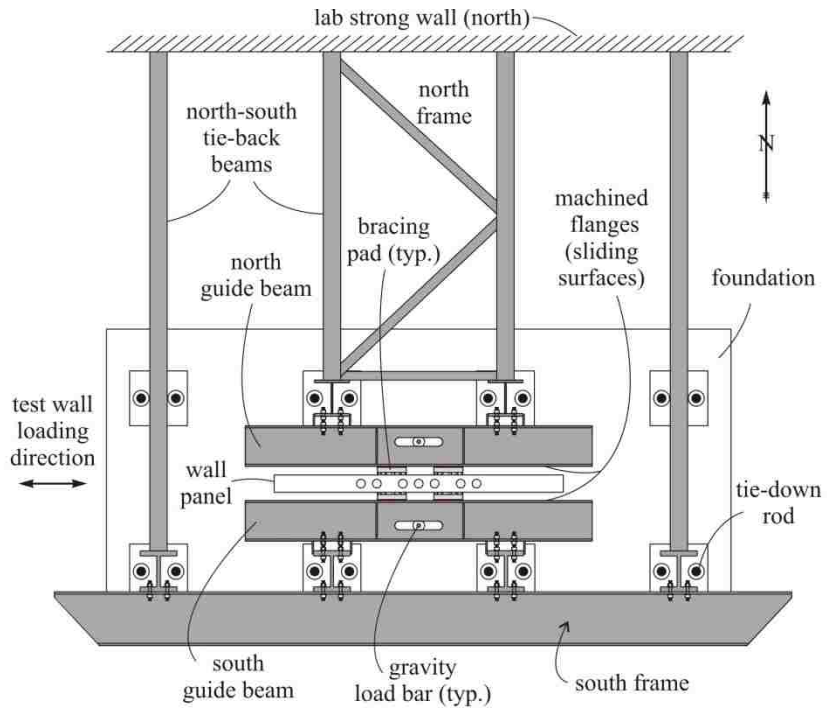
Figure 4-13 - Out-of-plan Bracing (Perez et al. 2004)
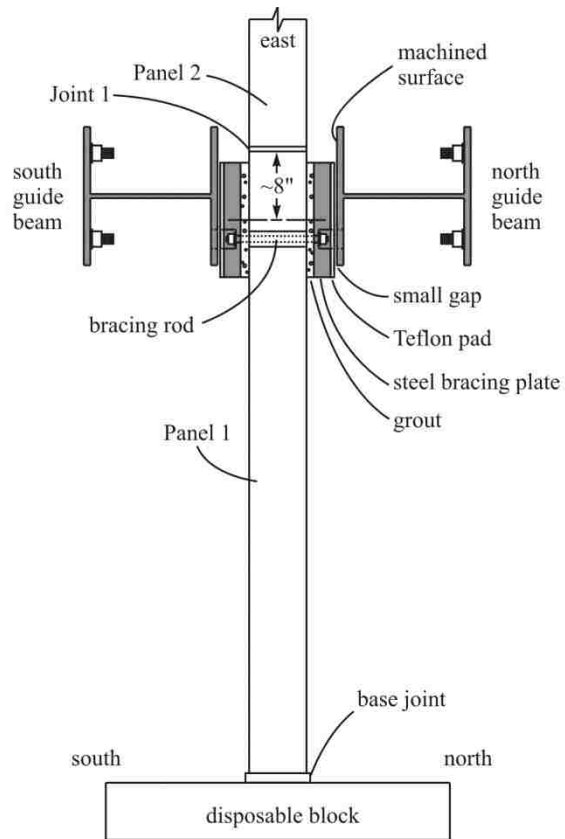
Figure 4-14 - Out of Plane Bracing (Perez et al. 2004)

Figure 4-15 - Lifting Attachment

LC = load cell
N = north side of wall
S = south side of wall
LB = loading block
RM = rotation meter
SP = string pot

Grav LC-N
Grav LC-S
Lat LC
W
E
LB SP-N
RM LB
LB SP-S
Floor 3 SP
Floor 2 SP
Floor 1 SP
RM $l_w/2$
RMB
LBYW
LBYE
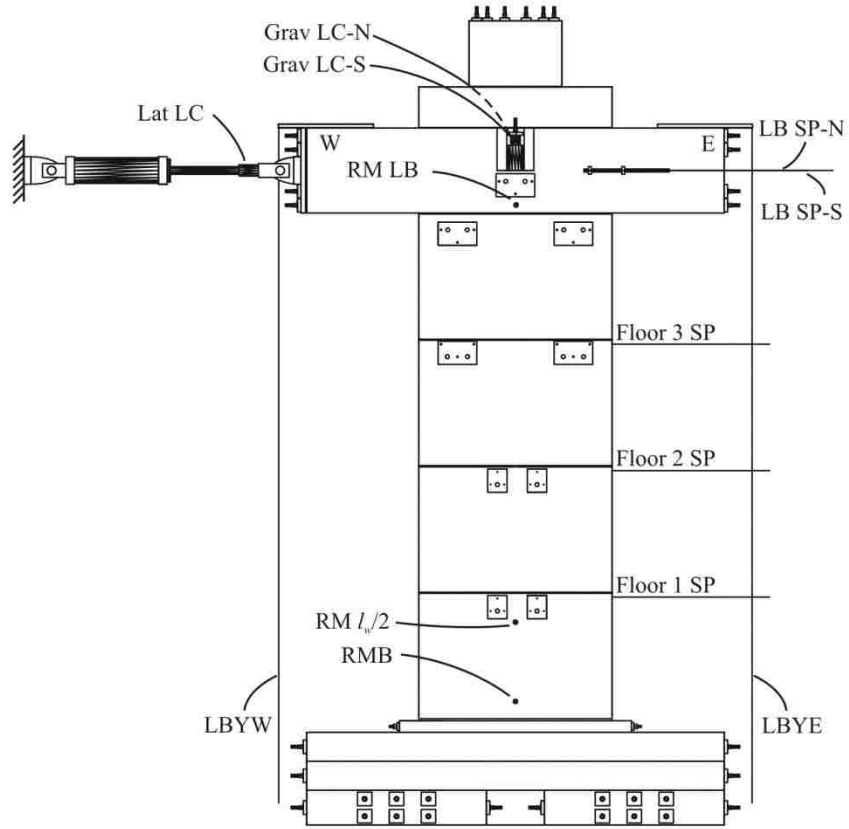
Figure 4-16 - Global Instrumentation Plan (Perez et al. 2004)

First Story Panel

GOE GO7 GO6 GO5 GO4 GO3 GO2 GO1 GOW

12.5" 18.75" 13.5" 13.5" 18.75" 12.5"

6.25" 6.25"
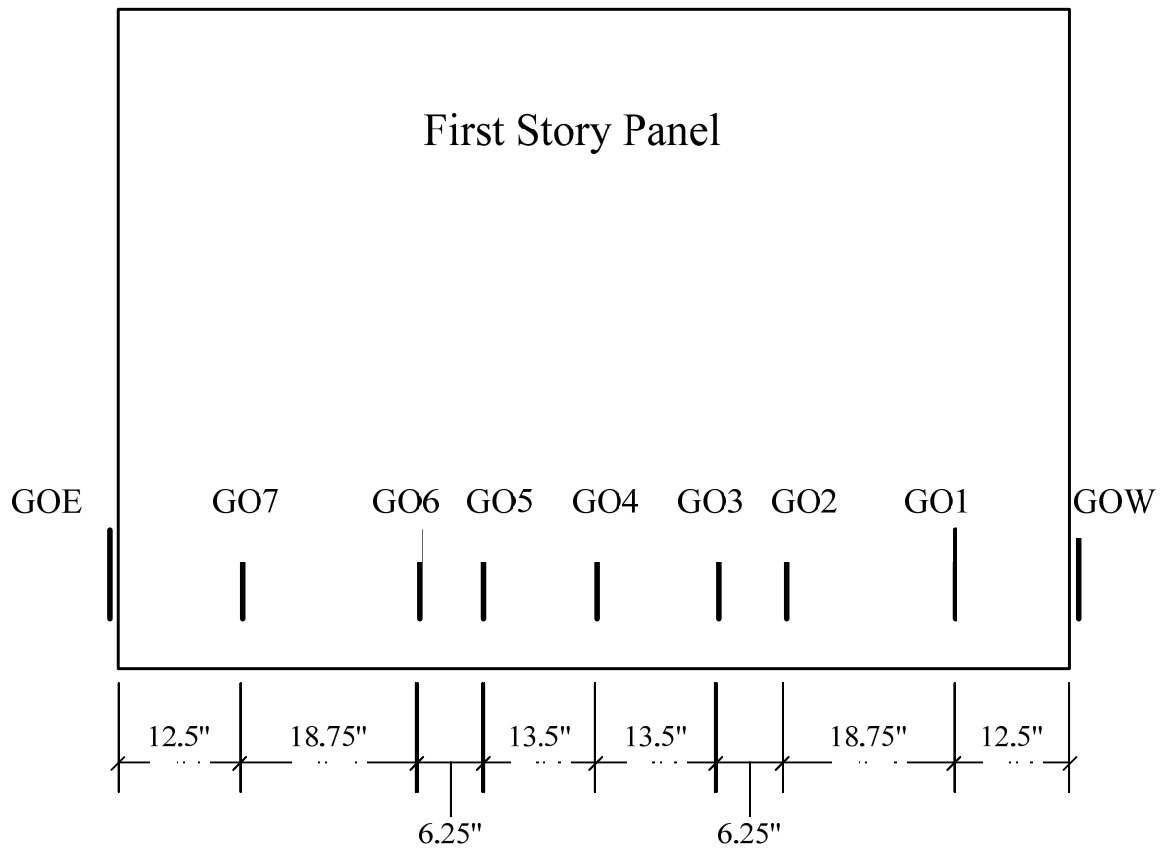
Figure 4-17 - Gap Opening Instrumentation

Figure 4-18 - Loading History for Experiment
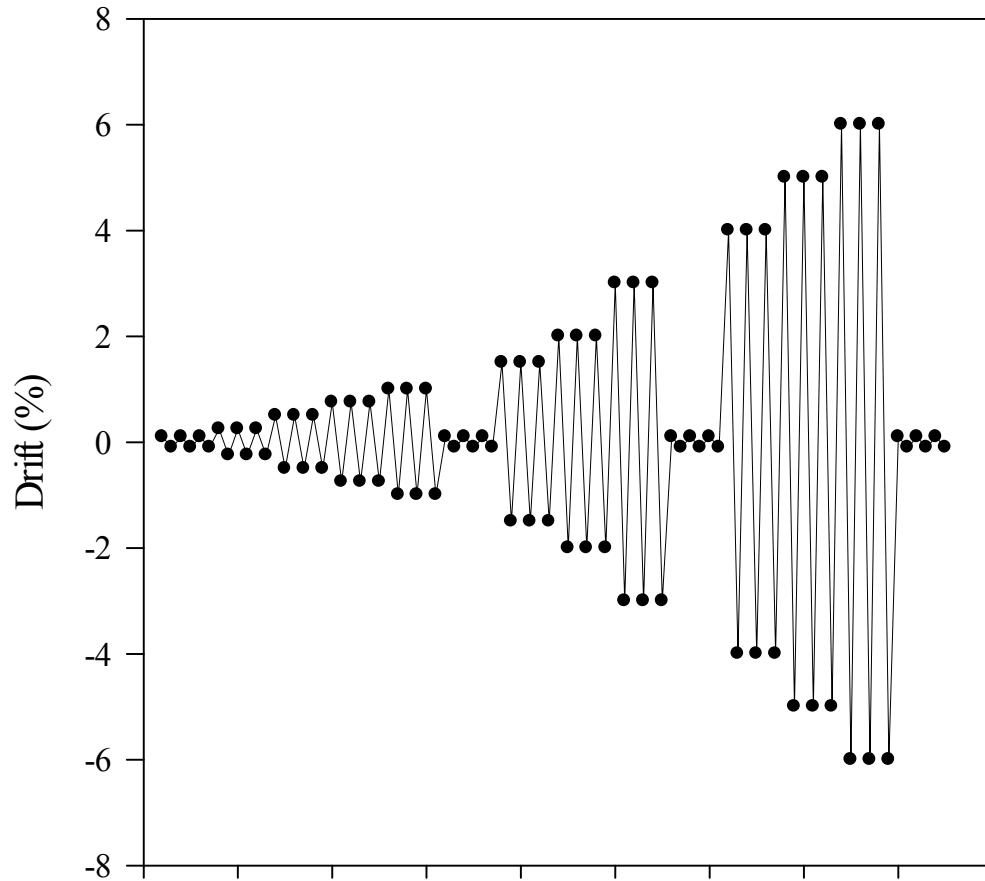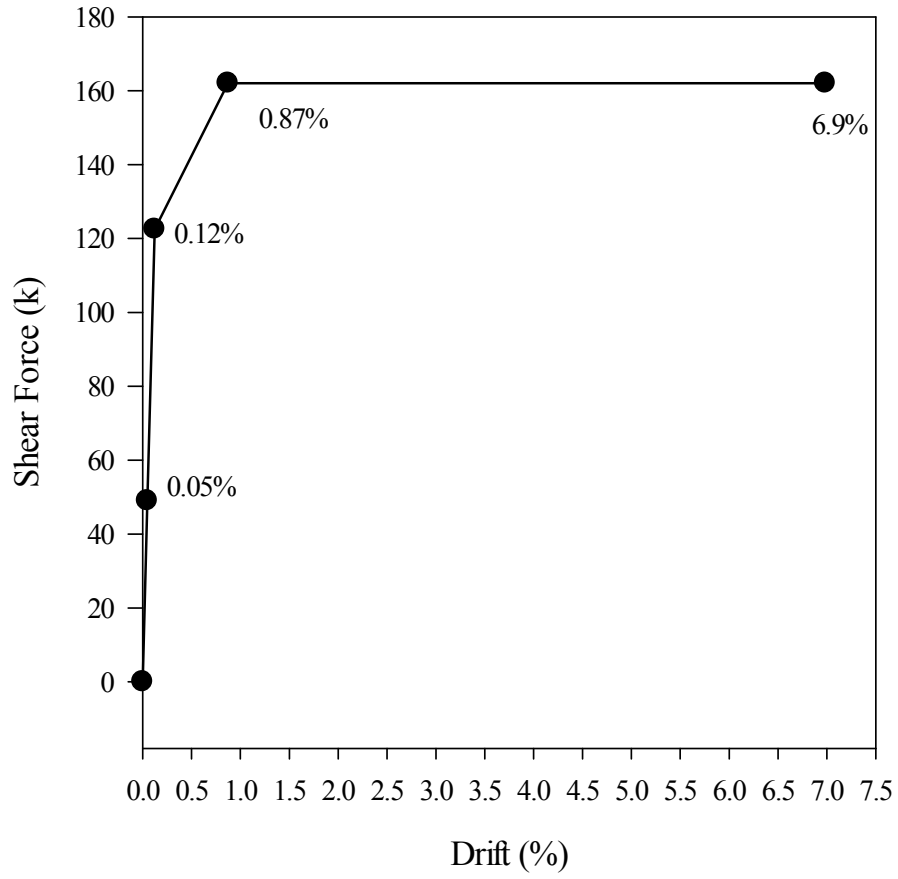
Figure 4-19 - Expected Monotonic Behavior

5   Experimental Results

5.1   Introduction

This chapter presents the results of the lateral load experiment on the plate-confined wall panel. General notes on the results presentation are given in Section 5.2. Section 5.3 presents a timeline of the experiment of the test organized by drift level. Sections 5.4 through 5.7 discuss individual measured responses of the wall across drift levels. Section 5.8 is a discussion of unexpected behaviors during the experiment.

5.2   General Notes

The behavior of the plate-confined system is presented herein both in a global and a local sense using data acquired from the instrumentation described in Chapter 4. The sign conventions for these measurements can be seen in Figure 4-16. As the wall rotates, the force imparted by the actuator on the wall shifts from horizontal to a combination of horizontal and vertical components. Perez et al. (2004) showed that the effects of the vertical component of force are negligible and for this reason, the vertical component is ignored for the plate-confined panel experiment. The force output from the actuator load cell is taken as horizontal.

5.3   Summary of Overall Behavior

Figure 5-1 shows the lateral load versus roof drift behavior of the plate-confined wall panel system. Immediately apparent is the shift of the hysteretic loop from the zero load point. This shift occurred do to premature damage at the top of the first-story wall panel on the west side. This event, referred to as Damage Event 1, is shown qualitatively in Figure 5-2. The west-side damage had little effect on the eastward behavior. Therefore, the eastward behavior will be used to quantify the performance of the system.

The wall was cycled from 0.1% to 2.0% drift with no visible damage to the bottom corners of the first story panel. These regions of TW3 and TW5 sustained heavy damage. On the first eastward cycle to 3.0% drift, the eastward, top corner of the first story panel failed, causing an overall loss of capacity of the wall. This damage, referred to as Damage Event 2, is shown qualitatively in Figure 5-2. This is considered the ultimate failure of the wall. At the time of failure, the wall was under 197 kips of lateral load, which greatly exceeded the capacity of the previous tests. The drift level at this damage event was 2.7% which is similar to the maximum drift (i.e., Θ_{cf}) of TW3.

The variation of gravity load versus roof drift is shown in Figure 5-3. The load varied slightly, within a range of about ±5%, with the exception of one occurrence where there was a steep drop in the force. This occurred after the first eastward half cycle in the 0.5% cycle group and is discussed further in Section 5.3.3

5.3.1 0.1% Roof Drift Cycle Group

The first cycle of the test was to 0.1% roof drift. This corresponded to a loading block displacement of 0.29 inches. This displacement was achieved in approximately one minute. The load at peak displacement was approximately ±85 kips for these cycles. The response was linear, no damage was observed and there were no audible sounds.

5.3.2 0.25% Roof Drift Cycle Group

The next cycle of the test was to 0.25% roof drift. This corresponded to a loading block displacement of 0.71 inches. This displacement was also achieved in one minute, as the previous cycle showed that the loading rate was too slow. During the first eastward half cycle, the mechanical limit switch attached to the loading block was tripped. The range of these switches was increased from this point on to prevent further interruption. The load at peak displacement was approximately ±130 kips for these cycles. The response was linear, no damage was observed and there were no audible sounds.

5.3.3 0.5% Roof Drift Cycle Group

The next cycle of the test was to 0.5% roof drift. This corresponded to a loading block displacement of 1.42 inches. This displacement was achieved in two minutes. The load at peak eastward displacement was approximately 151 kips. The westward behavior varied throughout the cycle group. Prior to the first westward cycle, some popping sounds were

heard, and the specimen experienced a large and instantaneous drop in gravity force from 176 kips to 109 kips. At the time of the drop, the wall was at the zero position after the first eastward half cycle. The test was paused so the gravity load could be adjusted and the wall inspected for damage. There was no visual evidence of damage and the test was continued. The first westward half cycle reached a peak load of -138 kips when the first unexpected damage to the wall occurred, causing the load to drop to -105 kips. Figure 5-4 shows a photograph of Damage Event 1 which occurred at the top west corner of the plate-confined panel and the bottom west of the second panel. The damage consisted of spalling of some of the cover concrete on the second panel, and spalling of a large piece of the concrete from between the plates at the top of the plate-confined panel. After the damage occurred the wall was cycled eastward again. All ensuing westward half cycles achieved a load level of approximately -116 kips at 0.5% roof drift. It should be noted that after Damage Event 1 the point at which the wall experienced zero lateral load and the point of zero roof drift no longer coincided with one another. At the zero roof drift level, there was approximately 85 kips of residual lateral load.

5.3.4   0.75% Roof Drift Cycle Group

The next cycle of the test was to 0.75% roof drift, corresponding to a loading block displacement of 2.14 inches. This drift level was achieved in two minutes. The peak eastward load was 164 kips while the peak westward load was -142 kips. This discrepancy is from the unsymmetrical wall panel conditions resulting from Damage

133

Event 1. At this drift level, there was substantial gap opening behavior, especially under eastward load. Figure 5-5 shows the gap opening at 0.75% eastward drift. The bond with the grout was broken and the wall panel was beginning to lift off the grout. It should be noted that the cracking which started with Damage Event 1 spread slightly during this cycle group, though there was no appreciable reduction in the westward load capacity within the drift cycle group.

5.3.5   1.0% Roof Drift Cycle Group

The next cycle of the test was to 1.0% roof drift. This corresponded to a loading block displacement of 2.85 inches. and was achieved in 2.5 minutes. The peak eastward load was 172 kips while the peak westward load was -159 kips. Again this is a result of Damage Event 1. Note that during the 1.0% cycle group a large piece of concrete from the top west corner of panel was removed by hand to prevent any damage to instrumentation around it. Figure 5-6 shows the specific area which was removed.

5.3.6   0.1% Roof Drift Cycle Group (2)

This was the second group of cycles to 0.1% roof drift, included as a stiffness degradation check. During the test it became apparent that the check would be irrelevant as the loads that developed during cycles to 0.1% drift were positive at both 0.1% drift and -0.1% drift. In other words, because the zero load point and zero drift point no longer

134

coincided with one another, the wall was being displaced around a position of zero drift only, not zero load. The load level varied from 66 kips to 114 kips. As such, one cycle of the three planned cycles was skipped.

5.3.7   1.5% Roof Drift Cycle Group

The next cycle of the test was to 1.5% roof drift. This corresponded to a loading block displacement of 4.27 inches. The peak eastward load was 184 kips while the peak westward load was -176 kips. The magnitude of the peak loads are closer at this cycle group than previous groups because at higher drift levels, the gap opening behavior at the base of the wall had greater effect on the global behavior than the damage caused by Damage Event 1. At this level, there was substantial gap opening behavior in both east and westward directions. Figure 5-7 shows the gap opening behavior during eastward loading.

5.3.8   2.0% Roof Drift Cycle Group

The next cycle of the test was to 2.0% roof drift. This corresponded to a loading block displacement of 5.70 inches. This displacement was reached in 5 minutes. The peak eastward load was 193 kips and the peak westward load was -187 kips. During this cycle group, spalling along the base of the second panel began to propagate towards the center of the wall.

5.3.9 3.0% Roof Drift Cycle Group

The next cycle of the test was to 3.0% roof drift. The corresponding loading block displacement was 8.54 inches. This displacement was not achieved. The wall system failed at 2.7% drift under eastward loading which corresponded to a loading block displacement of 7.6 inches. The load at this point was 197 kips. Westward loading was not applied after this damage under eastward loading occurred. The wall was returned to zero lateral load and the test was ended. Damage occurred in both the first and second panels. Figure 5-8 shows the spalling which occurred in the second panel. Figure 5-9 shows the damage that occured along the interface between the steel confinement plate and the concrete wall panel. Damage Event 2 started at the top east corner of the plate-confined panel, shown in Figure 5-10. A large piece of the concrete between the confinement plates spalled off as the second panel appears to have settled between the confinement plates of the first story panel. At the time of failure, there was gap opening both at the base joint and the joint between the first story plate-confined panel and the second panel as shown in Figure 5-11. This gap opening will be described in Section 5.8. Despite the premature failure, the confinement at the bottom corners of the plate-confined panel showed no evidence of damage, as seen in Figure 5-12.

136

5.4 PT Bar Forces

Figure 5-13 through Figure 5-18 show the PT bar force versus lateral roof drift for each

PT bar. The dotted line on each plot represents the actual yield point of the steel bars, at

172k of tensile force. Note that this actual yield force of 172 kips is larger than the yield

force assumed in design (150 kips). Figure 5-13 shows the behavior of PT1 which is

located the farthest to the west, and therefore reaches its highest force during eastward

loaded. It can be seen that at the failure of the entire system, PT1 had just reached the

yield point. It can also be seen that the force at zero lateral drift decreased by nearly 40%.

In previous tests reported by Perez et al. (2004), loss of prestress was due to yielding of

the PT steel, but as mentioned before, the PT steel did not yield until the end of the test.

Similar results can be seen for PT2. Conversely, Figure 5-18 shows the behavior of PT6

which did not reach yield at all, while experiencing a smaller loss of prestress (about

22%).

5.5 Gap Opening Behavior

The gap opening behavior at the base of the plate-confined panel under eastward loading

is shown in Figure 5-19. At 2% roof drift, the gap had opened to 1.6 inches but remained

relatively linear, indicating a lack of damage at the corner of the base panel. The

westward loading behavior is shown in Figure 5-20. There are several points to note

regarding gap opening under westward loading. Before Damage Event 1 (0.5% roof drift)

the gap had opened to around 0.1 inches and after the damage it stabilized at 0.04 inches.

Note also that the maximum gap opening achieved was 1.0 inches, which is substantially less than under eastward loading.

5.6   Lateral Displaced Shape

The displaced shape of the wall system is shown at peak displacement during the first cycle of each group in Figure 5-21. The peak displacements for the upper stories were similar for the loading in each direction. At the loading block level, the maximum eastward displacement was 5.7 inches while the maximum westward displacement was 5.8 inches. However, the displacement at the top of first story was not the same for the two loading directions. This discrepancy is discussed in Section 5.8. Lateral displacement (sliding) of the base of the wall was not instrumented because sliding of the base panel was not observed in the previous tests by Perez et al. (2004). From the top of the first story to the loading block, the wall appears to displace linearly.

5.7   Rotation Profiles

Figure 5-22 shows the rotation profile at maximum displacement during the first cycle. As expected, eastward loading shows near constant rotation. The majority of this rotation is due to the rigid body rotation of the entire wall system about the base. Under westward loading, rotation appears nearly constant over the height of the first panel, though smaller than the first panel rotation under eastward loading to the same drift level. The loading

block exhibits rotations much larger than the first story under westward loading, which suggests rotational deformation occurs above the first story, most likely at the joint between the first story plate-confined panel and the second panel. Figure 5-23 shows a schematic of this additional rotation, ω. Although it was not measured, substantial gap opening between the first and second panel was observed under westward loading.

5.8   Analysis of Unexpected Behavior

5.8.1   Discussion of Early Failure

The first story plate-confined wall panel failed at the top east corner (Damage Event 2) because the concrete axial strain exceeded the capacity of the concrete in the top corner of the plate-confined panel. In Chapter 3, a moment-curvature analysis of the wall was used to determine the required confinement ratio up the height of the wall. Recall that controlling failure criteria was assumed to be dilation of the confined concrete to the point which the confinement bolts fractured. This was expected to occur at the bottom of the first panel. The strain at the top of the first panel was expected to be so small, in fact, that confinement was not even needed there. The concrete would be sufficient alone. Figure 5-25 shows a schematic comparison of the compression resulting from a small contact zone at the base of the first story panel when gap opening is not present at the joint between the first and second panels and when it is present. In Figure 5-25 (a) note how at the top of the first story panel, the fan is very wide, suggesting that the compressive stress (and therefore the compressive strain) is very well distributed across

139

the panel. Figure 5-25 (b) shows how this compression fan would change if there was substantial gap opening at the joint between the first and second panels, which was observed during the test. The vertical compressive force must flow through a smaller area, increasing the stress in the area of contact between the two panels. The resulting strain at the top corner of the plate-confined panel at failure was likely much larger than expected. The in-plane transverse strain exceeded the capacity of the concrete and a large piece of concrete spalled off of the corner, allowing the wall to drop down violently causing a rapid spread of damage. The plates bent out, the second story panel settled in between the confinement plates of the first panel. There was substantial spalling along the joint between both panels as indicated in Figure 5-8 and Figure 5-9.

Neither the gap opening of the joint between the first and second panel, or the axial strain variation in the first and second panels were measured.

5.8.2 Delay of PT Yielding

The plate-confined wall panel did not experience the linear limit of the post-tensioning (LLP) at the same drift level as TW3 or TW5. This result can be attributed to the permanent damage which resulted from Damage Event 1 during the 0.5% drift cycles. After the damage at the top west corner of the plate-confined first panel, the average vertical displacement between the ends of the loading block was -0.1 inches whereas before the damage it was 0.014 inches. Throughout the test, as damaged slowly accrued at both top corners of the first panel, these vertical displacements became larger. This

measurement is not a true measure of the shortening of the wall, because the position at zero lateral drift was not the same as the position at zero lateral load. It is a linear approximation of the length of the chord along the centroid of the wall from the loading block to the base panel. Figure 5-26 shows the centroidal axis shortening (along the chord) at the end of each drift cycle. As the wall effectively shortens, the PT bars lose a portion of the original prestress as mentioned in Section 5.4. Therefore, the stress in the bars at the beginning of each half cycle is lower, which is the reason the bars yielded only near the end of the test. Figure 5-27 shows the PT force in each bar after each load cycle where the decrease in prestress force is evident.

5.8.3 Unsymmetric Lateral Behavior

Damage occurred in the top west corner of the plate-confined panel, causing the wall to exhibit different lateral behavior when loaded to the east as opposed to the west. Further discussion of this is provided in Chapter 6.
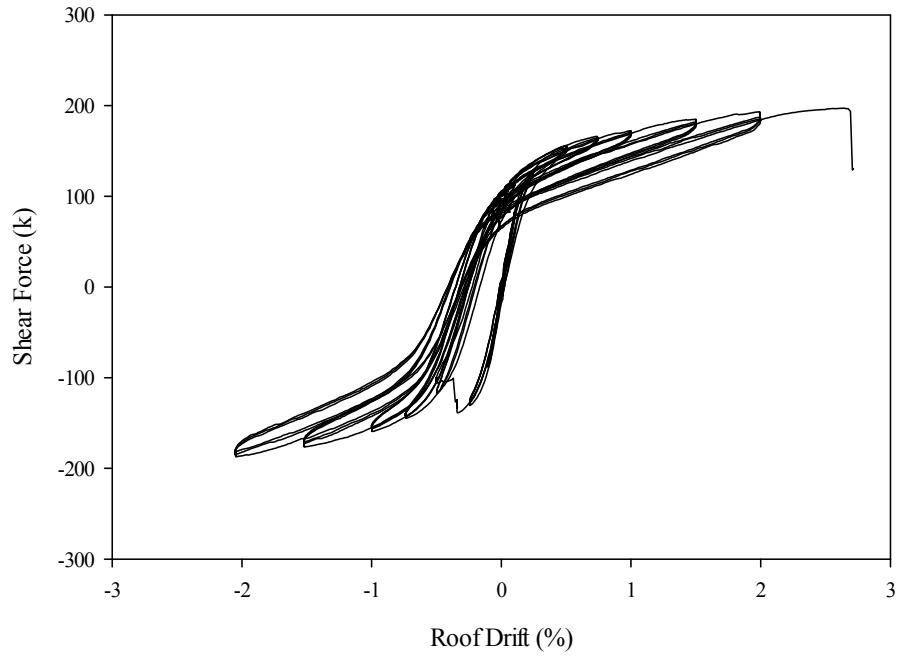
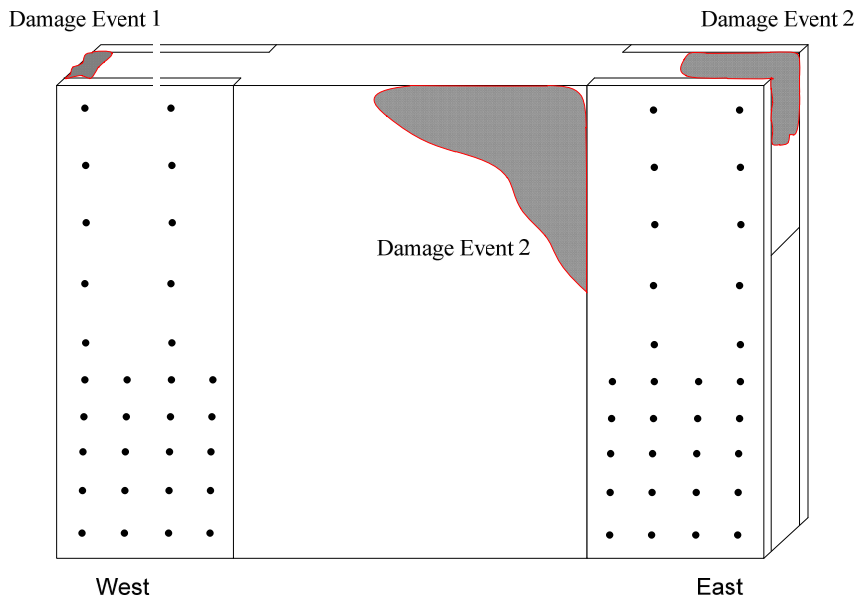**Figure 5-1 - Lateral Load vs. Roof Drift**

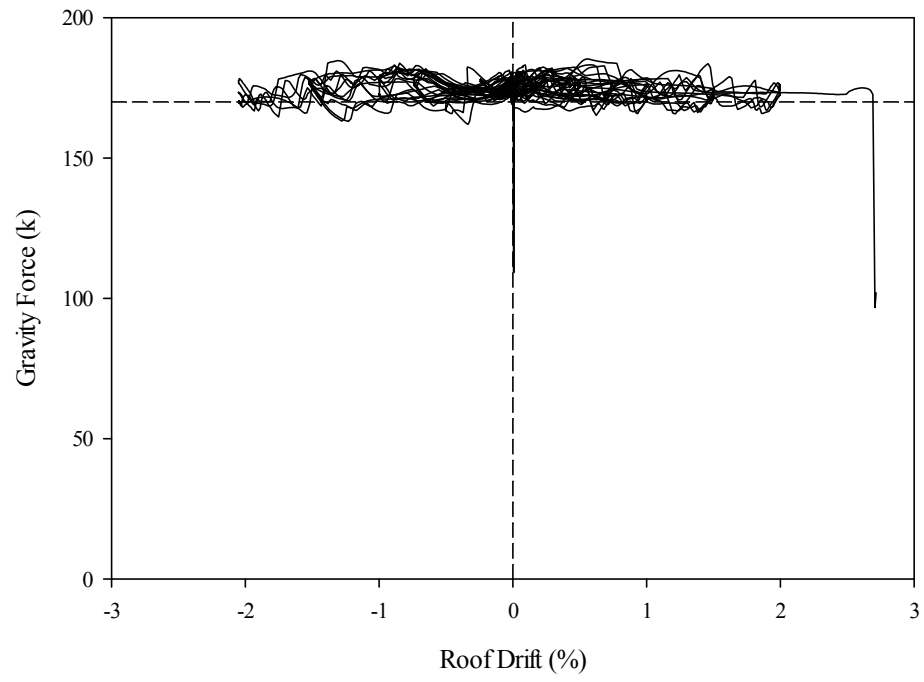**Figure 5-2 – Schematic Showing Locations of Damage during Test**

Figure 5-3 - Gravity Load vs. Roof Drift

Figure 5-4 - Damage Event 1 - Top Corner of Plate-Confined Panel (West Side)

Figure 5-5 - Gap Opening at 0.75% Roof Drift (Eastward Loading)

144

Figure 5-6 - Area of Concrete Removed During 1.0% Cycles (West Side)

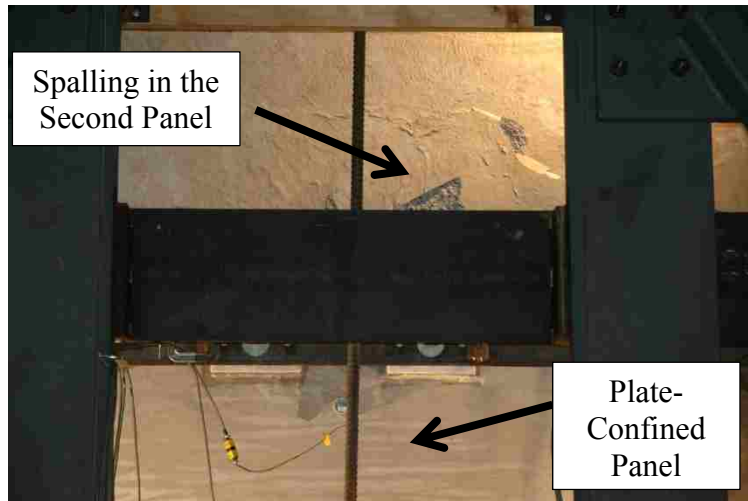
Figure 5-7 - Gap Opening at 1.5% Roof Drift (Eastward Loading)

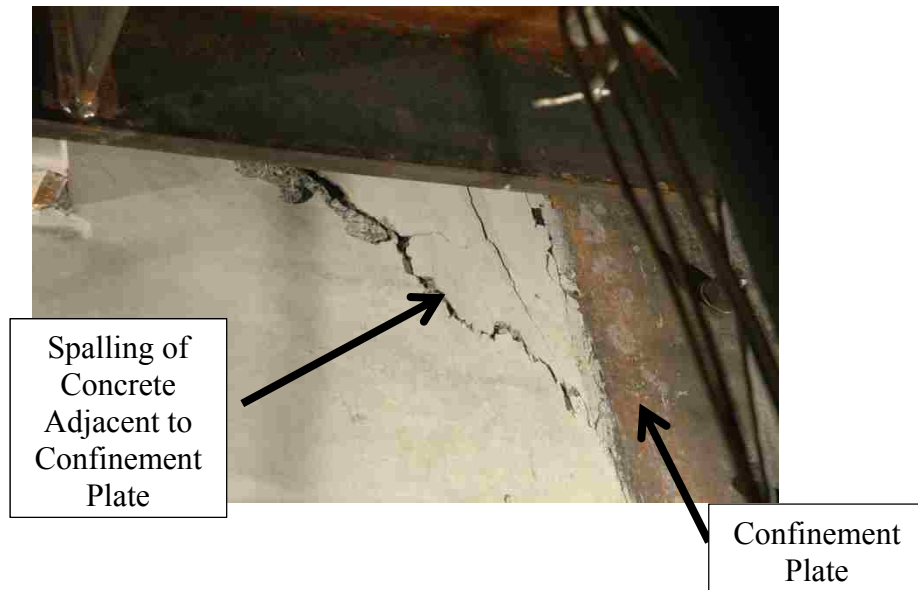**Figure 5-8 – Spalling in the Middle Region of the Second Panel**

Figure 5-9 – Spalling of Plate-Confined Panel

Figure 5-10 - Damage Event 2 - Confinement Failure at Top East Corner of Plate-Confined Panel
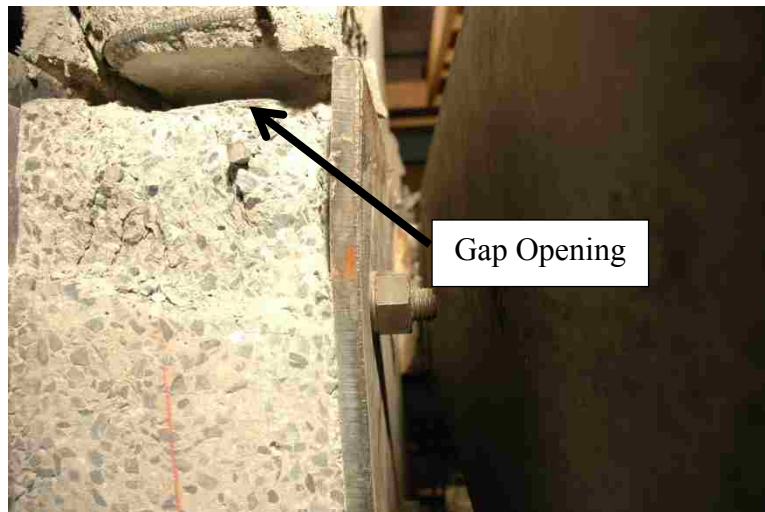

Gap Opening

Figure 5-11 - Gap Opening at Joint between First Story Plate-Confined Panel and Second Panel

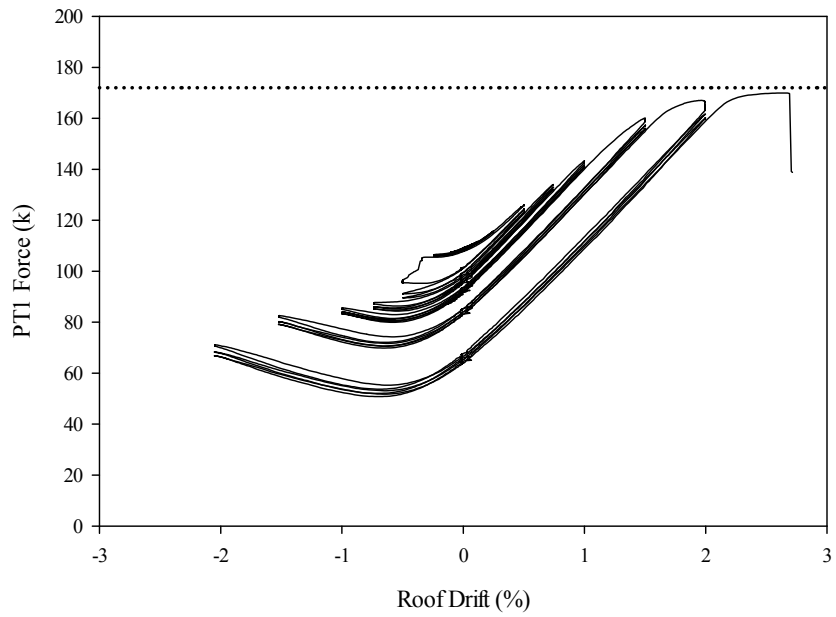**Figure 5-12 - Lack of Damage at Bottom Corner of Panel - East Side**
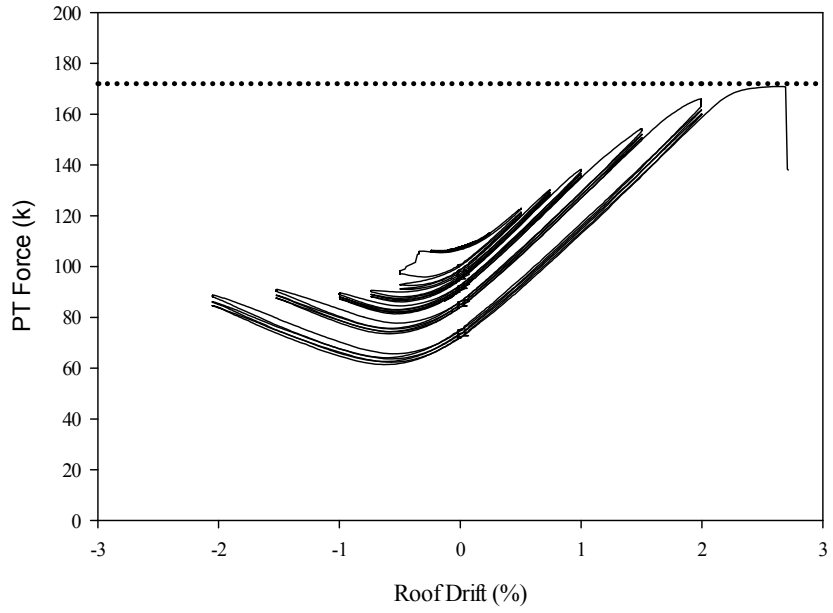

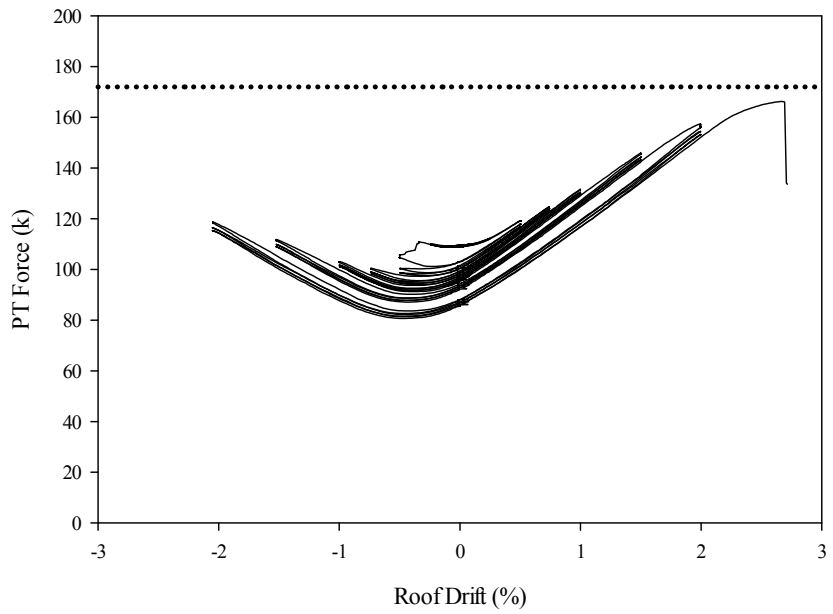**Figure 5-13 - PT1 vs. Roof Drift**

Figure 5-14 - PT2 vs. Roof Drift

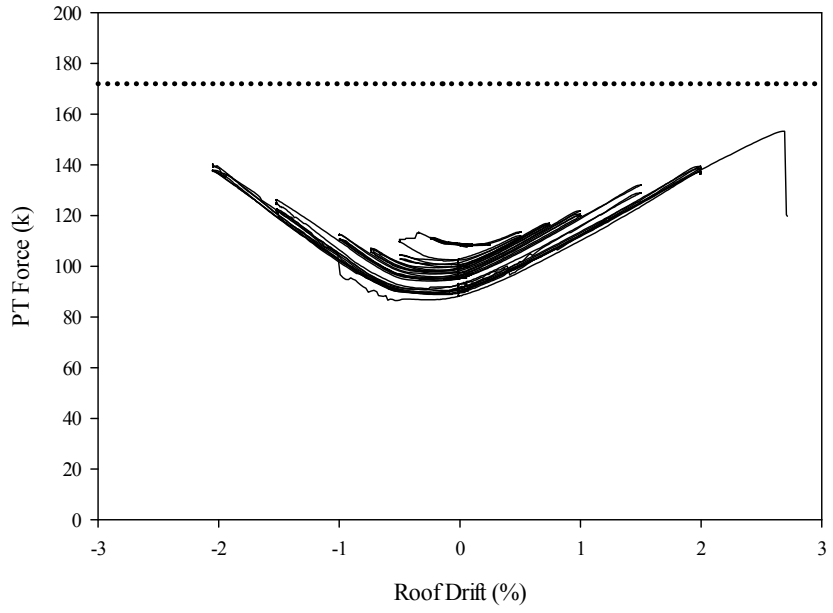**Figure 5-15 – PT3 vs. Roof Drift**

Figure 5-16 - PT4 vs. Roof Drift
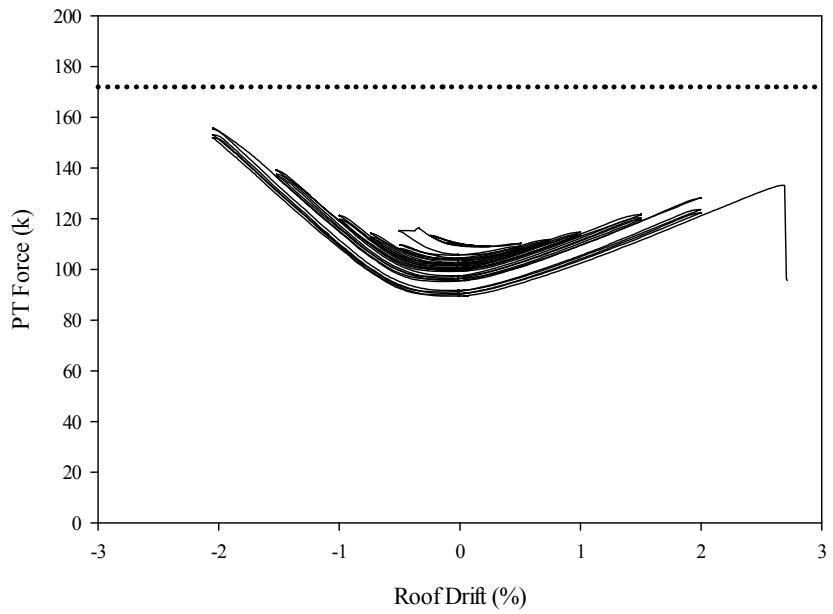

Figure 5-17 - PT5 vs Roof Drift

150
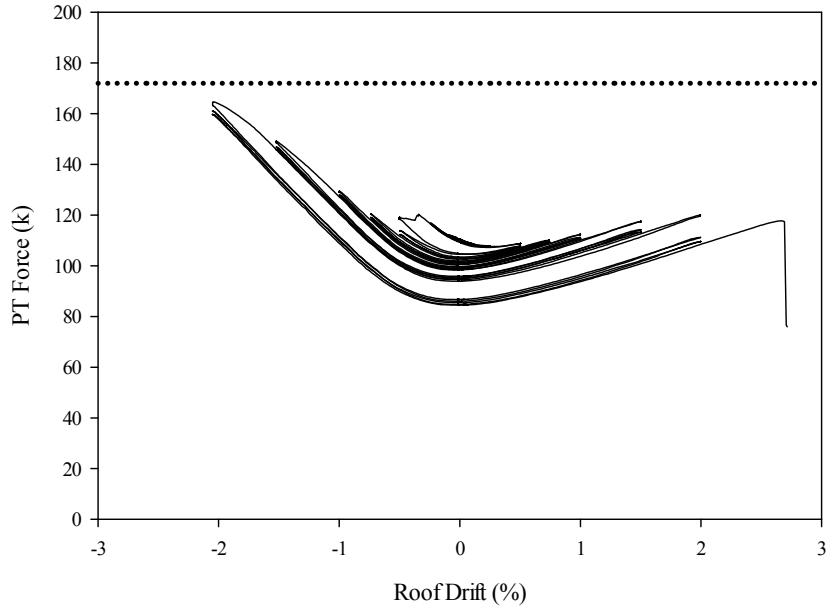
Figure 5-18 - PT6 vs Roof Drift
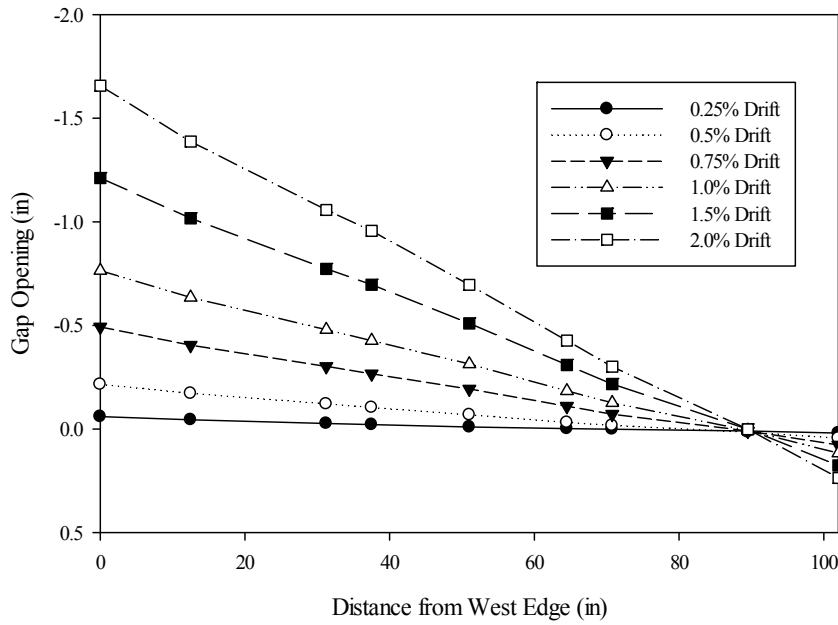
Figure 5-19 - Gap Opening - Eastward Loading

151
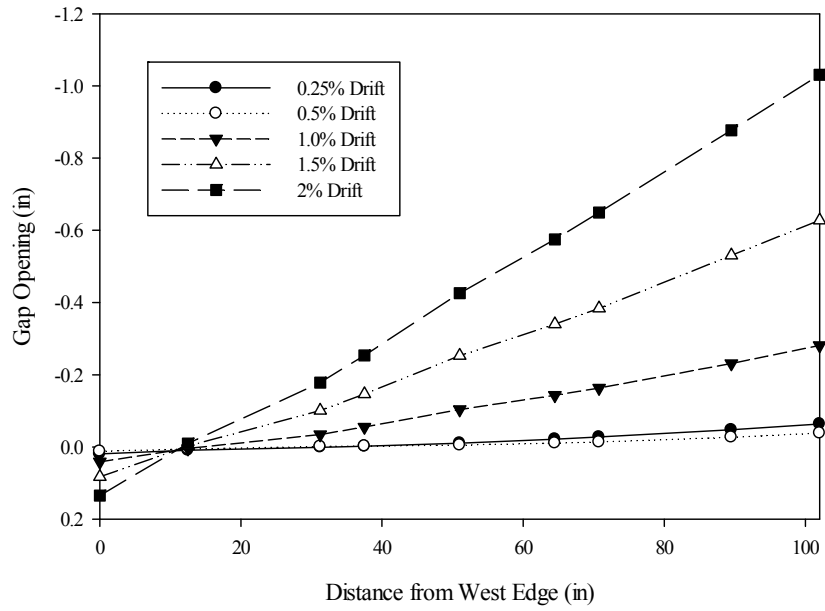
Figure 5-20 - Gap Opening - Westward Loading
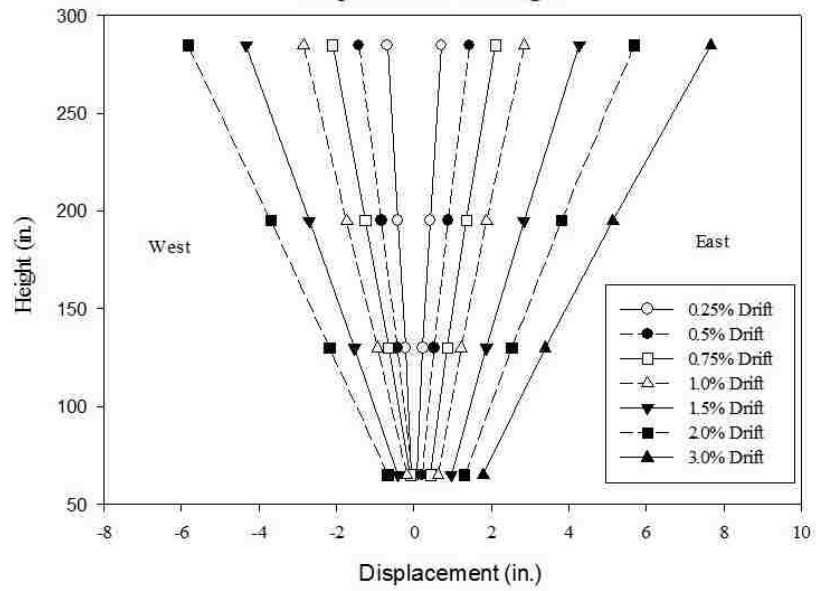
Figure 5-21 - Displaced Shapes at First Cycle for Each Roof Drift Level

152
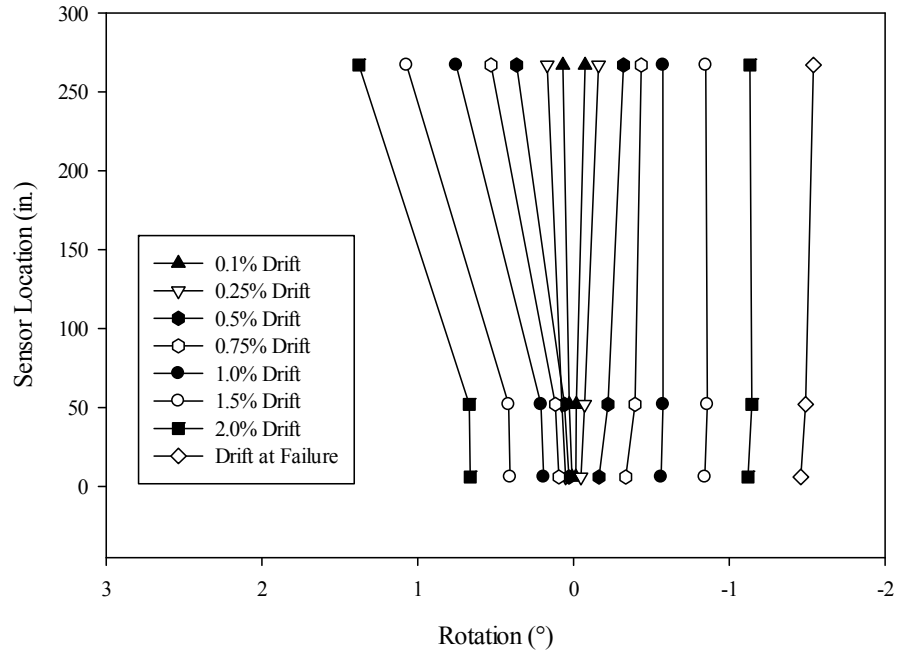
Figure 5-22 - Rotation Profiles
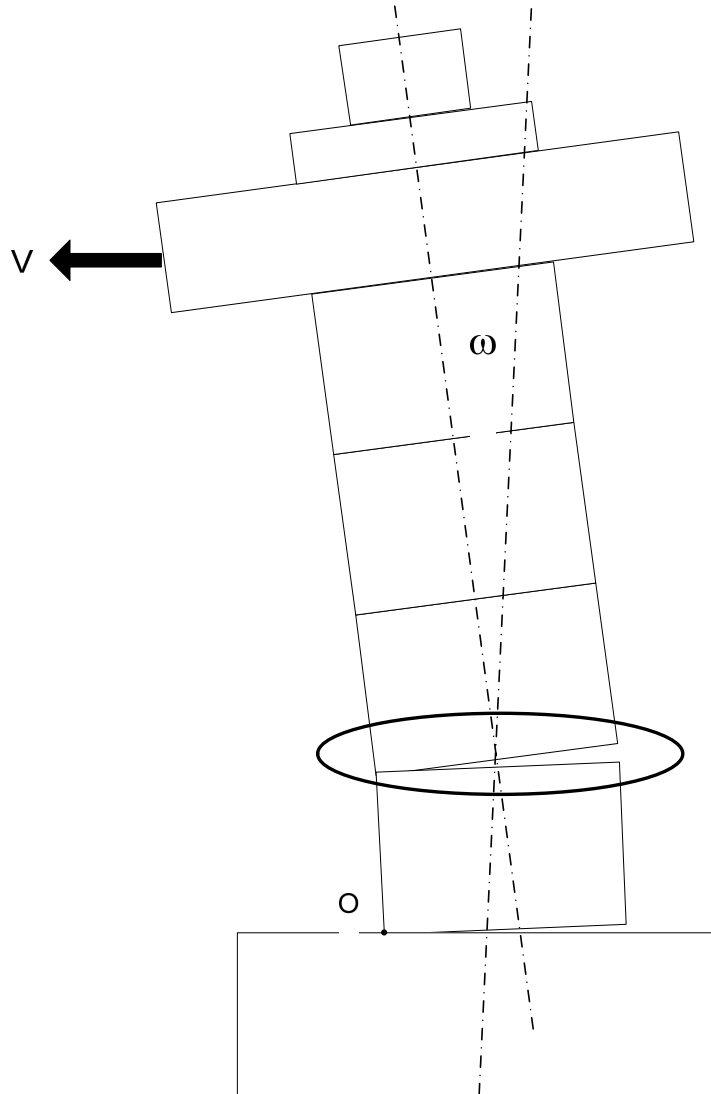
Figure 5-23 - Additional Rotation from Gap Opening at First Story

Figure 5-24 - Gap Opening at Joint between First and Second Panels

2% Roof Drift (Westward Loading)
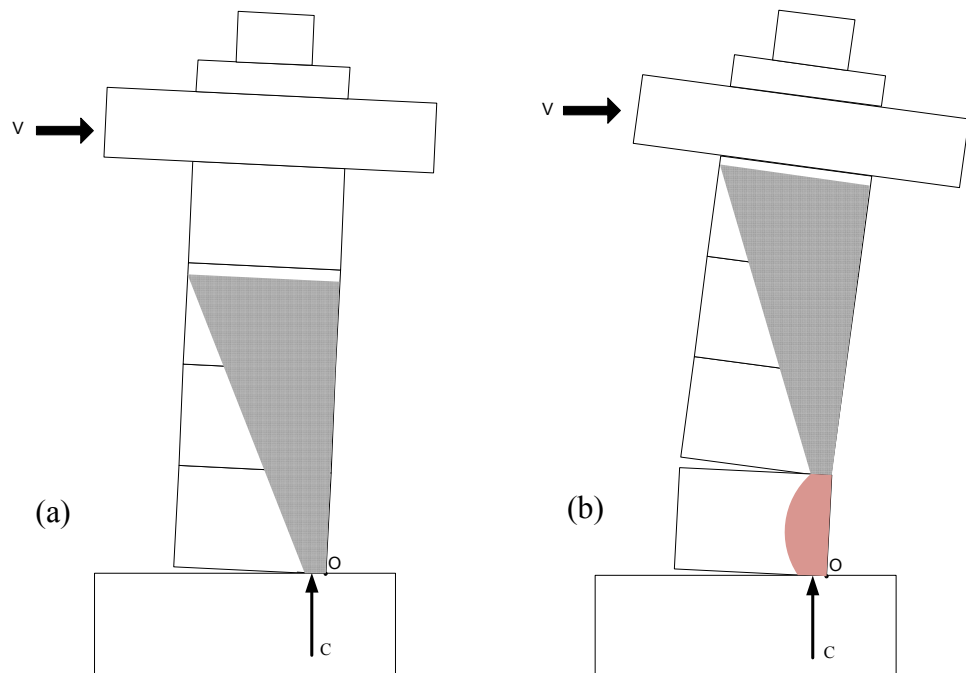
Figure 5-25 – Compression Fan with (a) No Gap Opening at the First Story

(b) Gap opening at the First Story
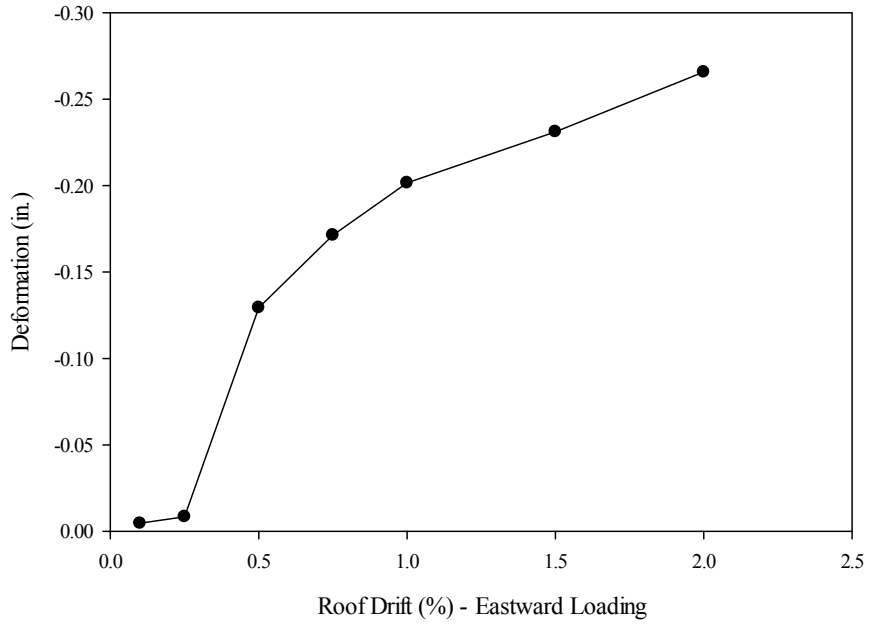
Figure 5-26 – Estimated Vertical Shortening of the Centroidal Axis of the Wall
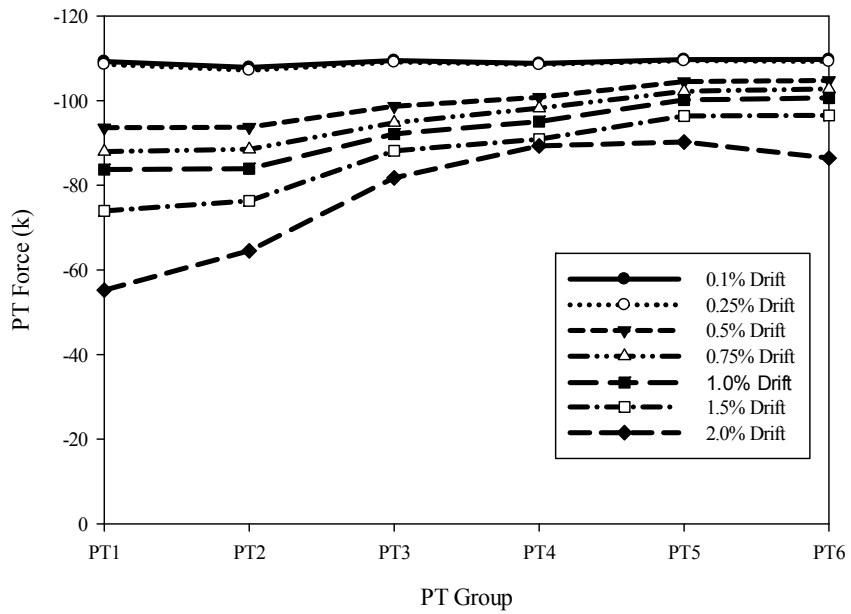
Figure 5-27 - PT Force at Zero Lateral Load after Each Cycle Group

156

6 Comparisons to Previous Experiment and Analytical Prediction

6.1 Introduction

This chapter presents comparisons of the plate-confined wall with test results for TW3 from Perez et al. (2004) and with the closed form predictions developed in Section 2.6. This research intended to develop a post-tensioned wall system with similar drift and load capacity of walls tested by Perez et al. (2004), without extensive damage at the bottom corners of the wall. Specifically, the original intention was to achieve the base shear capacity of TW3 and the lateral roof drift capacity of TW5 from Perez et al. (2004). The lateral roof drift capacity did not approach the capacity of TW5, and therefore no specific comparisons of the plate-confined wall results and TW5 were presented.

Sections 6.2 compares the plate-confined wall test results with the prior test results for TW3 of Perez et al. (2004). Section 6.3 compares the test results with predictions from the closed form analytical expressions. The comparisons of test results are based on the behavior of the first story as opposed to the entire structure. This places the emphasis on the behavior of the confined region at the bottom of the first story panel.

6.2 Comparison to TW3

6.2.1 Base Shear vs. First Story Drift

Figure 6-1 compares the base shear versus first story drift of the plate-confined wall and TW3 from Perez et al. (2004). There is an offset of the first story panel of the plate-

confined wall toward the east which gets larger as the test continues. This is a result of minor sliding of the base of the panel during eastward loading, which was not fully recovered upon westward loading because of damage near the joint between the first and second panels. The sliding was not anticipated and was therefore not measured directly. The displacement gage at the top of the first panel indicates a maximum residual displacement of 0.15 inches which corresponds to 0.25% first story drift.

Also visible in Figure 6-1 is the asymmetric behavior of the plate-confined system. Since damage occurred near the joint above the first story panel under westward loading, the plate-confined panel was subjected to less drift (first story drift) under westward loading. All further first story drift comparisons focus on the east side of the panel under eastward loading, adjusted for sliding by removing the residual displacement present at the end of each eastward half cycle, because the sliding is not quantifiable except at the time of zero lateral load, since the horizontal displacement at the base of the first story panel was not measured.

6.2.2   Base Shear vs. Drift at Perez et al. (2004) Limit State Levels

Figure 6-2 shows an envelope plot of the base shear versus first story drift for TW3 and the plate-confined panel under eastward loading. The points of the plot represent the limit states defined by Perez et al. (2004), reiterated in Chapter 2. This plot is a comparison of the base shear of the plate-confined wall with the base shear of TW3 at the first story drift level at which TW3 experienced the design limit states (DEC, ELL, LLP, and CCC).

158

6.2.2.1 Decompression of TW3

TW3 experienced decompression at 0.04% first story drift and a load of 55 kips. At the same drift level, the plate-confined wall was under 52.5 kips of base shear. This discrepancy in base shear is not large and it can be concluded that the wall systems decompressed at almost the same point, indicating that decompression is more dependent on the elastic deformation of the entire wall as opposed to the stiffness of the bottom corner detail.

6.2.2.2 Spalling of TW3

TW3 began to spall at 0.67% first story drift and a load of about 140 kips. At the same first story drift, the plate-confined wall was at 166 kips of base shear. This corresponds to 20% more load capacity. At this drift level, the plate-confined details at the bottom corners of the panel dominate the behavior of the system. The smaller contact zone length results in larger gap opening, which corresponds to more rigid body rotation of the panel. Figure 6-3 and Figure 6-4 show TW3 and the plate-confined wall, respectively, at 1% roof drift. This point falls in between the two limit states of concrete spalling and yielding of PT steel for TW3. TW3 clearly shows permanent damage beginning to develop at the confined corner, while the plate-confined wall exhibits no sign of damage.

6.2.2.3   Yielding of PT Steel of TW3

The post-tensioning bars of TW3 began to yield at 1.42% first story drift and a load of
150 kips. This was the load capacity of the wall. At the same first story drift, the plate-
confined wall was at 184 kips. This corresponds to a 22% more load capacity. It should
be reiterated that due to the damage at the top west corner, there was loss of prestress
which delayed yielding of the post-tensioning bars.

6.2.2.4   Crushing of TW3

TW3 failed at 2.57% first story drift and a load of 125 kips. At the same first story drift
level, the plate-confined wall was at 196 kips. This corresponds to 57% more load
capacity. Figure 6-5 shows TW3 at failure while Figure 6-6 shows the plate-confined
wall at failure. The damage seen at the bottom corner of TW3 is not seen at all for the
plate-confined wall. The failure which was experienced by the plate-confined wall was of
a similar, sudden nature, but was in a different location. Therefore the plate-confined wall
reached the same drift and carried a larger load without sustaining severe damage at the
bottom corners of the first story panel, where failure occurred in TW3. However, the
failure occurred at a similar drift level because of unanticipated damage at the top of the
first story panel.

6.3 Comparison to Predictions from Closed Form Expressions

Figure 6-7 shows the predicted monotonic behavior of the plate-confined wall compared to the behavior from the test. The figure indicates that the closed form expressions were accurate through the DEC and ELL stages. There is a substantial change in the slope of the plot after the 0.25% drift cycle, indicating softening. This occurs at the same load level as predicted analytically. The experiment showed approximately 21% more load capacity than the predictions. The plate-confined wall did not approach the predicted roof drift of 6.8%.

6.3.1 Difference in Load Capacity

The difference in load capacity results from a discrepancy in the assumed and actual yield stress of the PT bars. The design of the plate-confined panel and the analytical predictions were based on an assumed yield stress value, f_{py}, of 120 ksi. In reality, the bars yielded at a stress of 136 ksi which represents an increase of 13%. Figure 6-8 shows the updated predictions, including the correct yield stress for the PT bars. The experimental results align well with the adjusted analytical predictions in terms of capacity.

Note that the greater than expected PT bar forces produced a larger compressive force resultant and increased the axial compressive stress and strain in the concrete panel.
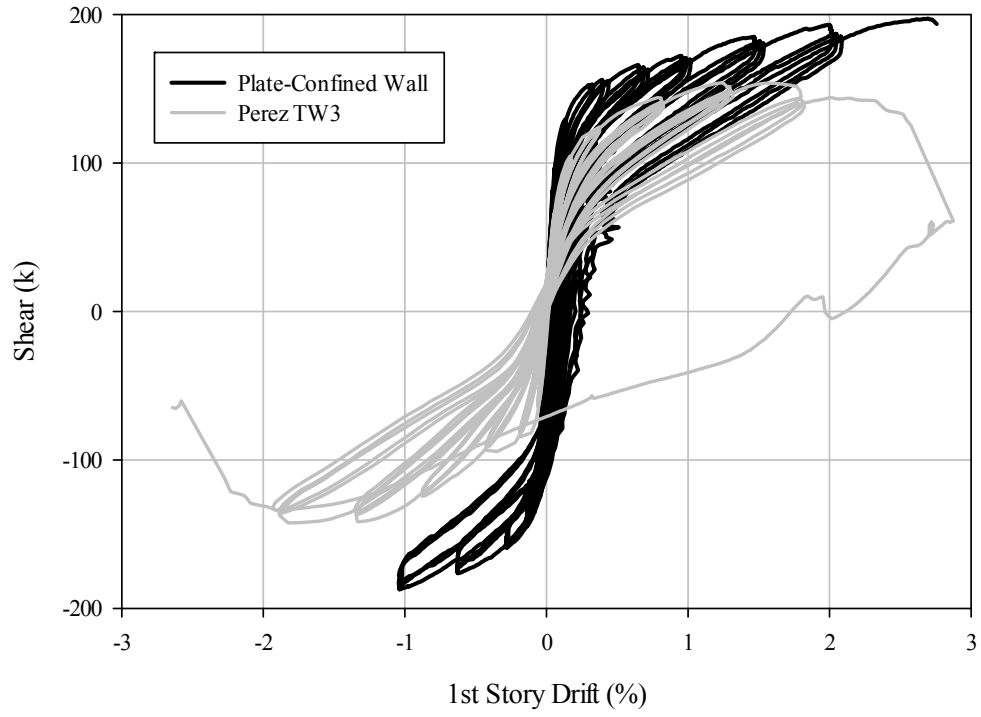
Figure 6-1 - Base Shear vs. 1st Story Drift

162
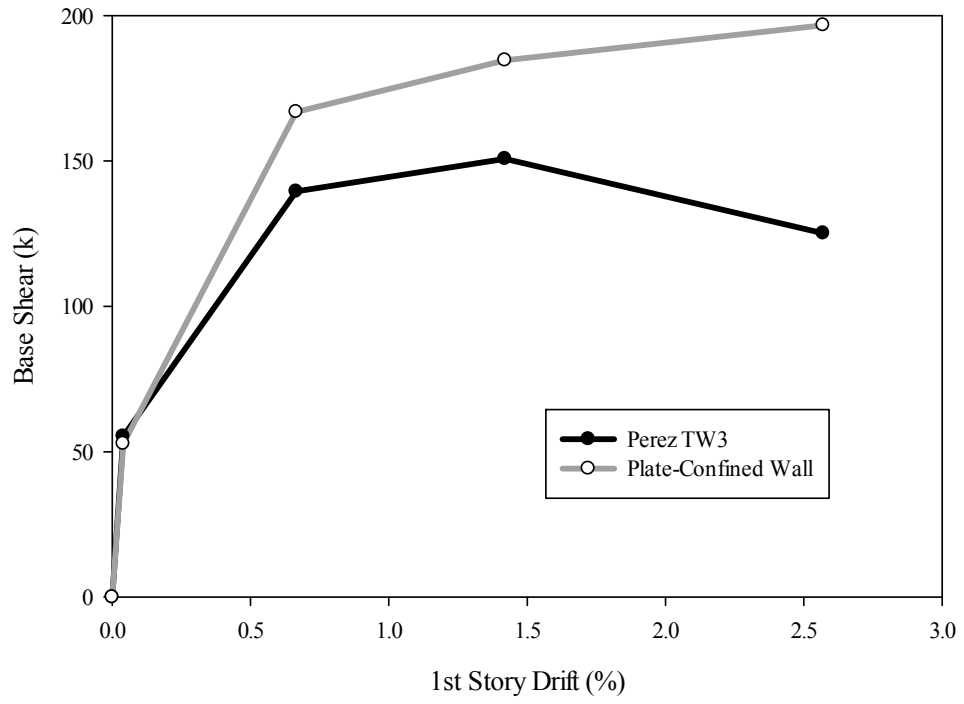
Figure 6-2 - Base Shear vs. First Story Drift at Limit States

Figure 6-3 - TW3 at 1% Roof Drift

Figure 6-4 - Plate-confined Wall at 1% Roof Drift

Figure 6-5 - TW3 at Failure

Figure 6-6 - Plate-confined Wall at Failure
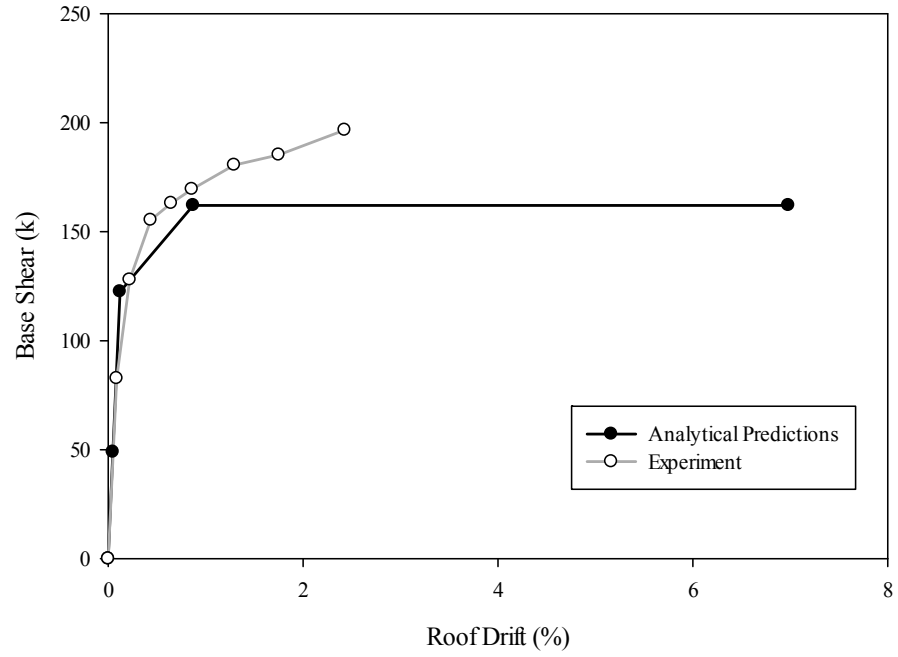
Figure 6-7 – Initial Prediction from Closed Form Analytical Expressions vs. Experimental Behavior

Figure 6-8 - Adjusted Prediction from Closed Form Analytical Expression vs. Experimental Behavior

7 Assessment of Plate-confined Panel Design Performance

7.1 Introduction

This chapter will discuss how the plate-confined wall panel performed experimentally as compared to the intended performance. Section 7.2 will explain the behaviors which differed greatly from the predictions by highlighting the main design assumptions which were violated during the test. Section 7.3 will provide a qualitative assessment of the panel performance.

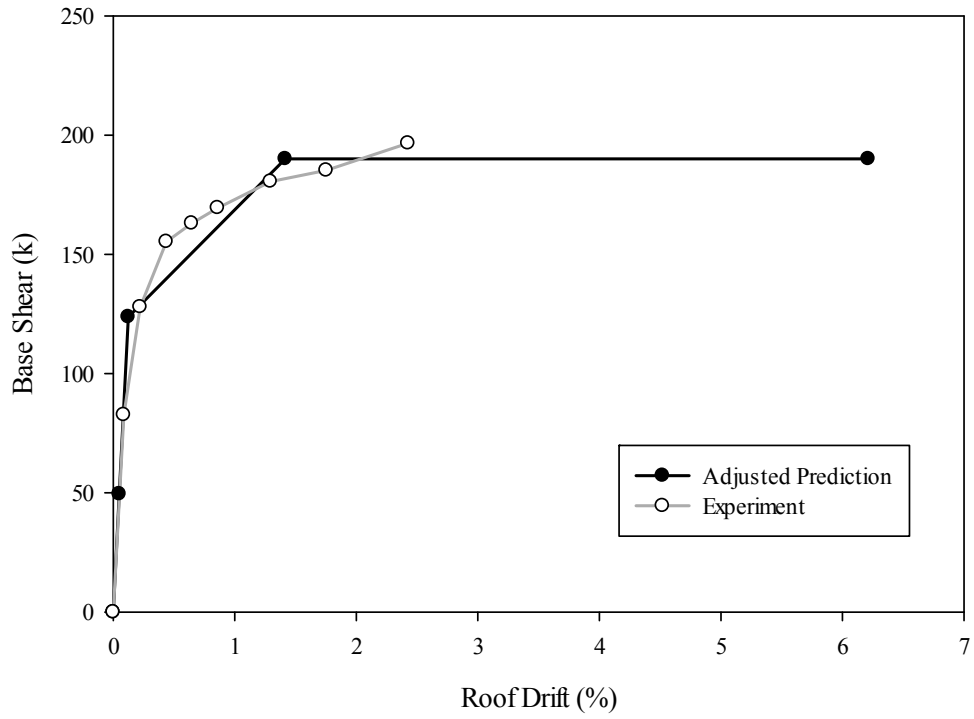## 7.2 Discussion of Deviations from Closed Form Predictions

As discussed in Chapter 2, the closed form predictions used for the panel option assessment and selection, and final panel design were dependent on several assumptions. The deviation of the actual behavior from that predicted using the closed form expressions was a result of these assumptions being violated. These assumptions, whether implicit or explicit, are reiterated and discussed in Sections 7.2.1 through 7.2.3.

Recall that in Section 6.3.1 the effect of the difference between the nominal yield stress (120ksi) and the actual yield stress (136 ksi) of the PT bars was quantified. The correlation of the experimental results with the analytical predictions improved when the actual yield stress was used in the prediction. The remaining discussion focuses on why the failure occurred in the top east corner of the plate-confined panel, and why the predicted drift capacity was not achieved.

168

7.2.1   Assumption of Gap Opening Only at the Base of the First-Story Panel

The assumption that gap opening would occur at the base of the first story panel only was violated during the test. Substantial gap opening was observed at the joint at the top of the first story panel, as evident in Figure 5-11. In Section 5.8, this gap opening and the effect that it had on the theoretical distribution of compression stress and strain over the height of the first story panel was discussed. The violation of this assumption was critical in developing damage at the top of the first story panel.

7.2.2   Assumption of Nominal Confinement at the Top of the Panel

The assumption that the top of the panel needed only a nominal amount of confinement for constructability was incorrect. Neglecting the gap opening at the top of the first story and underestimating the post-tensioning forces at yield resulted in an underestimate of the axial strain demand at the top of the first story panel. The axial strain resulting from the increased compressive force and the decrease in contact area between the first and second panels was much larger than expected. The decision to stop the end plate at 2/3 of the height of the panel was also critical. The in-plane transverse strain of the panel was expected to be small in the upper part of the panel. However, the larger axial compressive strains led to larger in-plane transverse tensile strains in the horizontal direction. The result was a large amount of spalling of the edge of the panel at the top corners of the first

169

story panel which was associated with both Damage Event 1 and the ultimate failure of the panel.

The rebar cage design was inadequate as a source of confinement. The spacing of the u-shaped bars on the ends of the longitudinal bars was too large to provide sufficient confinement. There was also a large amount of cover concrete left on the edges of the plate-confined panel, resulting in a region of completely unconfined concrete along the edge, where the compressive strains are the largest.

7.2.3   Assumption that Panel does not Slide at the Base

The decision to not measure lateral displacement at the base of the first story panel, based on prior tests by Perez et al. (2004), resulted in valuable information being lost. The panel appeared to slide towards the east, as shown in Figure 5-21. The sliding of the base and the damage in the top west corner of the plate-confined panel made it difficult to determine the actual behavior of the bottom corner region of the plate-confined panel.

7.3   Qualitative Panel Performance

The bottom corner regions of the plate-confined panel appeared to perform very well, though the early failure of the wall near the joint at the top of the first story panel, and construction issues made it difficult to identify the benefits of this panel design option. A qualitative assessment of the performance of the panel design is presented in this section.

7.3.1 Positive Panel Design Performance Assessment

The most apparent indicator of the positive performance of the plate-confined panel was the complete lack of damage at the bottom corners. The plate-confined panel developed almost no damage in this critical region, as opposed to the panels tested by Perez et al. (2004) which, after a major seismic event, would have required total replacement due to extensive spalling and rebar fracture. Even the damage from a minor seismic event would require some repair.

Additionally, the increase in lateral load capacity is seen as a positive outcome. The contact zone at the base of the panel was smaller, resulting in a larger base moment capacity with a corresponding larger base shear capacity.

7.3.2 Negative Panel Design Performance Assessment

The damage to the top corners and the upper interior region of the plate-confined panel was undesirable. This damage was due to the under-design of the panel as discussed in Section 7.2. The probable design corrections would require more bolts up the height of the plate-confined panel. This would make the wall more difficult and expensive to construct.

The material required and the preparation required to incorporate bolts, plates, ducts, and a rebar cage into one wall panel made construction difficult. Ensuring complete

consolidation of the concrete within the tight rebar cage is difficult as well. The plate-confined wall panel as designed in this study would not readily lend itself to rapid production.

7.3.3   Behavior as a Seismic Design System

Due to the damage that occurred at the top west corner of the first floor panel and the shortening of the wall, the plate-confined system did not exhibit the self-centering behavior that was expected. These failures were not anticipated and not accounted for in the design of the plate-confined panel. However, even if the design was adequate, this test suggests that it is difficult to limit damage under seismic loading.

The substantial effort required to install the plate-confined first story panel as a replacement panel into a damaged wall is an indicator that repairing these systems in a building after a seismic event is difficult.

8 Conclusions and Recommendations

8.1 Summary

The research presented herein was an effort to improve precast, post-tensioned concrete wall panels by investigating alternative panel designs. The work intended to improve the performance of the previous wall panels in two areas; lateral roof drift capacity and base shear capacity. A set of expressions for predicting the behavior of a precast, unbonded post-tensioned concrete shear wall with several different first story panel options was presented, based on prior work by Perez et al. (2004). The options considered were compared and a plate-confined panel design using steel plates with bolts through the thickness of the wall was selected. The experimental test setup, data acquisition and instrumentation and test plan for the plate-confined panel were presented.

8.2 Conclusions

The plate-confined wall panel detail did not reach the performance goal level of 6% lateral roof drift, though it did exceed the performance goal of 140 kips of base shear capacity. The following conclusions can be drawn from the study:

- The plate-confined wall panel behaved exceptionally well regarding local damage resistance within the plate-confined region.

- The damage that occurred was to the top of the first story panel, causing an unexpected and early failure.

173

- Gap opening at the joint between the first and second story panels led to the failure of the top of the first story panel from excessive compressive strains.

- Accumulation of damage in this region caused a loss of prestress force.

- Full confinement over the height of the first story panel edges is crucial to the performance of the system.

- Constructability and cost are a major concern for the plate-confined wall panel system.

- Incorporation of this system into an actual building presents an interesting challenge that warrants further investigation.

8.3   Recommendations for Future Work

Several future research areas were identified during this research which could be addressed. These recommendations for future work include:

- An in-depth investigation into how the axial strain varies along the height of the panel during a test should be conducted in order to develop an improved bolt pattern for the confinement plates.

- The sliding of the base of the first story panel should be addressed.

- Modifications to the design in order to avoid damage to the top of the panel should be analyzed to determine if it will result in damage somewhere else in the panel.

- Effort should be expended on increasing constructability of the plate-confined panel.

- An in-depth study of plate-confined wall panels within the entire structural system of a building should be conducted.

References

American Institute of Steel Construction. (2005). <u>Steel construction manual</u>. Chicago, Ill., American Institute of Steel Construction.

El-Sheikh, "Seismic Analysis, Behavior, and Design of Unbonded Post-Tensioned Precast Concrete Frames," Ph.D. Dissertation, Department of Civil and Environmental Engineering, Lehigh University, Bethlehem, PA, 1997.

Kurama, Y. C., "Seismic Analysis, Behavior, and Design of Unbonded Post-Tensioned Precast Concrete Walls," Ph.D. Dissertation, Department of Civil and Environmental Engineering, Lehigh University, Bethlehem, PA, 1997.

Oh, B., "A Plasticity Model for Confined Concrete Under Uniaxial Loading," Ph.D. Dissertation, Department of Civil and Environmental Engineering, Lehigh University, Bethlehem, PA, 2002.

Perez, F.J., Pessiki, S., and Sause, R. (2004), "Experimental and Analytical Lateral Load Response of Unbonded Post-Tensioned Precast Concrete Walls," *Advanced Technology for Large Structural Systems (ATLSS)* Rep. No. 04-11. Lehigh Univ., Bethlehem, PA.

Priestley, M., "Overview of PRESSS Research Program," *PCI Journal*, Precast/Prestressed Concrete Institute, Vol. 36, No. 4, July-August 1991, pp. 50-57.

Priestley, M. and Tao, J., "Seismic Response of Precast Prestressed Concrete Frames with Partially Debonded Tendons," *PCI Journal*, Precast/Prestressed Concrete Institute, Vol. 38, No. 1, January-February 1993, pp. 58-69.

Vita

Jeffrey Weidner was born on May 14, 1982 in Annapolis, MD to Daniel and Laura Weidner. He earned a Bachelor of Science in Architectural Engineering from Drexel University in Philadelphia, PA in 2005 before attending Lehigh University for a Master of Science in Structural Engineering. Currently Jeffrey is working towards a Doctorate in Structural Engineering at Drexel University and is recently married. Jeffrey plans to continue working the field of infrastructure condition assessment and management with a focus on bridges.